Universitat de Girona

WAVES AND TURBULENCE ON SUBMERGED AND EMERGENT AQUATIC VEGETATION

Dolors PUJOL COMPANY

Dipòsit legal: Gi. 747-2013
http://hdl.handle.net/10803/111336

Universitat de Girona

DOCTORAL THESIS

WAVES AND TURBULENCE ON SUBMERGED AND EMERGENT AQUATIC VEGETATION

Dolors Pujol Company

2013

Doctoral Programme in Experimental Sciences and Sustainability

Supervisors:

Teresa Serra Putellas

Jordi Colomer Feliu

Thesis submitted for the degree of Doctor of Philosophy by the University of Girona

La Dra. Teresa Serra Putellas i el Dr. Jordi Colomer Feliu, professors titulars del Departament de Física de la Universitat de Girona,

CERTIFIQUEN:

Que aquest treball, titulat “Waves and turbulence on submerged and emergent aquatic vegetation”, que presenta la Dolors Pujol Company per a l’obtenció del títol de doctora, ha estat realitzat sota la seva direcció i que compleix els requeriments per poder optar a Menció Internacional.

I perquè així consti, signen aquest certificat el 24 de gener de 2013.

Dra. Teresa Serra Putellas

Dr. Jordi Colomer Feliu

This Ph.D. thesis has been prepared as a collection of papers, in agreement with the regulations of the University of Girona. This thesis includes three original papers that have been published in peer-reviewed journals, and two papers that have not been yet published at the moment of preparing this thesis. The five papers have been published in (or submitted to) journals with impact factors within the first and second quartile, according to the 2011 Journal Citation Reports (JCR), for the subject categories *Oceanogrphy, Marine and Freshwater Biology* and *Multidisciplinary Geosciences*.

The complete references of the papers comprised in this thesis and the corresponding impact factor are:

Pujol, D., Colomer, J., Serra, T., Casamitjana, X., 2010. Effect of submerged aquatic vegetation on turbulence induced by an oscillating grid. Continental Shelf Research. 30, 1019-1029. (Impact factor: *2.088*; Journal *19 of 59 (0.32)*; 2nd quartile; Category *Oceanography*)

(http://www.sciencedirect.com/science/article/pii/S0278434310000762)

Pujol, D., Colomer, J., Serra, T., Casamitjana, X., 2012. A model for the effect of submerged aquatic vegetation on turbulence induced by an oscillating grid. Estuarine Coastal and Shelf Science. 114, 23-30. (Impact factor: *2.247*; Journal *20* of *97 (0.21)*; 1st quartile; Category *Marine and Freshwater Biology*)
(http://www.sciencedirect.com/science/article/pii/S0272771411003660)

Pujol, D., Nepf, H., 2012. Breaker-generated turbulence in and above a seagrass meadow. Continental Shelf Research. 49, 1-9. (Impact factor: *2.088*; Journal *19 of 59 (0.32)*; 2nd quartile; Category *Oceanography*)
(http://www.sciencedirect.com/science/article/pii/S0278434312002531)

Pujol, D., Serra, T., Colomer, J., Casamitjana, X., 2013. Flow structure in canopy models dominated by progressive waves. Journal of Hydrology (in press). (Impact factor: *2.656*; Journal *25 of 170 (0.15)*, 1st quartile; Category *Multidisciplinary Geosciences*)

Pujol, D., Casamitjana, X., Serra, T., Colomer, J., Canopy-scale turbulence under oscillatory flow. Submitted to Continental Shelf Research. (Impact factor: *2.088*; Journal *19 of 59 (0.32)*; 2nd quartile; Category *Oceanography*)

Agraïments

Aquesta tesi no hauria estat possible sense la col·laboració de moltes persones que m'han donat el seu suport.

Els meus dos tutors de tesi, el Dr. Jordi Colomer i la Dra. Teresa Serra del grup de Física Ambiental del Departament de Física, per confiar en mi. El seu entusiasme em va contagiar des del primer moment. També vull agrair el suport del Dr. Xavier Casamitjana i la seva ajuda en el tractament de dades. El treball en grup amb tots ells ha permès presentar els resultats d'aquesta tesi a congressos internacionals, en ciutats com Montpeller, Viena, Reykjavík i Otsu (Japó).

M'agradaria agrair a la Dra. Heidi Nepf i als membres del "Environmental Fluid Mechanics Lab" (MIT, Massachusetts, USA) per la seva amabilitat en rebre'm i en deixar-me formar part del seu grup durant uns mesos. En especial vull agrair l'ajuda del Dr. Mitul Luhar qui sempre estava disposat a donar-me un cop de mà.

No puc oblidar-me dels meus companys del despatx, dels companys del grup de recerca de Física Ambiental (Montse, Conxi, Toni, Nazha, Neus, Dani, Bruna, Àlex, Marianna) i de la Cristina, amb qui he compartit moltes estones en els últims mesos. Aquests quatre anys no haguessin estat tan divertits sense ells! I en Xicu Gòmez, laborant del Departament, que mai tenia un no per resposta.

Finalment, vull donar les gràcies a la meva família, en Carles i als amics per tot el suport donat.

Aquesta tesi ha estat finançada amb l'ajut del Ministerio de Ciencia e Innovación a través de CGL 2007-62483/HID i CGL 2010-17289 i amb l'ajut de la Beca de Recerca 08/11 de la Universitat de Girona.

Contents

List of Abbreviations

a: amplitude of the wave (Chapter 4 and 6)

a: frontal area per volume (Chapter 5)

α_w: attenuation of the wave velocity

A: total area

A_f: frontal area of the blade

A_∞^{rms}: root-mean-square wave orbital excursion length of the free-stream potential flow

C_d: drag coefficient

C_f: friction coefficient

C_m: inertial force coefficient

C_1, C_2, C_3: constant parameters

d: diameter of the plant

d_p: penetration depth

E: modulus of elasticity

ERV: emergent rigid vegetation

ε: dissipation

f: oscillating frequency

g: gravity constant

h: mean water height

h_s or h_v: height of the vegetation

h_{SRV}: height of the submerged rigid vegetation

h_{SFV}: height of the submerged flexible vegetation

h_{ERV}: height of the emergent rigid vegetation

H: height of the wave

k: wavenumber

k_m: added mass

l: second moment of area

ℓ_0: integral length scale

L_d: canopy drag length scale

L_s: canopy shear length scale

λ: wavelength

λ_1 and λ_2: geometrical and dynamical dimensional parameters

λ_f and λ_p: canopy parameters

M: space between grid bars

n: number of measurements (Chapter 6)

n: number of plants (Chapter 2)

n_s: stem density (plants/m^2)

OGT: oscillating grid turbulence

ppd: plant-to-plant distance

P_s: shear production

P_{wk}: turbulence production associated with canopy wakes

r: regression coefficient

ρ_w: density of the water

ρ_s: density of the flexible blades

R: rigid canopy model

Re_c: Reynolds number associated with the mean current

Re_G: Reynolds number of the oscillating grid

Re_w: Reynolds number associated with the wave velocity

s: stroke of the grid

S: distance between stems

S_{ww}: power spectral density

SAV: submerged aquatic vegetation

SPF: solid plant fraction (%)

SR: semi-rigid canopy model

SRV: submerged rigid vegetation

SFV: submerged flexible vegetation

t: time

t_b: thickness of the flexible blade

t_f: theoretical breaking time

T: transport of turbulence

TKE: turbulent kinetic energy

TKE_0: turbulent kinetic energy divided by water density

u or U_i or u_i: instantaneous velocity

U or U_c or u_c or <u> or $\bar{u}$: mean velocity

u' or U': turbulent velocity

u_0: root-mean-square of turbulent velocity

U_w or u_w: wave velocity

$U_{w,rms}$ or $u_{w,rms}$: root-mean-square of the wave velocity

$U_{\infty,w}^{rms}$: wave velocity root-mean-square unaffected by the canopy roughness

ν: kinematic viscosity

ω: radian frequency

w_b: width of the blade

z_c: distance from the virtual origin to the top of the canopy

z_m: distance from the virtual origin to the measurement

List of Figures

List of Tables

Abstract

Within the coastal zone, the ocean, land, and air interact to produce favourable habitats for many species. In particular, these zones are governed by physical forces originating from tidal currents, waves, winds and night convection amongst others, and characterized by the presence of seagrass meadows of varying characteristics and structure. That is, they can be submerged or emergent, or they can be dense or sparse. The aim of this thesis is to study the effects of flow structure and distribution in canopy models in which fluid is dominated by a) nearly isotropic turbulence with zero mean flow, b) progressive waves and c) breaking waves.

The first mechanism studied in this thesis is the pure and nearly isotropic turbulence generated by wind and night convection. Chapters 2 and 3 analyse the effect of submerged aquatic vegetation on a flow dominated by nearly isotropic turbulence with zero mean flow. Chapter 2 is focused on the feedback from the vegetation characteristics, between nearly isotropic turbulence and submerged aquatic vegetation. Oscillating grid turbulence is used to reproduce the effect of wind or night convections on seagrass models. Chapter 3 models, based on the results in Chapter 2, the effect of submerged aquatic vegetation.

Chapters 4 and 5 describe the vertical flow structure associated with progressive waves. The oscillatory flow is decomposed into three different terms: mean current, wave and turbulent velocity, from which both the shear stress and the turbulence kinetic energy are calculated. The study is conducted in a wave flume, with a vertical paddle, which generates progressive waves.

The third process studied is the interaction of submerged aquatic vegetation with breaking waves (Chapter 6). The turbulence is estimated by using an ensemble averaging technique. The instantaneous velocity is decomposed into the sum of the ensemble mean velocity, and the deviation from the ensemble mean. The levels of turbulence are associated with the loss of wave energy. This experiment was conducted at the Environmental Fluid Mechanics Lab (MIT, Massachusetts, USA), during a stay of 4 months, under the supervision of Professor Heidi Nepf.

The experiments were carried out in tanks and flumes where different mechanisms generated different turbulence intensities and wave conditions, and where different seagrass models (rigid, and flexible as well as models differing in canopy height, stem diameter and plant density) were employed. Flexible vegetation models were geometrically and dynamically similar to typical seagrasses for each process (nearly isotropic turbulence, progressive waves and breaking waves).

Chapter 7 illustrates the general results and a general discussion, and Chapter 8 presents the overall conclusion of this thesis.

In agreement with the regulations of the University of Girona, Chapters 2, 3 and 6 are an exact transcription of the published articles in Continental Shelf Research and Estuarine Coastal and

Shelf Science. A copy of these articles can be found in the appendix. Furthermore, the appendix contains a copy of a manuscript related to an experiment conducted with pure and nearly isotropic turbulence, in which a $k-\varepsilon$ turbulence model was used to simulate the results obtained in Chapters 2 and 3, and of which the author of this thesis is a co-author.

Resum

En zones costaneres, l'oceà, el terra i l'aire interactuen per produir un hàbitat favorable per moltes espècies. En particular, aquestes zones són governades per forces físiques originades per marees, onades, vent i convecció nocturna, entre d'altres i caracteritzades per la presència d'herbassars aquàtics amb diferents característiques i estructures. D'aquesta manera, l'herbassar pot ser submergit o emergent; dens o escás. Aquesta tesi té l'objectiu d'estudiar els efectes de l'estructura i la distribució del flux en models de plantes aquàtiques en un fluid dominat per a) turbulència quasi isotròpica amb flux mitjà zero, b) onades progressives i c) onades trencants.

El primer mecanisme estudiat en aquesta tesi ha estat la turbulència pura i quasi isotròpica generada pel vent o per la convenció nocturna. El Capítol 2 i 3 tenen l'objectiu d'analitzar l'efecte de la vegetación aquàtica submergida per turbulència quasi iostròpica. El Captítol 2 està centrat en l'estudi de la interacció entre la turblència quasi isotròpica i la vegetación aquàtic submergida. Una xarxa oscil·lant s'ha utilitzat per tal de reproduir l'efecte del vent o la convenció nocturna. El Capítol 3 té com objectiu modelar l'efecte de la vegetación aquàtic submergida basada en els resultats del Capítol 2.

Els Capítols 4 i 5 tenen l'objectiu de descriure l'estructura vertical del fluid associat a onades progressives. El moviment oscil·latori és descomposat en 3 termes diferents: current mitjà, velocitat de les onades i turbulència, a partir de les quals el cisallament i l'energia cinètica turbulenta són calculades. L'estudi és realitzat en un tanc d'onades, amb una pala vertical, des d'on es generen el camp d'onades.

El tercer procés estudiat és la interacció de la vegetación aquàtica submergida amb les onades trencants (Capítol 6). La turbulència és estimada utilitzant una tècnica conjunta de promitjos. La velocitat instantània és descompasada en la suma de velocitat mitjana, i la desviación d'aquesta velocitat mitjana. Els nivells de turbulència són associates amb la pèrdua d'energia de l'onada. Aquest expriment va ser realitzat al "Environmental Fluid Mechanics Lab" (MIT, Massachusetts, EUA), sota la supervisió de la Professora Heidi Nepf, durant una estada de 4 mesos.

Els experiments van ser realitzats en tancs i canals on diferents mecanismes generaven diferents intensitats de turbulència i condicions d'onades i, diferents models de vegetació aquàtica (rígida, flexible, altura de les plantes, diàmetre de la tija i, densitat de plantes) eren implamentades. Els models de vegetació flexible eren geomètrica i dinàmicament similars a les praderies de plantes aquàtiques per cada efecte (turbulència quasi isotròpica, onades progressives i onades trencants).

El Capítol 7 presenta els resultats i la discussió generals i, el Capítol 8 presenta les conclusions generals d'aquesta tesi.

D’acord amb les normes de la Universitat de Girona, els Capítols 2, 3 i 6 són una transcripció exacta dels articles ja publicats en el Continental Shelf Research i en l’ Estuarine Coastal and Shelf Science. Una còpia d’aquests articles es troba a l’annex. A més, l’annex també conté una còpia d’un article relacionat amb els experiments realitzats amb la turbulència quasi isotròpica, en el qual un model de turbulència $k-\varepsilon$ és utilitzat per simular els resultats obtinguts en el Capítol 2 i 3 i on l’autora d’aquesta tesi hi figura com a coautora.

Chapter 1: Introduction

Wetlands are distributed globally, covering ~ 4 % of the Earth's land surface (Prigent et al., 2001) and producing 2000 g/m^2 year of net primary production (22.6 % of the Earth's total) (Begon et al., 1986). Seagrass meadows in wetlands and coastal zones are an economically important component of that habitat because of the link between seagrass and fish production. For example, together with wetlands, seagrass beds support more than 80% of the annual fish yield in the Mediterranean (Batisse and Jeudy de Grissac, 1995).

Wetlands and coastal zones are systems governed by physical forces originating from tidal currents, waves, wind and night convection, amongst others, and by biophysical interactions between those processes and the organisms that inhabit the wetlands. Therefore, in natural systems, flows are a combination of steady, oscillatory and turbulent flows. This thesis starts from the hypothesis that aquatic vegetation plants modify the flow structure. So, the zone well inside the seagrass meadow is known to shelter or dampen the turbulent kinetic energy (TKE). The thesis aims to study the flow structure in different canopy models in a fluid dominated by a) nearly isotropic turbulence with zero mean flow, b) progressive waves and c) breaking waves. Unidirectional flows are outside of the scope of this study because they have been thoroughly studied in the past. However, a mean current in the direction of wave propagation is generated under progressive waves, and the interaction of this current with the vegetation has also been studied in this thesis. Specifically, this work has focused on the effects of different vegetation structures, in terms of density, stem diameter, height and rigidity, on the flow structure.

This Ph.D. thesis comprises of five papers related to the study of the effects of aquatic plants on a flow dominated by wave and nearly isotropic turbulence. Chapters 2 and 3, using an oscillating grid turbulence device, are related to the study of flow dominated by nearly isotropic turbulence with zero mean flow, Chapters 4 and 5 are focused on the interaction between the canopy bed and a flow dominated by waves. In particular, we have focused on the mean current, wave velocity (Chapter 4), and turbulent velocity and turbulent kinetic energy (Chapter 5). Finally, Chapter 6 studies the turbulent kinetic energy in a flow dominated by breaking waves.

The following sections in this introduction give a brief overview of the ecological implications of the presence of seagrass meadows, the mechanisms that generate turbulence inside a meadow as well as a summary of the calculations and methodology used for experiments.

1.1. Measurement of flow parameters in aquatic vegetation

The Eulerian model was considered suitable for describing the flow velocity in the experiments carried out. The Eulerian velocity field is defined as (u, v, w) in the (x, y, z) directions, respectively and measured at a fixed point in the space (x, y, z) coordinate system. The three components of velocity are recorded with a down-looking Acoustic Doppler Velocimeter (ADV). The ADV has three acoustic receivers and one acoustic transmitter, and provides water velocity measurements in three directions: two horizontal flow components (u and v) and a vertical component (w). Since turbulence has a high frequency, the ADV instrument is configured to transmit more than 10 acoustic signals per second. To avoid spikes, beam correlations from ADV measurements lower than 70% and values of instantaneous velocities higher than two standards deviation are discarded. From the measurements taken by the ADV, the three components of the turbulent velocities (u', v', w') can be calculated. Then, TKE is calculated from the following equation:

$$TKE = \frac{1}{2}\rho_w\left(\overline{u'^2} + \overline{v'^2} + \overline{w'^2}\right) \qquad (1.1)$$

where ρ_w is the water density and overbars represent time-averaged velocities. The calculation of turbulent components of the velocity is different for each fluid motion: nearly isotropic turbulence with zero mean flow, progressive waves and breaking waves. In the following sections the details of the calculations used to subtract the turbulent velocity are given.

1.2. Previous studies describing turbulence inside a meadow by unidirectional flow

Within shallow-water environments where seagrasses are abundant, local hydrodynamics can be drastically altered depending on both vegetation densities and flow conditions. Previous studies have successfully described the flow structure for submerged vegetation subjected to unidirectional flow using rigid and flexible vegetation models (Folkard, 2005; Ghisalberti and Nepf, 2006; Lefebre et al., 2010; Luhar et al., 2008; Nepf, 2011; Nepf, 1999; Nepf and Vivoni, 2000; Tanino and Nepf, 2008). In a zone without plants, and in a situation dominated by advection, the velocity profile follows the law of the wall. This logarithmic profile is described by the Kármán-Prandtl equation:

$$U_z = \frac{U^* \cdot \ln(z/z_0)}{\kappa} \qquad (1.2)$$

where U_z is the velocity at height z above the bed, U* is shear velocity, z_0 is the roughness length scale and, $\kappa = 0.4$ is the Von Kármán constant. For regions with adequate density of submerged aquatic vegetation, the logarithmic boundary layer disappears. In this situation, the velocity inside the submerged aquatic vegetation slows and is nearly constant over depth whereas, above the canopy the flow generally presents a logarithmic velocity profile (the velocity there follows the law of the wall) and vegetation may simply be considered as a form of macro-roughness (Nepf and Vivoni, 2000; Neumeier and Ciavola, 2004) (solid line of Fig. 1.1.a).

The current is partially dissipated by aquatic vegetation and afterwards converted to turbulent kinetic energy (TKE) within the meadow. Two distinct scales of turbulence have been identified within aquatic canopies. First, the drag discontinuity at the top of a submerged meadow produces a shear layer that generates canopy-scale turbulence that is transmitted downwards into the canopy down, d_p (Gambi et al., 1990; Nepf and Vivoni, 2000; Nepf and Ghisalberti, 2008). The shear-layer generates coherent vortices by Kelvin-Helmholtz (KH) instability (Ghisalberti and Nepf, 2002) (Fig. 1.1). Second, turbulence is generated in the wakes of individual blades and stems, if the Reynolds number based on the stem diameter (or blade width) is larger than about 200 (Anderson and Charters, 1982; Tanino and Nepf, 2008).

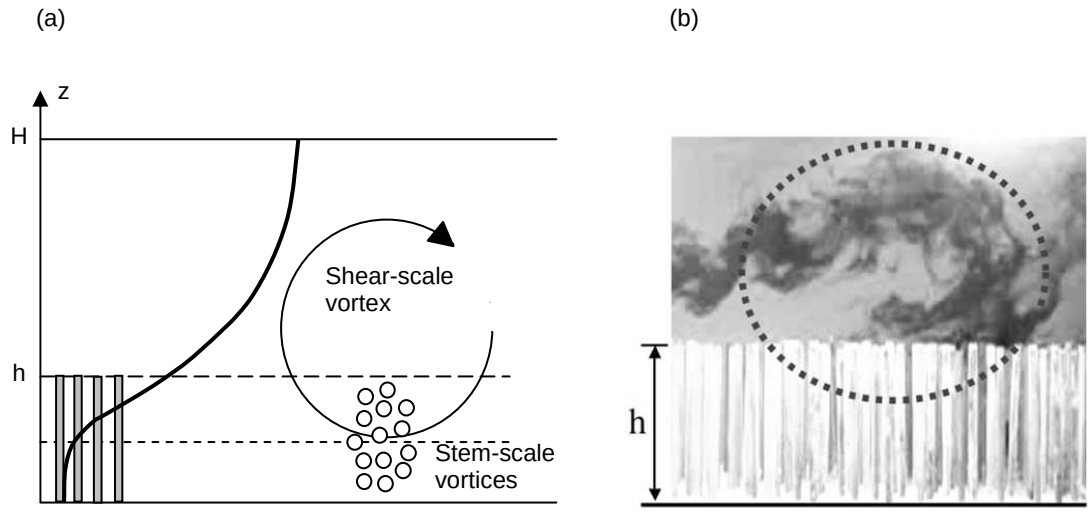

Figure 1.1. (a) Flow within and above a submerged canopy of height h in water depth H in unidirectional flow following the characteristic logarithmic velocity profile. The solid line is the profile of mean velocity. (b) Kelvin-Helmholtz (KH) instability above a submerged canopy of rigid cylinders is visualized using food dye. (Nepf and Ghisalberti, 2008).

A detailed description of the turbulence generated in the wakes of individual blades or stems is seen in Figure 1.2. This figure shows the flow structure behind a circular cylinder from a top-down perspective. Circular cylinders have been used to mimic submerged and emergent aquatic plants due to their similar geometry. Reynolds number is calculated as $Re = u \cdot d/\nu$,

where u is the velocity, d is the cylinder diameter and ν is the kinetic viscosity (= $1{\cdot}10^{-6}$ $m^2\ s^{-1}$). At low Re (Re < 10) the flow looks like an ideal fluid, characterized by the absence of vortices. At Reynolds numbers between 10 and 40, the cylinder bears a pair of attached eddies on its rear. Above 40, the pattern is no longer stable, and the vortices alternately detach, producing a wake of vortices rotating in opposite direction to that of its predecessor farther downstream. This pattern of alternating vortices is known as a "Von Kármán trail". Finally, between 100 and 200 the wide wake of turbulent eddies narrows rather abruptly. This phenomenon is called "separation of flow". Therefore, there is a production of TKE in that zone.

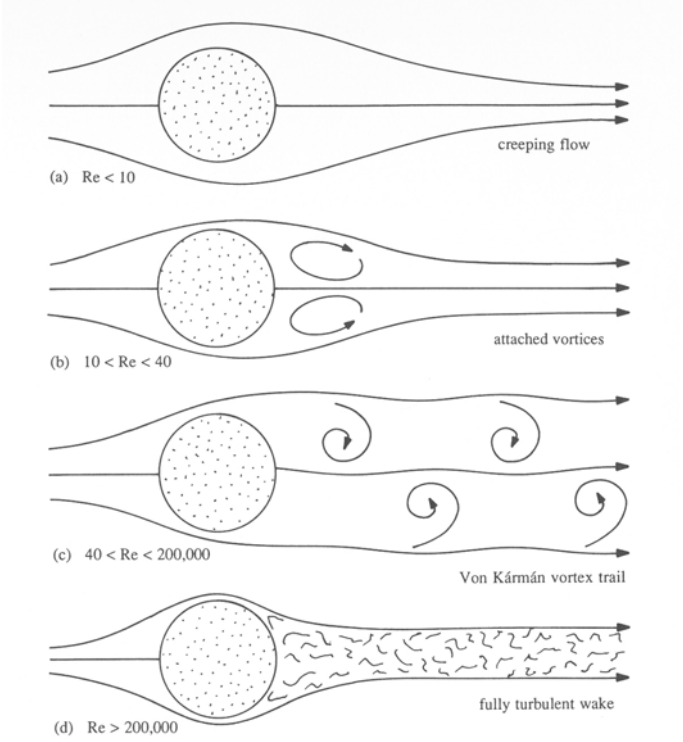

Figure. 1.2. Patterns of flow behind a circular cylinder. (a) Re < 10; b) 10 < Re < 40 c) 40 < Re < 200 and (d) Re > 200 (Vogel, 1994)

The production of turbulence may be enhanced by shear stress and stem wakes, but the associated drag leads to flow reduction, which in turn leads to reduce turbulence generation (Nepf et al., 1997). Therefore, because the level of turbulence inside a long meadow generally decreases with increasing stem density, sedimentation of particles also increases with increasing stem density (Bos et al., 2007; Leonard and Luther, 1995; Neumeier and Amos, 2006; Neumeier, 2007; van Katwijk et al., 2010; Ward et al., 1984).

1.3. Flow dominated by nearly isotropic turbulence

In wetlands, with weak tides and waves, turbulence created by night convection or by wind can interact with the plants and create an additional source of turbulent kinetic energy. Turbulence significantly affects the bottom boundary, and the interaction between turbulence and plant canopies is therefore particularly important.

Experiments with nearly isotropic turbulence with zero mean flow have been carried out to study different natural processes such as the mixing across density interfaces in stratified flows, like thermoclines or haloclines (Hopfinger and Toly, 1976; Nokes, 1988), the desorption of contaminants from sediment (Connolly et al., 1983), the mass transfer across a shear-free water-air interface (Brumley and Jirka, 1987), the resuspension and transport of sediment (Huppert et al., 1995; Orlins and Gulliver, 2003), the turbulent-dissipation model to perform a more accurate quantification of the experimental data (Matsunaga et al., 1999) and the aggregation dynamics in natural and engineered systems (Serra et al., 2008). Recently, some studies have put an emphasis on studying the influence of pure and nearly isotropic turbulence on the growth of different aquatic macrophyte species (Ellawala et al., 2011a; 2011b)

For stationary velocity records, the instantaneous velocities (u, v, w) are decomposed into the sum of time-averaged velocities ($\bar{u}$, $\bar{v}$, $\bar{w}$) and the turbulent components (u', v', w') (Fig. 1.3).

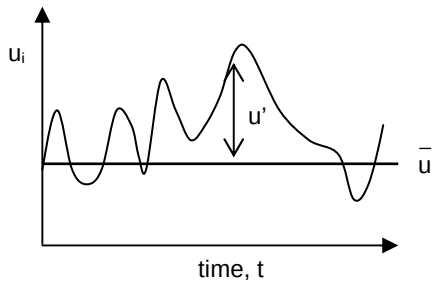

Figure 1.3. Sample of instantaneous velocity record

Therefore,

$$u' = u_i - \bar{u} \qquad (1.3)$$

This analysis is repeated for the v and w components.

1.4. Flow dominated by progressive waves

Some findings suggest that biological processes such as nutrient uptake may often be controlled by surface wave motions rather than the steady component of velocity that has received considerably more attention (Koch and Gust, 1999; Lowe et al., 2005b; Thomas and Cornelisen, 2003). Further, wave-induced forces are believed to set the distribution of seagrass populations (Fonseca and Bell, 1998). Specifically, waves have been noted to determine the upper depth limit distribution of submerged aquatic vegetation such as *Posidonia oceanica* (Infantes et al., 2009) and influence species size, morphology, and distribution patterns (Blanchette, 1997; Lewis, 1968; Menge, 1976).

For general wave flows, the instantaneous velocity, u_i can be descomposed as:

$$u_i = u_c + u_w + u' \qquad (1.4)$$

where u_c is the steady velocity associated with the current, u_w is the unsteady wave motion which represents spatial variations in the phase averaged velocity field, and u' is the turbulent velocity. u_c is the space and phase-averaged velocity found as (Lowe et al., 2005a; Luhar et al., 2010; Perrin et al., 2007, Sung and Yoo, 2001):

$$u_c = \frac{1}{2\pi}\int_0^{2\pi} u_i(\varphi)d\varphi \qquad (1.5)$$

where $u_i(\varphi)$is the instantaneous velocity according to the phase. Figure 1.4 shows a sample of instantaneous velocity (u_i) and steady velocity associated with the current (u_c) of experiments.

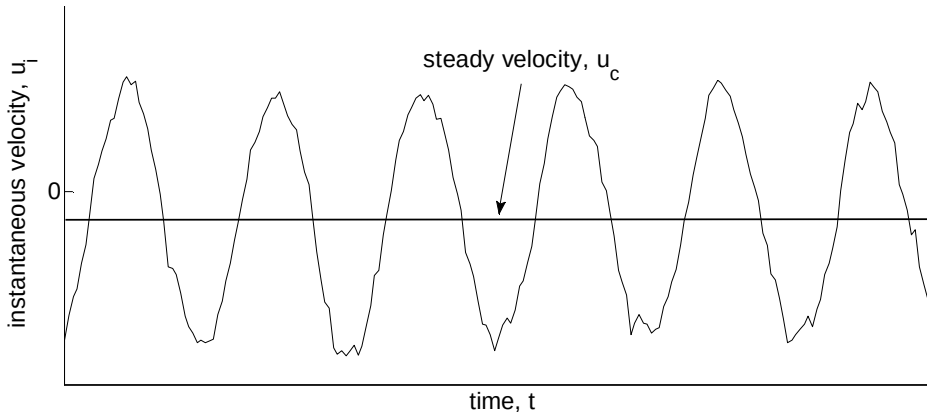

Figure 1.4. Sample of instantaneous velocity record (u_i)

Wave velocity, u_w, is obtained by using a phase averaging technique. For that, the Hilbert transform is used to average oscillatory flow velocities with a common phase, as in Wlezien and Way (1979). In order to compare the magnitude of the flow at different heights in the water column, the root mean squared (rms) velocities are calculated according to the following operation:

$$u_{w,rms} = \sqrt{\frac{1}{2\pi}\int_0^{2\pi}\left(u_i(\varphi) - u_c\right)^2 d\varphi} \qquad (1.6)$$

Then, turbulent velocity is calculated by subtracting the mean and the wave velocity from the instantaneous velocity:

$$u' = u_i - u_c - u_w \qquad (1.7)$$

This analysis is repeated for the v and w components.

1.5. Flow dominated by breaking waves

Ocean wave breaking is a random, intermittent and unsteady process caused by different mechanisms; such as wind blowing off the tops of waves (Banner and Phillips, 1974), or by wave-wave interaction, or wave instabilities (Melville, 1982). Wave breaking may be an important source of turbulence within a meadow, impacting both sediment retention and nutrient uptake. The most commonly used method for generating a repeatable, unsteady wave-breaking event is the constructive interference method used by Cummins (1962) and Davis and Zarnick (1964) to test ship models. Rapp and Melville (1990) extended this technique to generate an isolated breaker within a wave packet, which mimics transient wave breaking in the ocean. Following the method of Rapp and Melville (1990), the free surface displacement generated by the wavemaker, $\eta(x,t)$, was specified to be:

$$\eta(x,t) = \sum_{n=1}^{N} a_n \cdot \cos\left[k_n\left(x - x_f\right) - 2\pi f_n\left(t - t_f\right)\right], \qquad (1.8)$$

where a_n and k_n are the amplitude and wavenumber, respectively, of frequency component n; x_f is the distance from the wavemaker to the theoretical focusing location; t_f is the theoretical breaking time; and f_n is the nth frequency component. The wave signal was designed to create short period waves at the beginning of the packet and longer period waves at the end of the packet. Based on linear wave theory, the waves with a longer period travel at a higher celerity than those with a shorter period. Therefore, the longer-period waves catch up to the shorter-period waves, and the constructive interference produces a breaking event at a prescribed position and time. Figure 1.5 shows the ensemble mean surface displacements.

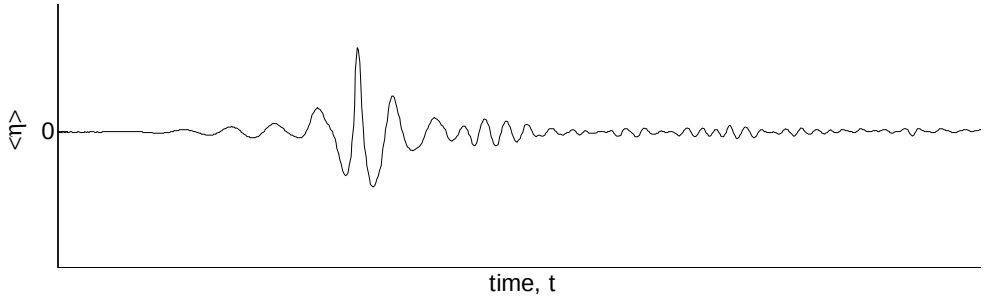

Figure 1.5. Ensemble mean surface displacements

In wave breaking, the turbulence is estimated using an ensemble averaging technique, described in Rapp and Melville (1990). The instantaneous velocity, $u_i(t)$, can be decomposed into the sum of the ensemble mean velocity, <u>(t), and the deviation from the ensemble mean, u'(t):

$$u_i(t) = \langle u \rangle(t) + u'(t) \qquad (1.9)$$

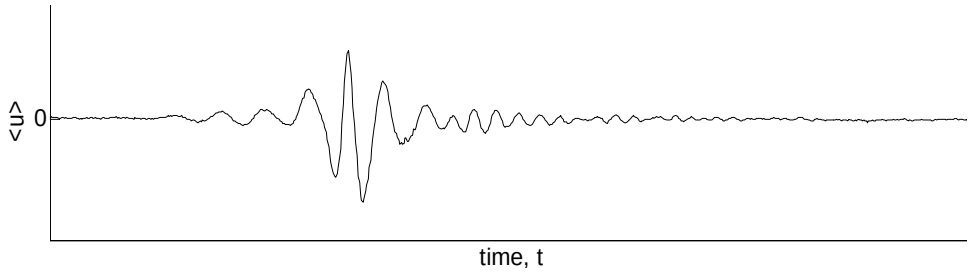

Figure 1.6. Ensemble mean horizontal velocity (<u>) as a function of time.

The deviation from the ensemble mean reflects three different sources:

$$u' = u'_t + u'_{rw} + u'_{mn}, \qquad (1.10)$$

where u'_t is the turbulence; u'_{rw} is motion associated with random waves generated by the breaking and u'_{mn} is the noise measurement.

Having estimated that the noise and random waves make relatively small contributions to u'_{rms}:

$$\left\langle u'^2_t \right\rangle \approx \left\langle u'^2 \right\rangle \qquad (1.11)$$

This analysis is repeated for the v and w components.

1.6. Ecological implications

Aquatic vegetation controls the mean and turbulent flow structure in coastal regions. Plants contribute to an addition drag which reduces both waves and currents and provides a refuge for fish, invertebrates and plankton (Ackerman and Okubo, 1993; Gambi et al., 1990; Nepf and Vivoni, 2000; Wilson et al., 1987). In particular, seagrass meadows reduce near-bed velocities, reducing local resuspension and promoting the retention of sediment (Fonseca and Fisher, 1986; Fonseca and Cahalan, 1992; Gleason et al., 1979; Granata et al., 2001; Reusch and Chapman, 1995). The reduction of resuspension improves water clarity, which in turn provides greater light penetration and consequently an increase in productivity, thus creating a positive feedback for seagrass growth (Ward et al., 1984).

1.6.1. Ecological implications under unidirectional flow

Studies of the flow structure under unidirectional flow demonstrate that properties such as plant density, plant height and stem flexibility are important parameters to take into account when studying the effect of a seagrass meadow and can modify the velocity amongst the aquatic plants (Ackerman and Okubo, 1993; Bouma et al., 2007; Ghisalberti and Nepf, 2006; Leonard and Crof, 2006; Nepf et al., 1997; Nepf and Vivoni, 2000; Peralta et al., 2008; Shi et al., 1995).

As an example, plant density plays an important role in determining flow structure. At low stem density, the mean velocity of the current can be converted to turbulent kinetic energy (TKE) by means of stem-wake turbulence (Nepf, 1999). Turbulence found inside the meadow has positive biological consequences, such as improvement in the transfer of CO_2 (in the form of bicarbonate) from the water to the surface layer of leaves. Without turbulence, the only physical mechanism capable of capturing CO_2 would be by means of molecular diffusion from the boundary layer, an extremely inefficient transport mechanism (Denny, 1988). Turbulence generated by the branches of the canopy could be the only turbulence, at the right scale, in the water motion able to enhance nutrient uptake and affect the exchange of gases and solutes (Anderson and Charters, 1982). However, at high stem density, the mean current is damped and dissipated by the canopy, a mechanism called sheltering. Nepf (1999) defined sheltering or dampening as a reduction in the in-emergent canopy macroscale diffusion due to a combination of reduced velocity and reduced eddy-scale relative to unvegetated zones. Neumeier and Amos (2006) and Neumeier (2007) found a reduction in turbulence near the bed, resulting in an enhancement of sediment deposition and a protection of the bed against subsequent erosion.

The differences between stiff and flexible canopies were described by Peralta et al. (2008). They concluded that a stiff canopy had a greater potential capacity to trap sediment, with the lateral expansion of the rigid canopy's populations resulting as a consequence of increased

sedimentation. However, a flexible canopy was more efficient at reducing erosion, so flexible shoots provide efficient protection against erosive forces.

1.6.2. Ecological implications under oscillatory flow

Some authors have studied the effects of seagrass or coral reef structures on a wave dominated flow in laboratory experiments (Coops et al., 1996; Koch and Gust, 1999; Lowe et al., 2005a; Luhar et al., 2010; Reidenbach et al., 2007). Seagrass meadows are an important ecosystem that may attenuate short-period waves (Möller et al., 1999) with a length scale from centimetres to tens of meters and a time in the order of the seconds. Extreme events such as storm surges or tsunamis are long-period waves hundreds of kilometres of length, with wave celerity from 10 to 100 times faster than standard ocean waves and a wave that quickly floods the coast over several minutes or days. Therefore, it is obvious that in these situations the wetland vegetation could not reduce the effects of storm surges or tsunamis (Feagin et al., 2010).

Experiments carried out to study the wave-induced currents inside the seagrass bed (Luhar et al., 2010) revealed that a unidirectional current is generated in the direction of wave propagation within the model seagrass bed when it is forced by a purely oscillatory wave-driven flow. The unidirectional mean current generated within the meadow under wave forcing plays a major role in determining both the health of the seagrass beds and their ecological contribution. This current could, for example, speed up the rate of water renewal within a meadow thus enhancing nutrient cycling expansion as well as influencing net sediment transport. In particular the enhancing of sediment transport is especially important for fine sediment and organic matter, where the majority of transport is in the form of suspended load. The mean current can also introduce a directional bias in the dispersal of seeds, spores and pollen, thereby dictating the direction of meadow (Luhar et al., 2010).

The ecological implications of plant movement under oscillatory flow have also been widely studied. Koch and Gust (1999) suggested that the periodic motion of seagrass blades could lead to enhanced mass transfer between the meadow and the overlying water column. In addition, the seagrass becomes fully extended and leans in the direction of flow for a longer part of the wave cycle. The blade posture can control light uptake. An increase in horizontally projected leaf also leads to higher photosynthesis. Therefore, under the wave crest, there is an enhancement of productivity in seagrass meadows (Zimmerman, 2003).

It is well known that many coral communities are located in nutrient limiting environments (Falter et al., 2004). Therefore, the capacity of transfer rates of material between seawater and the coral community will determine the fate of that community. Maximum shear and mass transport events have been observed near the top of the canopy, coinciding with ejection of vortices into

the flow, increasing the rate of turbulent exchange with the coral community. Therefore, that process could be one of the mechanisms which contributed to boosting the transfer of nutrients in the coral community (Reidenbach et al., 2007).

From another point of view, wave-induced forces are believed to establish the distribution of seagrass populations (Fonseca and Bell, 1998). Specifically, waves have been noted to determine the upper depth limit distribution of submerged aquatic vegetation such as *Posidonia oceanica* (Infantes et al., 2009) and influence species size, morphology, and distribution patterns (Blanchette, 1997; Lewis, 1968; Menge, 1976). Indeed, the disappearance of sandy beaches has been correlated with the regression of meadows (Batisse and Jeudy de Grissac, 1995).

References

Ackerman, J.D., Okubo, A., 1993. Reduced mixing in a marine macrophyte canopy. Funct. Ecol. 7, 305-309.

Anderson, S.M., Charters, A.C., 1982. A fluid dynamics study of seawater flow through *Gelidium nudifrons*. Limnol. Oceanogr. 27, 399-412.

Banner, M., Phillips, O., 1974. Incipient breaking of small-scale waves. J. Fluid Mech. 65, 647-656.

Batisse M., Jeudy de Grissac A., 1995. Marine region 3: Mediterranean, in: Kelleher G., Bleakley C., Wells S. (Eds.), A global representative system of marine protected areas, Book 1. Great Barrier Reef Marine Park Authority, World Bank, and World Conservation Union.

Begon M., Harper, J.L. and Townsend, C.R., 1986. Ecology: Individuals, Populations and Communities, 1st ed. Blackwell Science, Oxford.

Blanchette, C.A., 1997. Size and survival of intertidal plants in response to wave action: A case study with *Fucus gardneri*. Ecology 78, 1563-1578.

Bos, A.R., Bouma, T.J., de Kort, G.L.J., van Katwijk, M.M., 2007. Ecosystem engineering by annual intertidal seagrass beds: Sediment accretion and modification Estuarine Coastal Shelf Sci. 74, 344-348

Bouma, T.J., van Duren, L.A., Temmerman, S., Claverie, T., Blanco-Garcia, A., Ysebaert, T., Herman, P.M.J., 2007. Spatial flow and sedimentation patterns within patches of epibenthic structures: Combining field, flume and modelling experiments. Cont. Shelf Res. 27, 1020-1045 .

Brumley, B.H., Jirka, G.H., 1987. Near-surface turbulence in a grid-stirred tank. J. Fluid Mech. 183, 235-263.

Connolly, J.P., Armstrong, N.E., Miksad, R.W., 1983. Adsorption of hydrophobic pollutants in estuaries. J. Environ. Eng-ASCE. 109, 17-35.

Coops, H., VanderVelde, G., 1996. Effects of waves on helophyte stands: Mechanical characteristics of stems of *Phragmites australis* and *Scirpus lacustris*. Aquat. Bot. 53, 175-185.

Cummins, W. 1962. The impulse–response function and ship motion. Schiffstechnik Forschungsh. Schiffbau Schiffsmaschineubau. 9, 101-109.

Davis, M., Zarnick, E., 1964. Testing ship models in transient waves. Proc. Fifth Symp. on Naval Hydrodynamics, Washington, DC, Office of Naval Research. 509–540.

Denny, M.W., 1988. Biology and the mechanics of the wave-swept environment, Princeton University Press, Princeton.

Ellawala, C., Asaeda, T., Kawamura, K., 2011a. Influence of flow turbulence on growth and indole acetic acid and H_2O_2 metabolism of three aquatic macrophyte species. Aquat. Ecol. 45, 417-426.

Ellawala, C., Asaeda, T., Kawamura, K., 2011b. The effect of flow turbulence on plant growth and several growth regulators in *Egeria densa* Planchon. Flora. 206, 1085-1091.

Falter, J., Atkinson, M., Merrifield, M., 2004. Mass-transfer limitation of nutrient uptake by a wave-dominated reef flat community. Limnol. Oceanogr. 49, 1820-1831.

Feagin, R.A., Mukherjee, N., Shanker, K., Baird, A.H., Cinner, J., Kerr, A.M., Koedam, N., Sridhar, A., Arthur, R., Jayatissa, L.P., Lo Seen, D., Menon, M., Rodriguez, S., Shamsuddoha, M., Dahdouh-Guebas, F., 2010. Shelter from the storm? Use and misuse of coastal vegetation bioshields for managing natural disasters. Conservation Letters, 3, 1-11.

Folkard, A.M., 2005. Hydrodynamics of model *Posidonia oceanica* patches in shallow water. Limnol. Oceanogr. 50, 1592-1600.

Fonseca, M., Bell, S., 1998. Influence of physical setting on seagrass landscapes near Beaufort, North Carolina, USA. Mar. Ecol-Prog. Ser. 171, 109-121.

Fonseca, M., Cahalan, J.A., 1992. A preliminary evaluation of wave attenuation by 4 species of seagrass. Estuar. Coast. Shelf Sci. 35, 565-576.

Fonseca, M., Fisher, J., 1986. A comparison of canopy friction and sediment movement between 4 species of seagrass with reference to their ecology and restoration. Mar. Ecol-Prog. Ser. 29, 15-22.

Gambi, M.C., Nowell, A.R.M., Jumars, P.A., 1990. Flume observations on flow dynamics in *Zostera marina* (eelgrass) beds. Mar. Ecol. Prog. Ser. 61, 159-169

Ghisalberti, M., Nepf, H., 2002. Mixing layers and coherent structures in vegetated aquatic flows. J. Geophys. Res. Oceans. 107, C2

Ghisalberti, M., Nepf, H., 2006. The structure of the shear layer in flows over rigid and flexible canopies. Environ. Fluid. Mech. 6, 277-301.

Gleason, M., Pien, N., Fisher, J., 1979. Effects of stem density upon sediment retention by salt-marsh cord grass, *Spartina-Alterniflora Loisel*. Estuaries 2, 271-273.

Granata, T.C., Serra, T., Colomer, J., Casamitjana, X., Duarte, C.M., Gacia, E., 2001. Flow and particle distributions in a nearshore seagrass meadow before and after a storm. Mar. Ecol-Prog. Ser. 218, 95-106.

Hopfinger, E.J., Toly, J.A., 1976. Spatially decaying turbulence and its relation to mixing across density interfaces. J. Fluid Mech. 78, 155-175.

Huppert, H.E., Turner, J.S., Hallworth, M.A., 1995. Sedimentation and entrainment in dense layers of suspended particles stirred by an oscillating-grid. J. Fluid Mech. 289, 263-293.

Infantes, E., Terrados, J., Orfila, A., Canellas, B., Alvarez-Ellacuria, A., 2009. Wave energy and the upper depth limit distribution of *Posidonia oceanica*. Bot. Mar. 52, 419-427.

Koch, E.W., Gust, G., 1999. Water flow in tide- and wave-dominated beds of the seagrass *Thalassia testudinum*. Mar. Ecol-Prog. Ser. 184, 63-72.

Lefebvre, A., Thompson, C.E.L., Amos, C.L., 2010. Influence fo *Zostera marina* canopies on unidirectional flow, hydraulic roughness and sediment movement. Cont. Shelf Res. 30, 1783-1794.

Leonard, L.A., Croft, A.L., 2006. The effect of standing biomass on flow velocity and turbulence in *Spartina alterniflora* canopies. Estuar. Coast. Shelf Sci. 69, 325-336.

Leonard, L.A., Luther, M.E., 1995. Flow hydrodynamics in tidal marsh canopies. Limnol. Oceanogr. 40, 1474-1484.

Lewis, J., 1968. Water movements and their role in rocky shore ecology. Sarsia, 13-36.

Lowe, R., Koseff, J., Monismith, S., 2005a. Oscillatory flow through submerged canopies: 1. velocity structure. J. Geophys. Res. Oceans. 110, C10016.

Lowe, R., Koseff, J., Monismith, S., Falter, J., 2005b. Oscillatory flow through submerged canopies: 2. Canopy mass transfer. J. Geophys. Res. Oceans. 110, C10017.

Luhar, M., Rominger, J., Nepf, H., 2008. Interaction between flow, transport and vegetation spatial structure. Environ. Fluid Mech. 8, 423-439.

Luhar, M., Coutu, S., Infantes, E., Fox, S., Nepf, H., 2010. Wave-induced velocities inside a model seagrass bed. J. Geophys. Res. Oceans. 115, C12005.

Matsunaga, N., Sugihara, Y., Komatsu, T., Masuda, A., 1999. Quantitative properties of oscillating-grid turbulence in a homogeneous fluid. Fluid Dyn. Res. 25, 147-165.

Melville, W., 1982. The instability and breaking of deep-water Waves. J. Fluid Mech. 115, 165-185.

Menge, B., 1976. Organization of the New England rocky intertidal community: role of predation, competition, and environmental heterogeneity. Ecol. Monogr. 46, 355–393.

Moller, I., Spencer, T., French, J.R., Leggett, D.J., Dixon, M., 1999. Wave transformation over salt marshes: A field and numerical modelling study from north Norfolk, England. Estuar. Coast. Shelf Sci. 49, 411-426.

Nepf, H., Sullivan, J.A., Zavistoski, R.A., 1997. A model for diffusion within emergent vegetation. Limnol. Oceanogr. 42, 1735-1745.

Nepf, H., 1999. Drag, turbulence, and diffusion in flow through emergent vegetation. Water Resour. Res. 35, 479-489.

Nepf, H., Vivoni, E.R., 2000. Flow structure in depth-limited, vegetated flow. J. Geophys. Res. Oceans. 105, 28547-28557.

Nepf, H., Ghisalberti, M., 2008. Flow and transport in channels with submerged vegetation. Acta Geophys. 56, 753-777.

Nepf, H., 2011. Flow and transport in regions with aquatic vegetation. Annu. Rev. Fluid mech. 44, 123-142.

Neumeier, U., 2007. Velocity and turbulence variations at the edge of saltmarshes. Cont. Shelf Res. 27, 1046-1059.

Neumeier, U., Amos, C.L., 2006. The influence of vegetation on turbulence and flow velocities in European salt-marshes. Sedimentology 53, 259-277.

Neumeier, U., Ciavola, P., 2004. Flow resistance and associated sedimentary processes in a *Spartina maritime* salt-marsh. J. Coastal Res. 20, 435-447.

Nokes, R.I., 1988. On the entrainment rate across a density interface. J. Fluid Mech. 188, 185-204.

Orlins, J.J., Gulliver, J.S., 2003. Turbulence quantification and sediment resuspension in an oscillating grid chamber. Exp. Fluids 34, 662-677.

Peralta, G., van Duren, L.A., Morris, E.P., Bouma, T.J., 2008. Consequences of shoot density and stiffness for ecosystem engineering by benthic macrophytes in flow dominated areas: a hydrodynamic flume study. Mar. Ecol. Prog. Ser. 368, 103-115.

Perrin, R., Cid, E., Cazin, S., Sevrain, A., Braza, M., Moradei, F., Harran, G., 2007. Phase-averaged measurements of the turbulence properties in the near wake of a circular cylinder at high Reynolds number by 2C-PIV and 3C-PIV. Exp. Fluids 42, 93-109.

Prigent, C., Matthews, E., Aires, F., Rossow, W.B., 2001. Remote sensing of global wetland dynamics with multiple satellite data sets. Geophys. Res. Lett. 28, 4631-4634.

Rapp, R.J., Melville, W.K., 1990. Laboratory measurements of deep-water breaking waves. Philos. T. Roy. Soc. A. 331, 735-800.

Reidenbach, M.A., Koseff, J.R., Monismith, S.G., 2007. Laboratory experiments of fine-scale mixing and mass transport within a coral canopy. Phys.Fluids 19, 075107.

Reusch, T., Chapman, A., 1995. Storm effects on eelgrass (*Zostera-Marina L*) and blue mussel (*Mytilus-Edulis-L*) beds rid. J. Exp. Mar. Biol. Ecol. 192, 257-271.

Serra, T., Colomer, J., Logan, B.E., 2008. Efficiency of different shear devices on flocculation. Water Res. 42, 1113-1121.

Shi, Z., Pethick, J.S., Pye, K., 1995. Flow structure in and above the various heights of a saltmarsh canopy: a laboratory flume study. J. Coast. Res. 11, 1204-1209.

Sung, J., Yoo, J.Y., 2001. Three-dimensional phase averaging of time-resolved PIV measurement data. Meas Sci Technol 12, 655-662.

Tanino, Y., Nepf, H.M., 2008. Lateral dispersion in random cylinder arrays at high Reynolds number. J. Fluid Mech. 600, 339-371.

Thomas, F., Cornelisen, C., 2003. Ammonium uptake by seagrass communities: effects of oscillatory versus unidirectional flow. Mar. Ecol-Prog. Ser. 247, 51-57.

van Katwijk, M.M., Bos, A.R., Hermus, D.C.R., Suykerbuyk, W., 2010. Sediment modification by seagrass beds: Muddification and sandification induced by plant cover and environmental conditions. Estuarine Coastal and Shelf Science 89, 175-181.

Ward, L.G., Kemp, W.M., Boynton, W.R., 1984. The influence of waves and seagrass communities on suspended particulates in an estuarine embayment. Mar. Geol. 59, 85-103.

Wilson, K.A., Heck, K.L., Able, K.W., 1987. Juvenile blue-crab, *Callinectes-sapidus*, survival - an evaluation of eelgrass, *Zostera-marina*, as refuge. Fishery Bulletin, 85, 53-58.

Wlezien, R.W., Way, J.L., 1979. Techniques for the experimental investigation of the near wake of a circular-cylinder. AIAA J. 17, 563-570.

Zimmerman, R., 2003. A biooptical model of irradiance distribution and photosynthesis in seagrass canopies. Limnol.Oceanogr. 48, 568-585.

Chapter 2

Effect of submerged aquatic vegetation on turbulence induced by an oscillating grid

Pujol, D.[1], Colomer, J.[1], Serra, T.[1], Casamitjana, X.[1]

[1]Department of Physics, Escola Politècnica Superior-II, Campus Montilivi, 17071 Girona, Catalonia, Spain

Published in: *Continental Shelf Research, 30, 1019-1029*
http://www.sciencedirect.com/science/article/pii/S0278434310000762

Abstract In wetlands wind-induced turbulence significantly affects the bottom boundary, and the interaction between turbulence and plant canopies is therefore particularly important. The aim of this study is to advance understanding of the impact of this interaction in submerged aquatic vegetation (SAV) on vertical mixing in a fluid dominated by turbulence. Wind-generated turbulence was simulated in the laboratory using an oscillating grid. We quantify the vertical distribution of turbulent kinetic energy (TKE) above and within different types of vegetation, measured by an acoustic Doppler velocimeter. Experimental conditions are analysed in two canopy models (rigid and semi-rigid) with seven solid plant fractions (SPFs), three stem diameters (d) and three oscillation grid frequencies (f) and four natural SAVs (*Cladium mariscus, Potamogeton nodosus, Myriophyllum verticillatum and Ruppia maritima*). Our observations suggest that the TKE above the constructed canopies was higher than that found without plants. The vertical profile varied according to the diameters of the individual stems and the SPF. Within the canopies, two zones could be distinguished. The 'transition zone', situated a few centimetres below the top of the canopy, was characterised by a reduction in the TKE. Below the transition zone, the TKE progressively decayed as the stems dissipated the turbulence, creating a zone where the TKE was lower than in the zone without stems. This is a well-known effect of SAV on turbulence, called sheltering or dampening. This phenomenon was enhanced by a decrease in the stem diameter and an increase in the SPF of the canopies, due to the reduction of the plant-to-plant distance. We have, therefore, not only observed a sheltering, but quantified it. The development of the sheltering slowed as the frequency increased, because the vegetation could not prevent the penetration of the turbulence. In the semi-rigid model, no transition zone was found inside the canopies, while sheltering was found from the very top of the plants and was intensified inside the canopies. Finally, sheltering for SAVs was similar to sheltering produced by semi-rigid plants with widespread sheltering inside the canopy.

Keywords Wetlands; oscillating grid; model canopies; submerged aquatic vegetation; turbulence; sheltering.

2.1. Introduction

Wetlands are distributed globally, covering ~ 4% of the Earth's land surface (Prigent et al., 2001) and producing 2000 g/m^2/year of net primary production (22.6% of the Earth's total) (Begon et al., 1986). Even so, the world may have lost 50% of all its wetlands, mostly those used for agriculture, since 1900. SAV has numerous ecological functions, with some of the most important being flood storage and desynchronisation, but which all give structural support to food web development, increase the availability of the habitat, facilitate wastewater treatment from industrial, agricultural and municipal sources and help to store greenhouse gases (Gorham, 1991; Machate et al., 1997; Willems et al., 1997; Brooks, 1989). The vegetation can also regulate the abiotic condition of light, the temperature and the dissolved oxygen (Mazzella and Alberte, 1986).

Much research has been carried out to understand the effect of emergent (Nepf, 1999; Serra et al., 2004) and submerged canopies, either in laboratory flumes or in the field (Ackerman and Okubo, 1993; Koch and Gust, 1999; Sand-Jensen and Pedersen, 1999). With submerged plants in the laboratory, natural (Gambi et al., 1990; Jarvela, 2002) and artificial (Poggi et al., 2004; Ghisalberti and Nepf, 2006; Peralta et al., 2008) plants have been used. In all cases, submerged aquatic vegetation investigations indicate that, compared with unvegetated areas, the velocity of the flow is reduced through the canopy (Gambi et al., 1990; Ackerman and Okubo, 1993; Koch and Gust, 1999), causing a reduction in TKE and enhancing sedimentation (Leonard and Croft, 2006). Studies of sedimentation demonstrate that properties like plant density (Leonard and Crof, 2006; Bouma et al., 2007), and the height (Shi et al., 1995; Nepf and Vivoni, 2000), morphology (Leonard and Reed, 2002; Morris et al., 2008) and flexibility (Ghisalberti and Nepf, 2006; Peralta et al., 2008) of the stem cause the velocity of sedimentation and the concentration of flocs to vary. Eddies found inside the canopy are produced as a result of mechanical turbulence produced by the plants and transmitted downwards. This mechanical turbulence is caused by the wake turbulence generated locally by the stems, and the shear turbulence generated by the local velocity gradient (Neumeier and Amos, 2006). In this case, turbulence generated by wake production has a length scale equal to that of the canopy characteristics, much smaller than the characteristic length scale of shear-generated turbulence and quickly dissipated to heat (Raupach and Thom, 1981).

Many experiments have used wind or water tunnels to obtain isotropic turbulence. In these cases, however, the generated turbulence decayed rapidly and was subjected to significant time-mean motion. De Silva and Fernando (1994) demonstrated that an oscillating grid induces turbulence, and can be used as an alternative to wind tunnel experiments since this device produces isotropic turbulence with zero mean flow and with the essential properties of the turbulence (its length and velocity scales) being determined by grid geometry, the amplitude and frequency of oscillation and the distance from the grid (Nokes, 1988). The mechanical energy in the system is converted to TKE through grid oscillation (Matsunaga et al., 1999).

According to De Silva and Fernando (1994), a region is produced where turbulence is generated by jet and wake structures formed by the nature of the oscillation grid and corresponding to the open areas and the grid bars respectively. In this region the mean shear induced by the jets and wakes becomes insignificant because they merge into one another. The turbulence quantities close to the grid are expected to be statically stationary (Holzner et al., 2006). Furthermore, the turbulence may be considered isotropic, and the corresponding measurements are often compared with predictions from theories of isotropic turbulence (De Silva and Fernando, 1994). Therefore, the design is well able to individualise the effect of turbulence, as the mean flow within the system is zero. That is of major interest in wetlands where turbulence induced by the wind is sometimes the only agent affecting the bottom boundary, and the study of the specific interaction between turbulence and plant canopies is particularly significant.

The turbulence generated by the grid has been extensively studied, both theoretically and experimentally, in the laboratory. The design has been used in the investigation of many scientific and engineering problems, such as the study of the resuspension of sediment and transport (Orlins and Gulliver, 2003), the mixing across density interfaces in stratified flows like thermoclines or haloclines (Hopfinger and Toly, 1976; Nokes, 1988), the mass transfer across a shear-free water-air interface (Brumley and Jirka, 1987), the aggregation dynamics in natural and engineered systems (Serra et al., 2008) and the desorption of contaminants from sediment (Connolly et al., 1983).

Our experiments are aimed at studying the feedback vegetation characteristics between oscillating grid turbulence (OGT) and SAVs in terms of a wide variety of parameters, such as stem diameter, solid plant fraction and plant rigidity, which can mimic processes in the field. The study therefore complements other experiments carried out on channel systems.

2.2. Materials and methods

2.2.1. Experimental device

The experiments were conducted with an OGT (Fig. 2.1a) that consisted of a Plexiglas box with interior dimensions of 28 x 28 x 49 cm. A Plexiglas grid was fitted over the top of the tank at a distance of z_0 = 0.02 m from the water surface (Fig 2.1b). The square, 1 cm thick grid was composed of 5 x 5 bars, with a width between the bars of (M*)* = 0.05 m for a mesh spacing corresponding to a solidity of 31% (defined as the fractional solid area occupied by bars). It was placed horizontally and oscillated vertically with a fixed stroke of s = 0.05 m, and variable frequencies of f = 0.8, 1.6 and 2.8 Hz. A clearance of 5 mm between the sidewalls and the grid was maintained. The grid was suspended inside the tank at a height of 0.365 m from the tank bottom and was driven by a variable-speed motor located outside the tank.

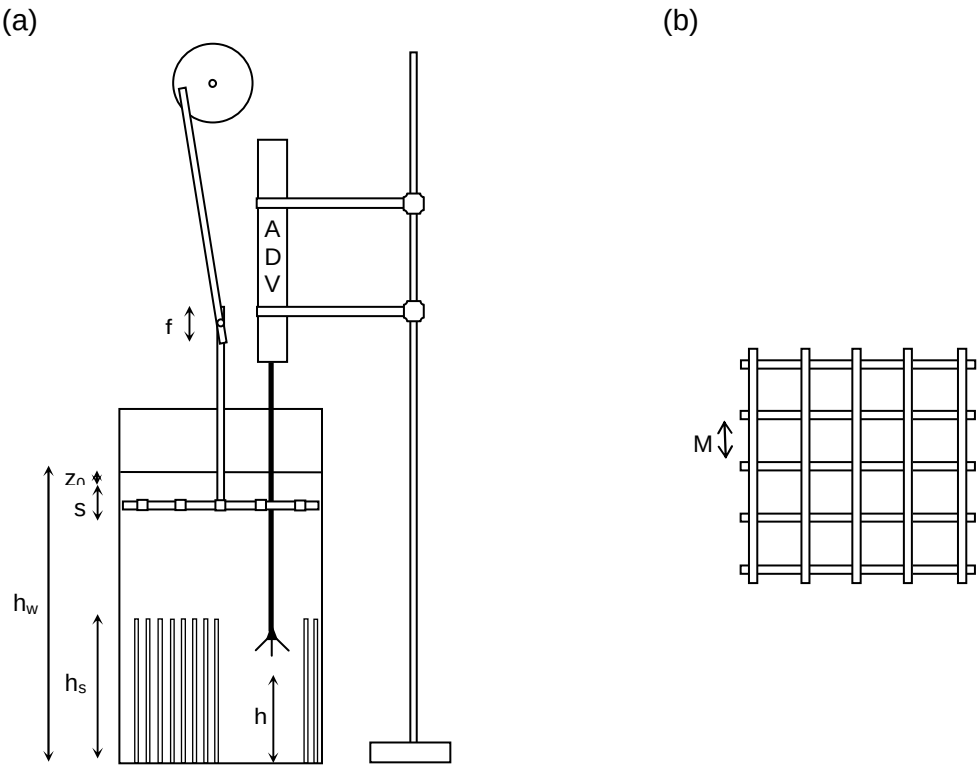

Figure 2.1. Schematic view of the laboratory experiment: (a) the structure of the device used in this study, where h_w is the height of the water column (0.41m); h_s is the height of the stem (0.17m); s is the stroke of the grid situated at the top (0.05m); z_0 is the distance between the water surface and the highest position of the mesh (0.02m); h is the height of the velocity samples (0.25, 0.23, 0.21, 0.20, 0.18, 0.17, 0.16, 0.14, 0.12, 0.10, 0.08, 0.06, 0.05, 0.04 m above the bed); and f is the grid frequency (0.8, 1.6, 2.8 Hz); (b) the grid where M is the width (0.05 m).

The turbulence generated by OGT is based on grid parameters such as M and s. Variations in the horizontal (u_0, v_0) and vertical (w_0) RMS velocities and the integral length scale (ℓ_0) of turbulence with distance z (measured from a virtual origin) can be expressed as:

$$u_0 = C_1 \cdot s^{3/2} \cdot M^{1/2} \cdot f \cdot z^{-1} \quad (2.1)$$

$$v_0 = C_2 \cdot s^{3/2} \cdot M^{1/2} \cdot f \cdot z^{-1} \quad (2.2)$$

$$\ell_0 = C_3 \cdot z \quad (2.3)$$

where C_1 = 0.22, C_2 = 0.25 and C_3 = 0.10 are constants that depend on the grid's geometry (DeSilva and Fernando, 1994; Hopfinger and Toly, 1976).

To calculate the grid's Reynolds number, Re_G, we used the equation of DeSilva and Fernando (1994), based on $Re_G = u_0 \ell_0/\nu$ and Eqs. (2.1) and (2.3):

$$Re_G = \frac{C_1 \cdot C_3 \cdot s^{3/2} \cdot M^{1/2} \cdot f}{\nu} \quad (2.4)$$

where ν is the kinematic viscosity ($0.93 \cdot 10^{-6}$ m^2/s). This resulted in the Reynolds values for f = 0.8, 1.6 and 2.8 Hz working out as 47, 95 and 166 respectively, from which we assumed that the flow was fully turbulent (Serra et al., 2008).

2.2.2. Methods of analysis

To obtain reliable velocity records, the mean quantities have to remain constant over the period of the study. For stationary velocity records, the instantaneous velocities (u, v and w) are decomposed into the sum of time-averaged velocities (U, V and W) and the turbulent components (u', v' and w'), which meant the TKE could be calculated from the following equation:

$$TKE = \frac{1}{2}\rho_w(\overline{u'^2} + \overline{v'^2} + \overline{w'^2}) \quad (2.5)$$

where ρ_w is the water density.

The TKE difference (ΔTKE) between samples with and without plants was expressed as a percentage and calculated according to:

$$\Delta TKE_h = \frac{TKE_{SAV} - TKE_{noSAV}}{TKE_{noSAV}} \times 100 \quad (2.6)$$

where h is the height of the samples, TKE_{SAV} is the TKE measured with a canopy at height h and TKE_{noSAV} is the TKE measured without a canopy at height h.

2.2.3. Measuring technique

Flow velocities were recorded with an acoustic Doppler velocimeter (ADV) (the Sontek/YSI 16-MHz MicroADV). The ADV has three acoustic receivers and one acoustic transmitter, and provides water velocity measurements in three directions: two horizontal flow components (u and v) and a vertical component (w). The acoustic frequency was 16 MHz, the sampling volume was 0.09 cm^3 and the distance to the sampling volume was 5 cm. The electronic noise of the measurements was smaller than the natural fluctuations caused by the turbulence. The ADV, which was operated manually, was mounted on a movable vertical frame so it could acquire single point measurements. For all experiments the ADV was placed at 7 cm of one side wall

(1.4 mesh size) and at 12 cm from the other side wall (2.4 mesh size) as suggested by Orlins and Gulliver (2003), who used an oscillating grid chamber to quantify the turbulence and sediment resuspension, with enough distance to wall to not measure their effects. In addition, the mesh endings were designed to reduce mean-secondary circulation. For each experiment, a vertical turbulence profile was taken over a height of 0.05 - 0.25 m, with 13 height positions in total, from the bottom of the tank.

In order to obtain valid data acquisition within the canopy, just a few stems were removed to avoid blocking the pathway of the ADV beam, as was done by Neumeier and Ciavola (2004) and Neumeier and Amos (2006). To minimise the effect of this 'hole', its shape was specifically designed to allow the ADV acoustic receivers and the acoustic transmitter to perform properly. To test the effect of the 'hole', we measured the velocities half a centimeter above the top of the canopy with and without plants. A comparison of the two measurements showed that at the highest SPF the difference was around 10% whereas at the lowest the difference was around 3%. We therefore concluded that the 'hole' contributed little to modify the hydrodynamics in that system.

The ADV instrument was configured to transmit 10 acoustic signals per second with a sampling time interval of 5 minutes (i.e. 3000 records per sample). The measurements were taken after oscillating the grid for about 10 minutes so that the turbulence was fully established. Each measurement was repeated five times. In addition, to avoid spikes, beam correlations from ADV measurements lower than 80% were removed. Finally, time-series records were used to calculate the turbulent velocities, and the results of repeated profiles at the same point were averaged.

2.2.4. Vegetation quantification

The characteristics of SAV vary greatly in terms of height, stem diameter, plant density, geometry and morphology. In order to obtain features in the laboratory similar to those in the field, 51 different situations were studied featuring two different canopy models, seven SPFs, three stem diameters, and three oscillating frequencies (Table 2.1).

Table 2.1. Summary of the 17 different situations studied with different SPFs, diameters and canopy models (R = rigid canopy model and SR = semi-rigid canopy model).

	SPF						
d (mm)	**0.6%**	**3%**	**5%**	**8%**	**10%**	**15%**	**25%**
4mm	SR	SR	R, SR	SR	R, SR	R	R
6mm			R		R	R	R
10mm			R		R	R	R

For each situation the oscillation frequencies were 0.8, 1.6 and 2.8 Hz.

The rigid canopy model consisted of rigid cylinders made of PVC (Fig. 2.2a left). The density of the canopy was implemented by four different SPFs. According to Serra et al. (2004) the SPF can be defined as the fractional plant area at the bottom occupied by stems:

$$SPF = \frac{n \cdot \pi \cdot (d/2)^2}{A} \qquad (2.7)$$

where n is the number of plants, d is the diameter of the plant and A is the total area studied. SPFs of 5, 10, 15 and 25% and cylinder diameters of 4, 6 and 10 mm were used for this study. The distribution of each SPF was made by means of a computer randomisation function with the distributions shown in Figure 2.3.

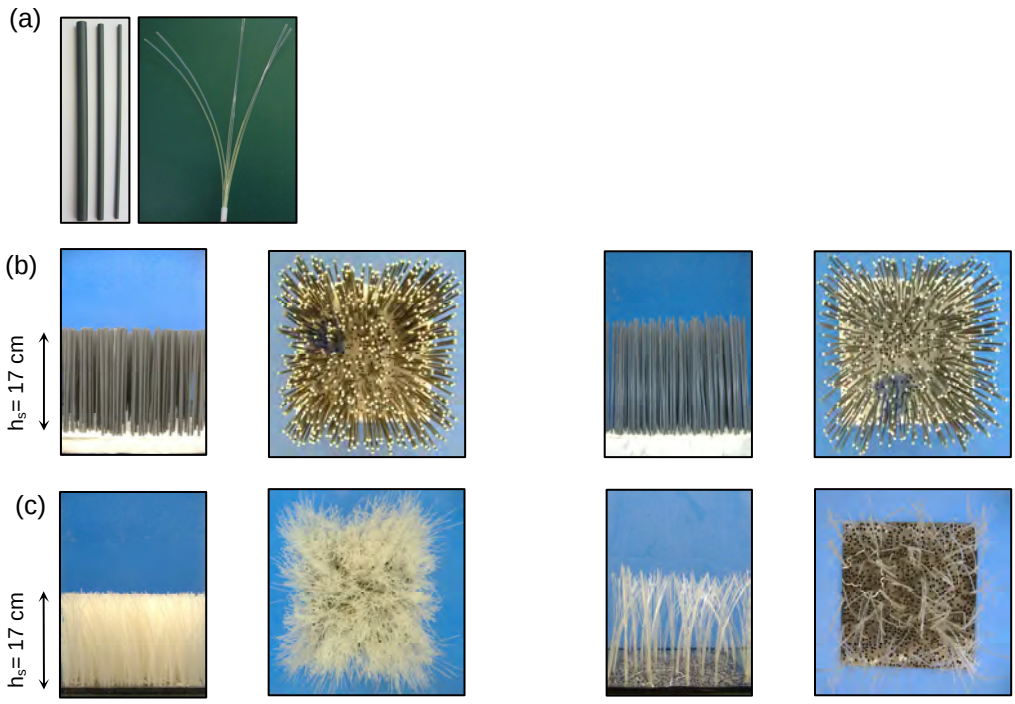

Figure 2.2. Photographs of vegetation studied: a) rigid canopy (d = 10, 6 and 4 mm) on the left and semi-rigid (d = 4 mm) on the right; b) lateral and top view of the rigid canopy (on the left, SPF = 10%, d = 4 mm and on the right, SPF = 5%, d = 4 mm); c) lateral and top view of the semi-rigid canopy (on the left, SPF = 10%, d = 4 mm and on the right, SPF = 0.6%, d = 4 mm).

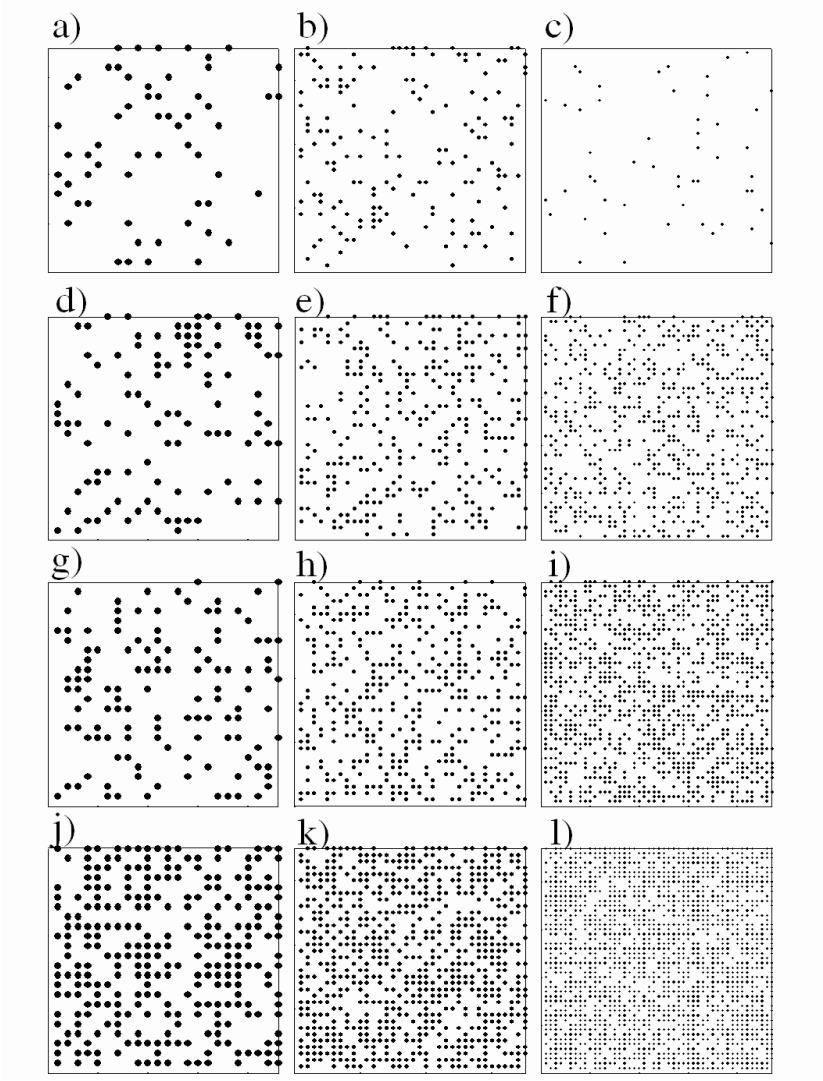

Figure 2.3. A plot of distributions for each feature: a) d = 10 mm, SPF = 5%; b) d= 6 mm, SPF = 5%; c) d = 4 mm, SPF = 5%; d) d = 10 mm, SPF = 10%; e) d = 6 mm, SPF = 10%; f) d = 4 mm, SPF = 10%; g) d = 10 mm, SPF = 15%; h) d = 6 mm, SPF = 15%; i) d = 4 mm, SPF = 15%; j) d = 10 mm, SPF = 25%; k) d = 6 mm, SPF = 25%; l) d = 4 mm, SPF = 25%.

A semi-rigid canopy model was made of nylon threads each 1.6 mm in diameter (Fig. 2.2c). To compare semi-rigid to rigid plants at d = 4 mm, 6 nylon threads were stacked together at the base to mimic the equivalent stem diameter. Due to the difficulty of determining SPFs with this canopy, three techniques were used for their calculation. The first was based on the application of equation (2.7) at the base of the canopy with five different SPFs (0.6, 3, 5, 8 and 10%) being considered. The second was based on determining the lateral obstruction ratio obtained from a binarised black and white picture using image analysis software (Neumeier, 2005). This software was designed to distinguish between black and white zones in order to calculate the area of the canopy. In this case, the lateral obstruction was 31, 83, 97, 98 and 99%. The third method consisted of calculating the vegetation cover at the top of the canopy using a similar

method to that developed by Neumeier (2005). In this case, for each situation studied photographs of the top were taken with a black background (the colour was the opposite of the canopy colour). We averaged the results over five pictures to calculate that the vegetation cover at the top of the canopy was 21, 56, 57, 74 and 76% (Table 2.2).

Table 2.2. Comparison of the three different techniques for measuring the SPF.

SPF (Bottom view, according to Serra et al., 2004)	Lateral obstruction (Lateral view according to Neumeier, 2005)	Vegetation cover (Top view)
0.6%	30.9%	20.6%
3%	82.7%	55.5%
5%	96.9%	57.3%
8%	98.1%	74.4%
10%	99.1%	76%

Real plants were used to compare the results obtained with those obtained for rigid and semi-rigid plant canopies. Four real plants were used for the study: *Cladium mariscus*, *Potamogeton nodosus*, *Myriophyllum verticillatum* and *Ruppia maritima* (Fig. 2.4). The density of each natural plant was 459 shoots/m^2. These plants were selected to give different SPF distributions and different morphologies. All of them are submerged aquatic vegetation in their natural media, with three of them developing in freshwater environments and one in a salty environment (*R. maritima*). The plants were cut at a height of 17 cm so that results could be compared with those obtained with previous models of rigid and semi-rigid canopies. *C. mariscus* (Fig. 2.4a) has a similar morphology to *R. maritima*: both have stem diameters of less than 2 mm. However, while *R. maritima* leaves are narrower, *C. mariscus* leaves are stiffer and wider. *M. verticillatum* (Fig 4 b) has compound and divided leaves, like feathers, and its stem is around 4 mm in diameter. *P. nodosus* (Fig. 2.4c) has a long stem with wide horizontal leaves and a diameter between 4 and 5 mm. Both *P. nodosus* and *M. verticillatum* have leaves that grow at each level of the stem and perpendicular to it. In addition, the vertical SPF is distributed homogeneously through the stem. *R. maritima* (Fig. 2.4d) has long, narrow upward leaves and lives in salt marshes.

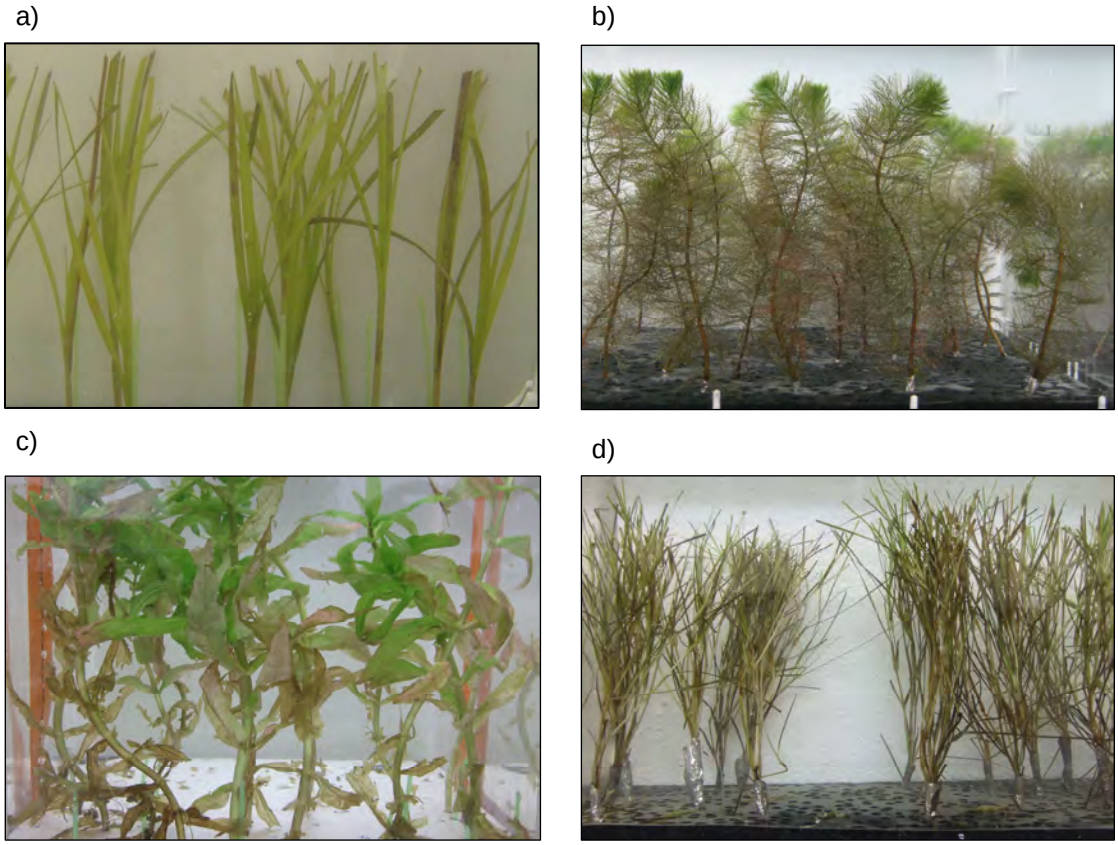

Figure 2.4. Illustrations of the submerged aquatic vegetation studied: a) *Cladium mariscus*; b) *Myriophyllum verticillatum*; c) *Potamogeton nodosus*; d) *Ruppia martitima*.

2.3. Results

The experiments with no SAV showed that TKE decreased following power decay, with the greatest values closest to the grid and decreasing towards the bottom of the tank (Fig. 2.5). TKE values were most different close to the grid at the different frequencies studied. Near the bottom, the results at the three frequencies studied were almost equal. The uncertainty in the data acquisition was calculated using the equation described by Kline and McClintock (1953) for the propagation of errors in physical measurements.

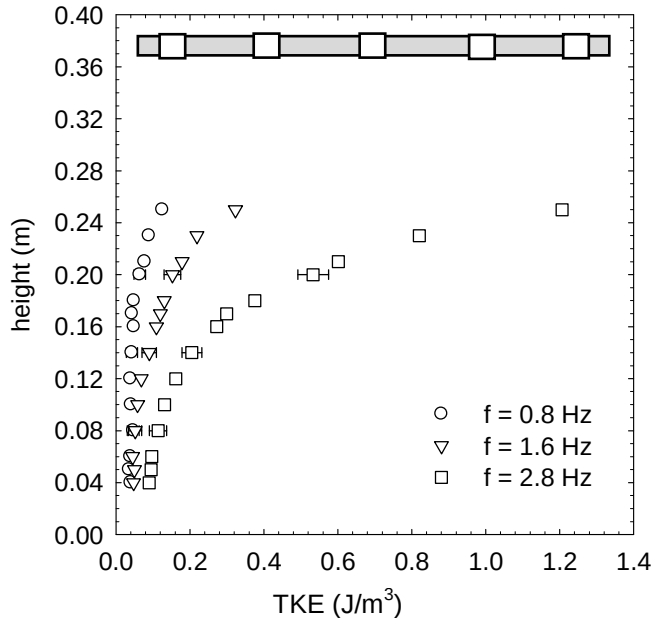

Figure 2.5. TKE profile with no SAV at 0.8 (circles), 1.6 (triangles) and 2.8 Hz (squares) frequencies. The horizontal error bars represent the uncertainty of experimental runs.

2.3.1. Experiments with the rigid canopy model

Three hydrodynamic regions with depth could be distinguished from all the TKE profiles for experiments with rigid canopies. The first was situated above the canopy, from 0.25 to 0.17 m above the bed. In all of the experiments the TKE was greater in this region than without plants (Fig. 2.6). The second region behaved like a transition zone and was situated below the top of the canopy to the depth where the TKE was lower than that found with no SAV. This depth depends on the stem diameter and canopy density at any depth. At the lowest diameter (d = 4 mm), the depth of the transition zone is 0.16 m (Fig. 2.6c and d), but as the stem diameter increases, the transition zone is more accentuated and can reach 0.08 m when d = 10 mm. Well inside the canopy, the TKE decayed progressively, creating a third zone where it was lower than that found where there was no SAV. The gradient of this zone was the lowest of the three.

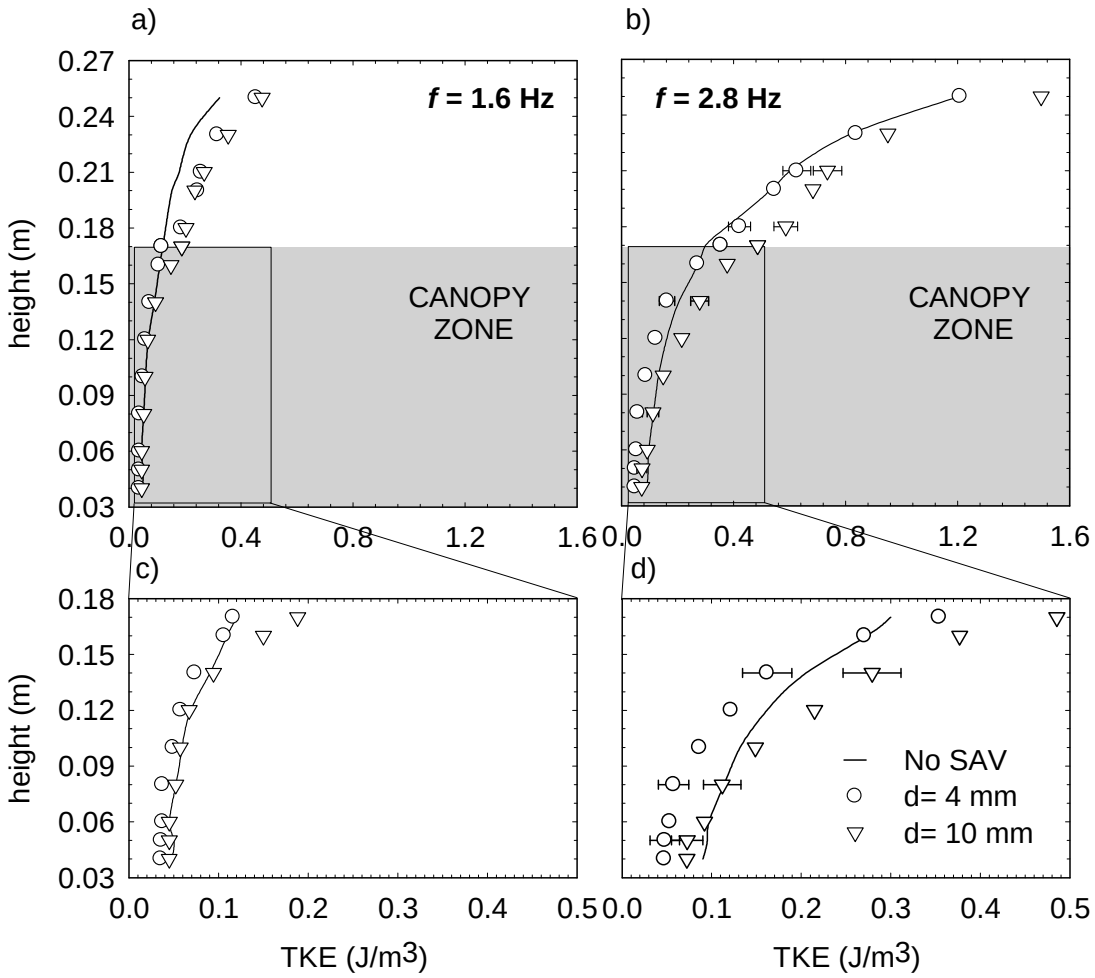

Figure 2.6. TKE profiles of rigid canopy at SPF = 25%, 4 (circles) and 10 mm (triangles) in diameter and with no SAV (solid line): a) f = 1.6 Hz; b) f = 2.8 Hz. Enlargement of the canopy zone: c) f = 1.6 Hz; d) f = 2.8 Hz. The horizontal error bars represent the uncertainty of experimental runs.

One cm above the constructed canopy (hereafter h_s+1) the ΔTKE was greatest and always positive for the largest stem diameters (56%) and the largest SPF and f (Table 2.3). Positive values of ΔTKE indicate a gain in TKE, and negative values indicate a decrease. Down in the canopy, the ΔTKE suffered a progressive decrease in the transition zone, one cm below the top of the canopy (hereafter h_s-1), and well inside the canopy (hereafter h_s/2, half the height of the stems). It was only positive for the lowest SPF (5%) and the largest stem diameter (d = 10 mm) (Table 2.3). The smallest ΔTKE was found in the constructed canopy with the smallest stem diameter (d = 4 mm) for all the SPFs and f.

Table 2.3. The TKE difference (%) for rigid canopies at four SPFs (5, 10, 15 and 25%), three stem diameters (10, 6 and 4 mm), and for semi-rigid canopies at three SPFs (5, 8 and 10%) at two frequencies (1.6 and 2.8 Hz) at three different heights (h_s+1, h_s-1 and h_s/2).

	SPF (%)	d (mm)	1.6 Hz			2.8 Hz		
			h_s+1	h_s-1	h_s/2	h_s+1	h_s-1	h_s/2
RIGID CANOPY	5	4	19.6	27.9	-12.8	6.9	18.9	3.8
		6	20.0	35.2	-3.4	10.1	43.5	-1.9
		10	22.4	53.4	18.5	9.9	38.2	16.7
	10	4	16.5	20.0	-18.8	4.6	10.7	-31.9
		6	18.6	23.2	-1.06	12.8	28.6	-26.8
		10	24.6	41.6	-4.4	14.9	51.1	-7.6
	15	4	26.1	8.9	-26.0	6.9	0.4	-33.7
		6	40.6	21.5	-25.4	23.9	21.5	-39.5
		10	46.3	45.8	-6.4	29.5	43.3	-4.9
	25	4	42.0	-3.2	-28.8	12.2	-0.9	-50.7
		6	35.2	0.9	-30.0	29.1	25.6	-50.8
		10	55.9	37.0	-14.0	56.2	37.9	-4.2
SEMI RIGID CANOPY	5	4	25.5	-3.2	-18.2	12.2	-13.9	-34.5
	8		28.2	-5.0	-25.9	17.8	-15.0	-13.9
	10		35.7	-22.9	-34.6	36.5	-13.9	-52.9

Besides the stem diameter, the SPF was also found to play an important role in TKE profiles. Above the constructed canopy (h_s+1), the greater the SPF the greater the ΔTKE (Fig. 2.7a). For SPF = 25% it was found to be between ~2 (d = 4 mm) and ~ 6 (d =10 mm) times larger than the ΔTKE found when the SPF was 5%. In the transition zone, 1 cm below the top of the constructed canopy (h_s-1), the ΔTKE showed a slight decrease with an increase in the SPF, especially for the smallest diameters (Fig 2.7b). Inside the constructed canopy (h_s/2) the reduction in the TKE was greater and increased with the SPF (Fig 2.7c); this relationship was found with the stems with smallest diameters. The differences in ΔTKE between h_s+1 and h_s/2 with all diameters were more evident with larger SPFs at all the oscillating grid frequencies (Table 2.3). For instance, the difference in ΔTKE above and well inside the constructed canopy at SPF = 25%, d = 4 mm and f = 2.8 Hz was 62.9%, whereas the difference in ΔTKE between the two zones at SPF = 5%, d = 4 mm and f = 2.8 Hz was only 3.1%.

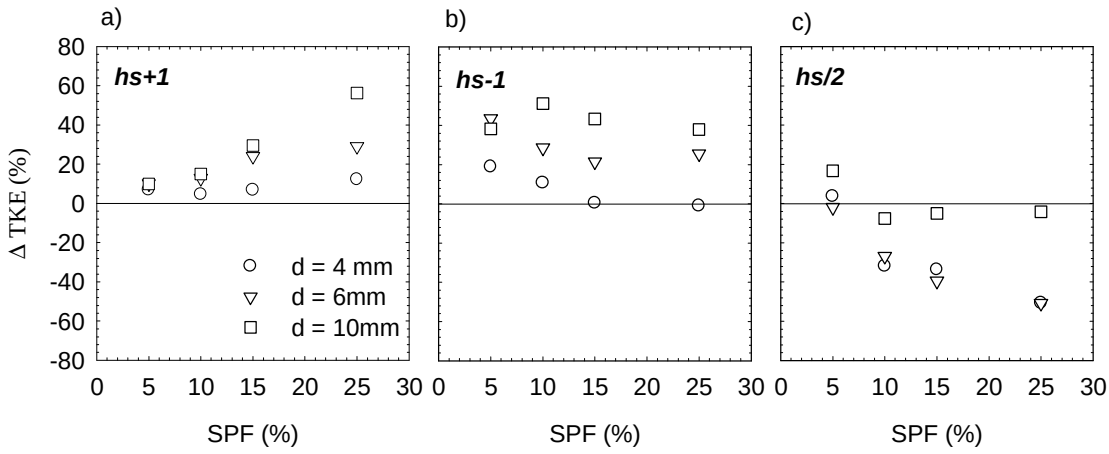

Figure 2.7. TKE differences (ΔTKE) of rigid canopy at 4 (circles), 6 (triangles) and 10 mm (squares) in diameter and f = 2.8 Hz: a) h_s+1; b) h_s-1; c) h_s/2.

2.3.2. Experiments with a semi-rigid canopy model

In contrast to the rigid model, the transition zone practically disappeared when the constructed semi-rigid canopy was used, and only two regions could be found, one above the canopy (h_s+1), and the other well inside it (h_s/2) (Fig. 2.8). Above the semi-rigid canopy (h_s+1), the ΔTKE increased with the SPF at all three frequencies (Figs. 2.9a, b and c). Inside the constructed canopy (h_s/2), the reduction in the ΔTKE was found to increase with the SPF, as was found with the rigid canopy model. For instance, the ΔTKE at h_s+1 for SPF = 10%, d = 4 mm and f = 1.6 Hz was found to be 16.5%, while the ΔTKE under the same conditions for the semi-rigid canopy model was found to be around 35% (Table 2.3). In addition, at h_s/2, the ΔTKE for the rigid canopy (with the same variables as before) was 19% (Table 2.3), lower than the ΔTKE for the semi-rigid canopy model (~34%). The differences between the ΔTKE in both zones (h_s+1 and h_s/2) were more evident as the SPF increased.

2.3.3. Experiments with field SAV

As shown in Figure 10, field SAV behaved similarly to what was found with the semi-rigid constructed canopy. The vertical distribution of TKE also allowed us to describe results found with SAV in two zones: above (h_s+1) and inside the SAV (h_s/2). *C. mariscus* and *R. maritima* both had a TKE vertical profile close to that of the semi-rigid model. They had similar morphologies, long, narrow, upward leaves with a heterogeneous vertical distribution, with the major biomass in the upper part. Near the bottom both had less dense canopies. *M. verticillatum* and *P. nodosus* were the plants that reduced the TKE inside the canopy to the greatest extent. For instance, at h_s-1 the reduction in the ΔTKE was more than 50% of its total.

A drastic change in TKE between the two zones caused the disappearance of the transition zone. This phenomenon is shown in Figure 11. Inside the canopy ($h_s/2$) the reduction in ΔTKE was greatest for *P. nodosus* and *R. maritima*, especially at higher frequencies.

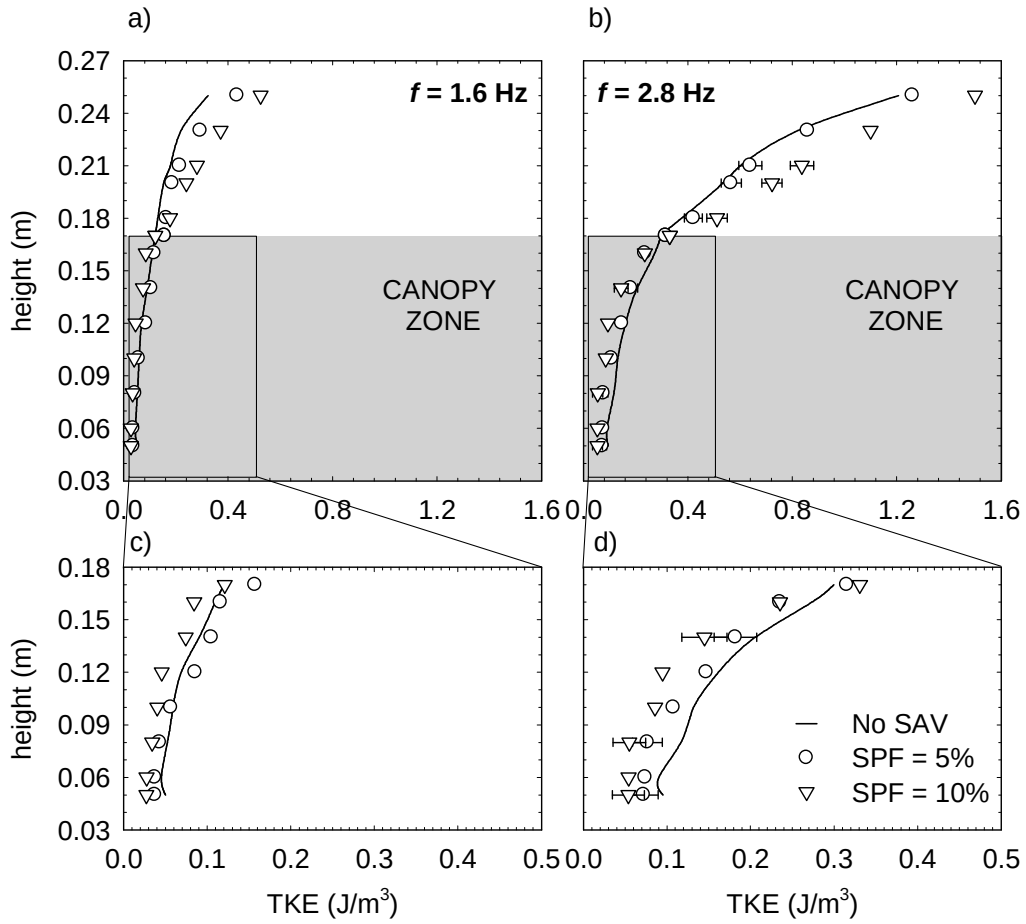

Figure 2.8. TKE profiles of semi-rigid canopy at 5 (circles) and 10% (triangles) of SPF and with no SAV (solid line): a) f = 1.6 Hz; b) f = 2.8 Hz. Enlargement of the canopy zone: c) f = 1.6 Hz; d) f = 2.8 Hz. The horizontal error bars represent the uncertainty of experimental runs.

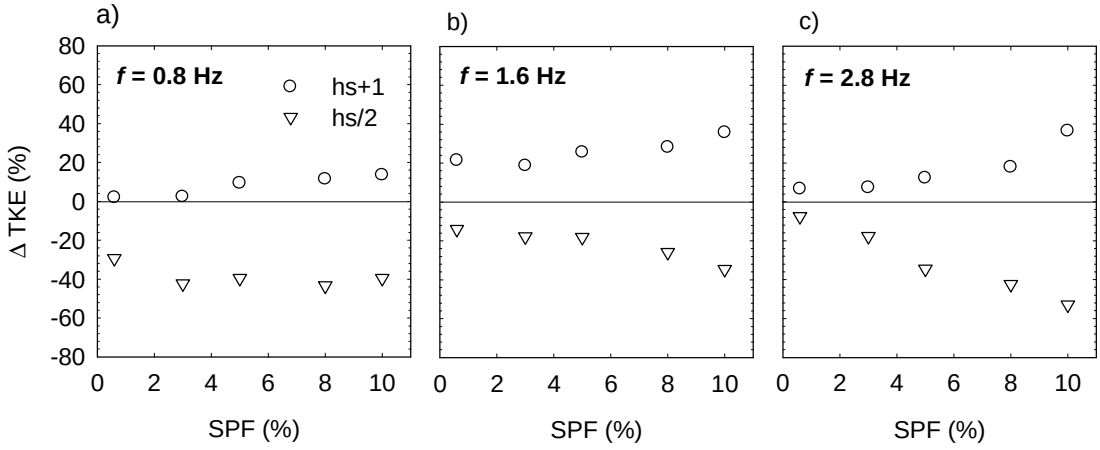

Figure 2.9.TKE differences (ΔTKE) of semi-rigid canopy at h_s+1 (circles) and $h_s/2$ (triangles): a) f = 0.8 Hz; b) f = 1.6 Hz; c) f = 2.8 Hz.

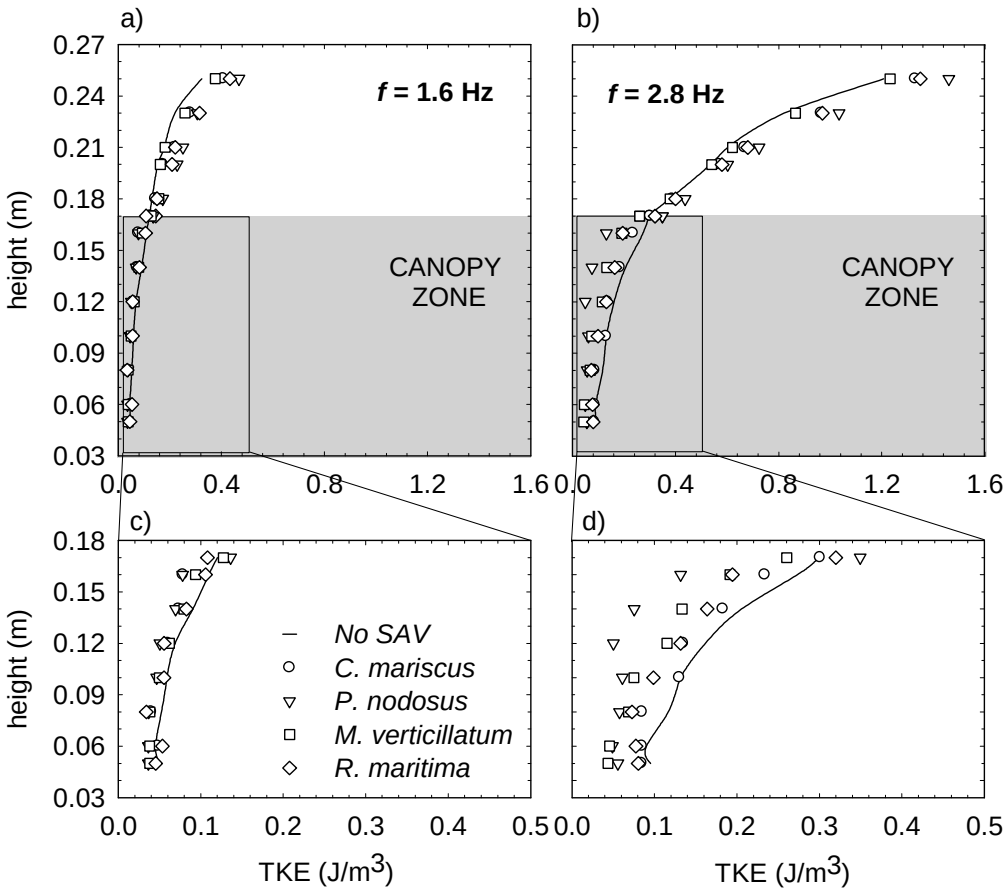

Figure 2.10. TKE profiles of *Cladium mariscus* (circles), *Potamogeton nodosus* (triangles), *Myriophyllum verticillatum* (squares) and *Ruppia maritima* (diamonds) with no SAV (solid line): a) f = 1.6 Hz; b) f = 2.8 Hz. Enlargement of the canopy zone: c) f = 1.6 Hz; d) f = 2.8 Hz.

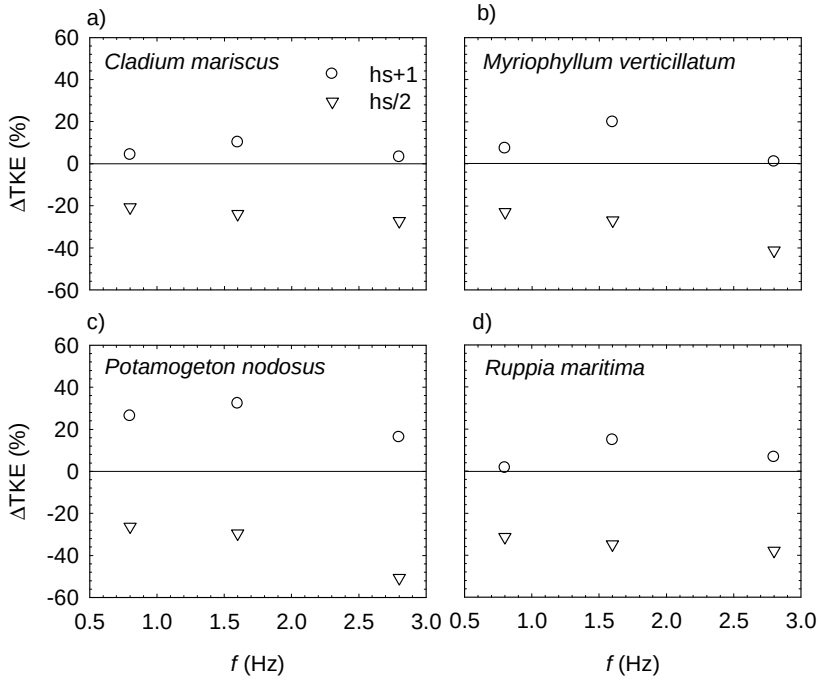

Figure 2.11. TKE differences (ΔTKE) in real plants at h_s+1(circles) and h_s/2 (triangles): a) *Cladium mariscus*; b) *Myriophyllum verticillatum*; c) *Potamogeton nodosus*; d) *Ruppia maritima*.

2.4. Discussion

2.4.1. Turbulence in submerged rigid constructed canopies

With the rigid constructed canopies, the vertical behaviour of the TKE profile allowed us to divide the flow into three zones: one above the canopy, another completely within the canopy and a transitional zone situated inside the top of the canopy. The zones were different in terms of their hydrodynamic behaviour. In our 36 experiments, the largest TKE values were found above the constructed canopies. This result, and the fact that the TKE increased with the SPF, can be explained in terms of the TKE being redistributed at a lower volume due to the presence of the constructed canopy, relative to the 'free-canopy' experiment. Most of the energy was concentrated above the canopy, and therefore the vegetation acted as a 'false rough floor' for the flow.

The results of this study suggest that within the canopy, interaction between water flow and the constructed canopies reduces the TKE measured relative to 'unvegetated' experiments. This reduction appears to be related to SPF, as others have been previously found with advection through vegetation (Nepf, 1999; Leonard and Croft, 2006). In our experiments, the depth of this zone depends on stem diameter and SPF. A reduction in the first and an increment in the second reduced the plant-to-plant distance, resulting in a reduction in the depth of the transition zone. On the other hand, well inside the constructed canopies, at $h_s/2$, the SPF was not the only variable that reduced the flow; the stem diameter also played an important role in dissipating turbulence. More precisely, the reduction in turbulence, or sheltering produced by the canopy, was enhanced as the stem diameter decreased and the SPF of the canopies increased. In other words, the enhancement of the sheltering can be explained by the reduction in the stem diameter and the increment in the SPF, that both caused a reduction in the plant-to-plant distance. Nepf (1999) defined sheltering or dampening as a reduction in the in-emergent canopy macroscale diffusion due to a combination of reduced velocity and reduced eddy-scale relative to unvegetated zones. Other authors have described sheltering in the same terms as Leonard and Croft (2006) and Neumeier and Amos (2006). For example, Neumeier and Amos (2006) found a reduction in turbulence near the bed in three different vegetation types. They pointed out that this effect should enhance sediment deposition and protect the bed against subsequent erosion.

Oscillating grid frequency was the agent generating the turbulence in the system. In this system the number of eddies increases as the oscillating grid frequency increases. All through the tank, at all levels and under all experimental conditions, there was a positive relationship between oscillating frequency and TKE. The behaviour of the sheltering inside the constructed canopy for the largest SPF produced the greatest ΔTKE at any diameter and frequency, because turbulence was highly dissipated inside the dense canopy. On the other hand, the reduction in energy at low frequencies suggests that the vegetation inhibits the production of larger turbulent

eddies, and it is likely that it also contributes to the breakdown of larger eddies into smaller ones (Christiansen et al., 2000). At the same time, with an increase in the grid oscillating frequency, the constructed canopy can not absorb so much energy and there is a displacement in the transmission of the energy downwards inside the canopy from the upper zone. As a result, and as shown in Table 2.3, the ΔTKE (%) at h_s-1 is positive for d = 10 mm, SPF = 25% and f = 1.6 Hz and around zero for the smallest diameters.

2.4.2. Turbulence in submerged semi-rigid constructed canopies

Experiments carried out with the semi-rigid model canopies showed that the transitional hydrodynamic regime disappeared, resulting in a steep gradient of TKE above and below the plants. This process was attributed to the morphology of the semi-rigid stems, where the thick stem at the base of the plant gradually divided at the top and its branches merged with the branches of its neighbours, resulting in an increase in the SPF at the top of the canopy. While the SPF obtained at the bottom of the rigid model was the same as that calculated at the top (Serra et al., 2004), the SPF calculated at the bottom of the semi-rigid SAV was completely different to the vegetation cover at the top. This shows that the role of the vegetation as a 'false rough floor' was enhanced in the semi-rigid model. More precisely, an extreme canopy condition of lateral obstruction = 99% (see column 2 in Table 2.2) dissipated the turbulence and increased the sheltering within the canopy. Within the canopy, sheltering was also greater as the SPF increased, even at the higher oscillating grid frequencies, which is evidence of the role of vegetation controlling high energy events in the field.

2.4.3. Turbulence in submerged aquatic vegetation

Nepf and Vivoni (2000) showed that the bending of the canopy effectively increased the local frontal area, thereby increasing the SPF at the top of the canopy. The depth of the zone affected by the sheltering was set by the depth of submergence and by canopy morphology, density and flexibility (Nepf and Vivoni, 2000). Shi and Hughes (2002) have studied the differences in plant flexibility as a stem property affecting the hydrodynamic flow. Other authors, such as Leonard and Luther (1995), Yang (1998) and Leonard and Croft (2006), have focused on the morphology of the plants and shown that the presence of elements oblique to the flow, such as leaves, inhibits the vertical transport of turbulence in the canopy.

Using SAV, the transitional zone disappeared due to the layout of the leaves, which isolated the two zones. The movement of the real plants contributed to enhancing the sheltering and resulted in the removal of the transitional zone by means of the undulating movements (Ackerman and Okubo, 1993). As the frequency increased, the sheltering intensified due to the

fact that there was greater movement of the plants at the top, which incremented the attenuation of the turbulence inside the canopy. This phenomenon did not appear in either the rigid or semi-rigid canopy models as in both of these the stems did not move at all.

C. mariscus and *R. maritima* had similar TKE profiles relative to the semi-rigid constructed canopies because their design was thought to mimic this kind of natural canopy as a just step. The difference between these natural plants (Fig. 2.10d) is found in their flexibility. The leaves of *R. maritima* were not as stiff or as wide, so the plant bent more easily, thereby enhancing the attenuation of the TKE inside the canopy. *M. verticillatum* and *P. nodosus* were the plants that reduced the TKE inside the canopy most (Figure 2.11) since they have a more complex structure. The latticework structure of the leaves of *M. verticillatum* around the stem enhanced the sheltering below. This plant had a lot of compound and divided leaves, which resulted in a featherlike structure. *P. nodosus* leaves were the widest and were positioned perpendicular to the stem. The morphology of the leaves enhanced the effect of the plants acting as a 'false rough floor', and increased the TKE gradient between the two zones.

2.5. Conclusions

The vertical TKE profiles in a system with a submerged rigid canopy subjected to turbulence generated by an oscillating grid were divided into three zones: one above the canopy and two inside the canopy. Above the canopy, the TKE found for all SPFs was greater than in those zones without any vegetation. This phenomenon was attributed to the redistribution of TKE at a lower volume, enhanced mainly by the largest SPFs.

The inner zone nearer the top of the canopy is called the transition zone. Although it was situated inside the plants, the TKE was still greater than that found without any plants. The third zone is situated below the transition zone and is defined as the region where the TKE was lower than TKE found in 'unvegetated' experiments. This phenomenon was called sheltering or dampening, and along with the depth of the transition zone was enhanced with a decrease in the stem diameter and an increase in the SPF of the canopies that caused a reduction in the plant-to-plant distance. We have, therefore, not only observed a sheltering, but quantified it. The development of the sheltering was reduced as frequency increased, due to the fact that vegetation could not prevent the penetration of the turbulence.

The semi-rigid model canopies prevented the development of a transitional zone, and a steep gradient of TKE above and inside the canopy was found. This process can be attributed to the morphology of the semi-rigid canopy, which produced a major increase in the SPF at the top of the canopy, since the distribution of the vertical biomass was not uniform. The experiments with SAV revealed that the transitional zone disappeared due to the layout of the leaves, which isolated the two zones. The movement of the real plants contributed to enhancing the sheltering

and reducing the transitional zone. As the frequency increased, the sheltering intensified because there was greater movement of the plants at the top, thus incrementing the attenuation of the turbulence inside the canopy.

Acknowledgements This research was funded by the *Ministerio de Ciencia e Innovación* of the Spanish Government through grant CGL 2007-62483/HID to the University of Girona. Dolors Pujol was supported by research fellowship BR08/11 of the University of Girona. The cost of the article publication was subsidized by a grant of the University of Girona. We would like to acknowledge the contributions of Xicu Gómez and Teresa Martí of the Department of Physics at the University of Girona and Amélie Dasre from the *Institut Universitaire et Technologique du Creusot* (France).

References

Ackerman, J.D., Okubo, A., 1993. Reduced mixing in a marine macrophyte canopy. Funct. Ecol. 7, 305-309.

Begon M., Harper, J.L. and Townsend, C.R., 1986. Ecology: Individuals, Populations and Communities, 1st ed. Blackwell Science, Oxford.

Bouma, T.J., van Duren, L.A., Temmerman, S., Claverie, T., Blanco-Garcia, A., Ysebaert, T., Herman, P.M.J., 2007. Spatial flow and sedimentation patterns within patches of epibenthic structures: Combining field, flume and modelling experiments. Cont. Shelf Res. 27, 1020-1045.

Brooks, R.,1989. An overview of ecological functions and economic values of wetlands, in: Majumdar, S., Brooks, R., Brenner, F., Tiner, R. (Eds.), Wetlands Ecology and Conservation: Emphasis in Pennsylvania.The Pennsylvania Academy of Science, New Jersey, pp. 11–20.

Brumley, B.H., Jirka, G.H., 1987. Near-surface turbulence in a grid-stirred tank. J. Fluid Mech. 183, 235-263.

Christiansen, T., Wiberg, P.L., Milligan, T.G., 2000. Flow and sediment transport on a tidal salt marsh surface. Estuar. Coast. Shelf Sci. 50, 315-331.

Connolly, J.P., Armstrong, N.E., Miksad, R.W., 1983. Adsorption of hydrophobic pollutants in estuaries. J. Environ. Eng-Asce. 109, 17-35.

Desilva, I.P.D., Fernando, H.J.S., 1994. Oscillating grids as a source of nearly isotropic turbulence. Phys. Fluids 6, 2455-2464.

Gambi, M.C., Nowell, A.R.M., Jumars, P.A., 1990. Flume observations on flow dynamics in *Zostera marina* (eelgrass) beds. Mar. Ecol. Prog. Ser. 61, 159-169

Ghisalberti, M., Nepf, H., 2006. The structure of the shear layer in flows over rigid and flexible canopies. Environ. Fluid Mech. 6, 277-301.

Gorham, E., 1991. Northern peatlands: role in the carbon cycle and probable responses to climatic warming. Ecol. Appl. 1, 182-195.

Holzner, M., Liberzon, A., Guala, M., Tsinober, A., Kinzelbach, W., 2006. Generalized detection of a turbulent front generated by an oscillating grid. Exp. Fluids 41, 711-719.

Hopfinger, E.J., Toly, J.A., 1976. Spatially decaying turbulence and its relation to mixing across density interfaces. J. Fluid Mech. 78, 155-175.

Jarvela, J., 2002. Flow resistance of flexible and stiff vegetation: a flume study with natural plants. J. Hydrol. 269, 44-54.

Kline, S.J., McClintock, F.A., 1953. Describing the uncertainties in single-sample experiments. Mech. Eng. 75, 3-8.

Koch, E.W., Gust, G., 1999. Water flow in tide- and wave-dominated beds of the seagrass *Thalassia testudinum*. Mar. Ecol. Prog. Ser. 184, 63-72.

Leonard, L.A., Croft, A.L., 2006. The effect of standing biomass on flow velocity and turbulence in *Spartina alterniflora* canopies. Estuar. Coast. Shelf Sci. 69, 325-336.

Leonard, L.A., Luther, M.E., 1995. Flow hydrodynamics in tidal marsh canopies. Limnol. Oceanogr. 40, 1474-1484.

Leonard, L.A., Reed, D.J., 2002. Hydrodynamics and sediment transport through tidal marsh canopies. J. Coast. Res. 36, 459-469.

Machate, T., Noll, H., Behrens, H., Kettrup, A., 1997. Degradation of phenanthrene and hydraulic characteristics in a constructed wetland. Water Res. 31, 554-560.

Matsunaga, N., Sugihara, Y., Komatsu, T., Masuda, A., 1999. Quantitative properties of oscillating-grid turbulence in a homogeneous fluid. Fluid Dyn. Res. 25, 147-165.

Mazzella, L., Alberte, R.S., 1986. Light adaptation and the role of autotrophic epiphytes in primary production of the temperate seagrass, *Zostera marina* L. J. Exp. Mar. Biol. Ecol. 100, 165-180.

Morris, E.P., Peralta, G., Brun, F.G., van Duren, L., Bouma, T.J., Perez-Llorens, J.L., 2008. Interaction between hydrodynamics and seagrass canopy structure: spatially explicit effects on ammonium uptake rates. Limnol. Oceanogr. 53, 1531-1539.

Nepf, H.M., 1999. Drag, turbulence, and diffusion in flow through emergent vegetation. Water Resour. Res. 35, 479-489.

Nepf, H.M., Vivoni, E.R., 2000. Flow structure in depth-limited, vegetated flow. J. Geophys. Res. 105, 28547-28557.

Neumeier, U., 2007. Velocity and turbulence variations at the edge of saltmarshes. Cont. Shelf Res. 27, 1046-1059.

Neumeier, U., 2005. Quantification of vertical density variations of salt-marsh vegetation. Estuar. Coast. Shelf Sci. 63, 489-496.

Neumeier, U., Amos, C.L., 2006. The influence of vegetation on turbulence and flow velocities in European salt-marshes. Sedimentology 53, 259-277.

Neumeier, U., Ciavola, P. 2004. Flow resistance and associated sedimentary processes in a *Spartina maritima* salt-marsh. J. Coast. Res. 20, 435-447.

Nokes, R.I., 1988. On the entrainment rate across a density interface. J. Fluid Mech. 188, 185-204.

Orlins, J.J., Gulliver, J.S., 2003. Turbulence quantification and sediment resuspension in an oscillating grid chamber. Exp. Fluids 34, 662-677.

Peralta, G., van Duren, L.A., Morris, E.P., Bouma, T.J., 2008. Consequences of shoot density and stiffness for ecosystem engineering by benthic macrophytes in flow dominated areas: a hydrodynamic flume study. Mar. Ecol. Prog. Ser. 368, 103-115.

Poggi, D., Katul, G.G., Albertson, J.D., 2004. Momentum transfer and turbulent kinetic energy budgets within a dense model canopy. Bound.-Layer Meteorol. 111, 589-614.

Prigent, C., Matthews, E., Aires, F., Rossow, W.B., 2001. Remote sensing of global wetland dynamics with multiple satellite data sets. Geophys. Res. Lett. 28, 4631-4634.

Raupach, M.R., Thom, A.S., 1981. Turbulence in and above plant canopies. Annu. Rev. Fluid Mech. 13, 97-129.

Sand-Jensen, K., Pedersen, O., 1999. Velocity gradients and turbulence around macrophyte stands in streams. Freshwater Biol. 42, 315-328.

Serra, T., Colomer, J., Logan, B.E., 2008. Efficiency of different shear devices on flocculation. Water Res. 42, 1113-1121.

Serra, T., Fernando, H.J.S., Rodriguez, R.V., 2004. Effects of emergent vegetation on lateral diffusion in wetlands. Water Res. 38, 139-147.

Shi, Z., Hughes, J.M.R., 2002. Laboratory flume studies of microflow environments of aquatic plants. Hydrol. Processes 16, 3279-3289.

Shi, Z., Pethick, J.S., Pye, K., 1995. Flow structure in and above the various heights of a saltmarsh canopy: a laboratory flume study. J. Coast. Res. 11, 1204-1209.

Willems, H.P.L., Rotelli, M.D., Berry, D.F., Smith, E.P., Reneau, R.B., Mostaghimi, S., 1997. Nitrate removal in riparian wetland soils: effects of flow rate, temperature, nitrate concentration and soil depth. Water Res. 31, 841-849.

Yang, S.L., 1998. The role of Scirpus marsh in attenuation of hydrodynamics and retention of fine sediment in the Yangtze estuary. Estuar. Coast. Shelf Sci. 47, 227-233.

Chapter 3

A model for the effect of submerged aquatic vegetation on turbulence induced by an oscillating grid

Pujol, D.[1], Colomer, J.[1], Serra, T.[1], Casamitjana, X.[1]

[1]Department of Physics, Escola Politècnica Superior-II, Campus Montilivi, 17071 Girona, Catalonia, Spain

Published in: *Estuarine Coastal and Shelf Science, 114, 23-30*

http://www.sciencedirect.com/science/article/pii/S0272771411003660

Abstract The aim of this study is to model, under controlled laboratory conditions, the effect of submerged aquatic vegetation (SAV) on turbulence generated in a water column by an oscillating grid turbulence (OGT). Velocity profiles have been measured by an acoustic Doppler velocimeter (MicroADV). Experimental conditions are analysed in two canopy models (rigid and semi-rigid), using nine plant-to-plant distances (ppd), three stem diameters (d), four types of natural SAV (*Cladium mariscus*, *Potamogeton nodosus*, *Myriophyllum verticillatum* and *Ruppia maritima*) and two oscillation grid frequencies (f). To quantify this response, we have developed a non-dimensional model, with a specific turbulent kinetic energy (TKE), f, stroke (s), d, ppd, distance from the virtual origin to the measurement (z_m) and space between grid bars (M). The experimental data show that, at $z_m/z_c < 1$ the turbulent kinetic energy decays with z_m, according to the well-known power law, z_m^{-2}, and does no depend on the vegetation characteristics. In contrast, at $z_m/z_c > 1$, TKE decreases faster with z_m and scales to the model variables according to $TKE_0/(f^2 \cdot s^2) = (d/ppd)^{-0.25} \cdot (z_m/M)^{-3}$. Therefore, at $z_m/z_c > 1$ the TKE is affected by the geometric characteristics of the plants (both diameter and plant-to-plant distance), an effect called sheltering. Results from semi-rigid canopies and natural SAV are found to scale with the non-dimensional model proposed for rigid canopies. We also discuss the practical implications for field conditions (wind and natural SAV).

Keywords Oscillating grid turbulence, submerged aquatic vegetation, non-dimensional model, turbulent kinetic energy, power law, sheltering.

3.1. Introduction

Wetlands are shallow water ecosystems situated between land and water bodies. These transitional zones are governed by physical forces originating from tidal currents, waves and wind and by biophysical interactions between those forces and the organisms that inhabit the wetlands (Bouma et al., 2007). Although the impact of aquatic vegetation on the control of mass transport has been widely studied (Christiansen et al., 2000; Granata et al., 2001; Manning and Dyer, 1999), it is still unclear how the different characteristics of aquatic vegetation influence the behaviour of the turbulent kinetic energy (TKE) under different flow regimes. We know that the presence of submerged aquatic vegetation (SAV) in salt marshes and the associated development of sheltering promote sedimentation as a result of longer particle residence times, and also decrease the resuspension of sediment from the bottom, thereby preventing its erosion. These geophysical processes, which determine the budget of particle transport, have biological consequences such as an increase in food availability and the provision of shelter to animals. In addition, aquatic plants also have physical consequences, such as flood storage and desynchronisation during rain and drought periods and acts as a bioshield during short periods of waves (Feagin et al., 2009). However, due in part to their limited capacity for adaptation, wetlands are considered to be among the ecosystems most vulnerable to climate change (Bates et al., 2008).

In natural systems, where pure turbulence and zero mean flow are rare, flows are a combination of steady, oscillatory and turbulent flows. In an effort to understand the real world we attempt to isolate each physical process. So this study is a first step toward understanding the effects of turbulence induced by wind on submerged aquatic plants. To generate nearly homogeneous and isotropic turbulence that mimics the effect of the wind on a water column, we used oscillating grid turbulence device (OGT). Many other experiments have used wind or water tunnels to obtain isotropic turbulence. In these cases, however, the generated turbulence decayed rapidly and was subjected to significant time-mean motion (DeSilva and Fernando, 1994). The device we used produces nearly homogenous and isotropic turbulence 2-3 mesh sizes away from the grid (DeSilva and Fernando, 1994). Furthermore, OGT produces no net flow direction, and thus no mean shear. Although there is shear produced by the oscillating grid, the temporal mean shear is zero, and since there is no mean shear in the OGT devices, the system can be used to study turbulence behaviour under differing operating conditions and to verify predictive models for use in real-world applications (Orlins and Gulliver, 2003). OGT has been used extensively to study different natural processes such as the mixing across density interfaces in stratified flows, like thermoclines or haloclines (Hopfinger and Toly, 1976; Nokes, 1988; Granata et al., 2001), the desorption of contaminants from sediment (Connolly et al., 1983), mass transfer across a shear-free water-air interface (Brumley and Jirka, 1987), the study of the resuspension and transport of sediment (Huppert et al., 1995; Orlins and Gulliver, 2003), the study of a turbulent-dissipation model to perform a more accurate quantification of

the experimental data (Matsunaga et al., 1999) and the aggregation dynamics in natural and engineered systems (Serra et al., 2008).

Ecotones in coastal lagoon landscapes feature different aquatic environments where SAV proliferate. For our study, we have chosen four characteristic plant species that occur along the freshwater – brackish water – coastal lagoon ecotone comprising Cladium mariscus, Myriophyllum verticillatum, Potamogeton nodosus and Ruppia maritima. Particle resuspension is higher in unvegetated areas than in vegetated zones, especially during energetic flow and wave events (Green et al., 1997; Lynch et al., 1997; Boon et al., 1996; Granata et al., 2001). Furthermore, because drag increases with biomass, the pattern flow is modified by both the canopy density (Peterson et al., 2004; Eckman 1987; Gambi et al., 1990; Leonard and Luther, 1995; Nepf, 1999) and the plant architecture (plant height, shape and distribution of leaves), altering the redistribution of particles inside the meadow (Granata et al., 2001; Leonard and Croft, 2006). Therefore, SAV controls the particle transport. As a result of flow modification total suspended solids decreases within the plant stand due to decreased advection, particle settling, reduced resuspension, and collisions with plant stems (Gruber, 2009). This is a well-known phenomenon called sheltering (Nepf, 1999; Leonard and Croft, 2006; Neumeier and Amos, 2006; Pujol et al., 2010). However, as pointed by Kosten et al. (2009), no relationship has been found between the plant density and the water clearing effect. Our objective is to examine the effect of different model canopies on turbulence to better understand the effect of the SAV on turbulence and to infer non-dimensional models that describe this interaction.

3.2. Materials and Methods

Laboratory measurements were conducted in an oscillating grid chamber consisting of a Plexiglas box with interior dimensions of 28 x 28 x 49 cm (Fig. 3.1). The tank was filled with a homogeneous fluid (water). This device generates turbulence from vertical oscillations produced by a horizontal square grid. In our design, the grid was situated at the top of the water column, 0.365 m from the tank bottom, and was controlled by a variable-speed motor located outside the tank. The grid consisted of 5 x 5 bars with a square section. The mesh size of the grid was 4.5 cm, and the width of the squares between bars was 1 cm, corresponding to a solidity of 31% (defined as the fractional solid area occupied by bars). A clearance of 5 mm was maintained between the sidewalls and the grid. In addition, the mesh endings were designed to reduce mean secondary circulation, as suggested by Fernando and DeSilva (1993), who proved that the distance between the wall and the closest bar parallel to the wall had to be M/2. The stroke of the grid oscillation was fixed at 5 cm. For each experiment, the grid was set to oscillate at frequencies of 1.6 and 2.8 Hz.

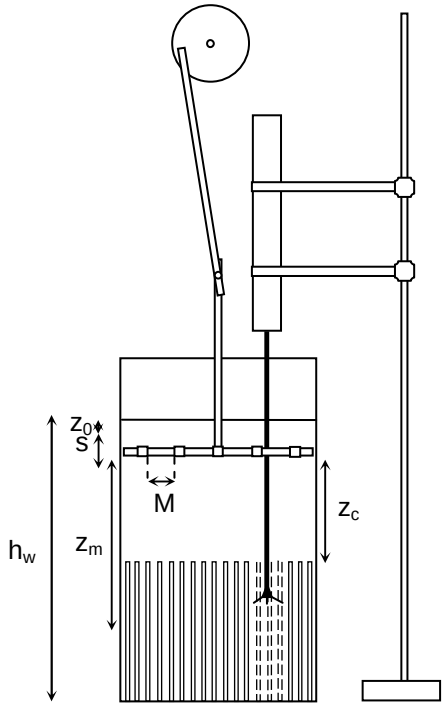

Figure 3.1. Schematic view of the laboratory experiment: the structure of the device used in this study, where h_w is the height of the water column (0.41m); z_c, the distance from the grid to the top of the canopy (0.16m); s, the stroke of the grid situated at the top (0.05m); z_0, the distance between the water surface and the highest position of the mesh (0.02m); z_m, distance from the virtual origin to the measurement (0.1, 0.12, 0.13, 0.15, 0.16, 0.21, 0.23, 0.25, 0.27, 0.28 m); f, the grid frequency (1.6, 2.8 Hz); and M, the width between bars (0.045 m).

The measurements were taken after the grid was oscillated for 10 min, in order to ensure that the measurements only included fully developed turbulence in a statistically steady state. We used an acoustic Doppler velocimeter (the Sontek/YSI 16-MHz MicroADV), which is commonly used to quantify turbulence characteristics, including the energy dissipation level (Colomer and Fernando, 1999). This high resolution instrument, with an acoustic frequency of 16 MHz, is ideal for use in laboratory turbulence studies. More details and the measurement technique used in this experiment are given in Pujol et al. (2010). The experimental measurements were taken at points along the vertical axis with the top measurement being two mesh sizes away from the grid, the minimum distance at which well-developed turbulence may be expected (Thompson and Turner, 1975; Atkinson et al., 1987). Therefore, the experimental measurements were carried out from 0.135 m to 0.315 m from the virtual origin proposed by Hopfinger and Toly (1976) where z_m = (1/2s+1 cm) ±0.5 cm. As mentioned by these authors, this origin is crucial to determining the exponent in the decay power law for turbulent kinetic energy with depth.

To simulate as close as possible the effect of natural SAV on field turbulence within a water column, we used different geometric characteristics of plants. Experimental conditions were analysed in a rigid canopy model (Fig. 3.3a), with nine different plant-to-plant distances and

three stem diameters. Some of the distributions for different ppd and d are shown in Figure 3.2. Furthermore, we studied a semi-rigid canopy model (Fig. 3.3b) with five different plant-to-plant distances, one stem diameter and four types of natural SAV (*Cladium mariscus*, *Potamogeton nodosus*, *Myriophyllum verticillatum* and *Ruppia maritima*) to validate the analytical model. Table 1 and table 2 shows the experimental conditions tested.

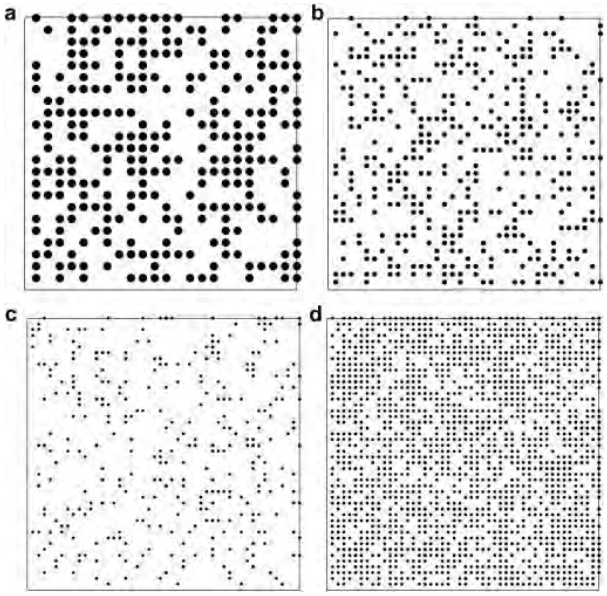

Figure 3.2. Different distributions for some feature: a) d = 10 mm, ppd = 8 mm; b) d = 6 mm, ppd = 8.7 mm; c) d = 4 mm, ppd = 12.5 mm; and d) d = 4 mm, ppd = 3.1 mm.

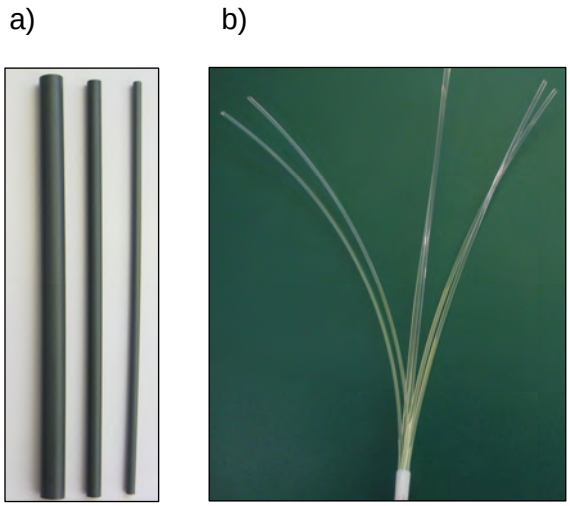

Figure 3.3. Photographs of the vegetation canopy model studied: a) rigid canopy (d = 10, 6 and 4 mm); b) semi-rigid canopy (d = 4 mm, at the base).

Table 3.1. Summary of the 28 different set-ups studied with different plant–to-plant distances, diameters, canopy models (R = rigid canopy model and SR = semi-rigid canopy model) and Reynolds number of the grid (Re_G). For each set-up the oscillation frequencies were 1.6 and 2.8 Hz. The height of the plants was 17 cm.

Run no.	Canopy model	f (Hz)	d (cm)	ppd (cm)	Re_G
1	R	1.6	0.4	1.25	95
2	R	1.6	0.4	0.57	95
3	R	1.6	0.4	0.31	95
4	R	1.6	0.6	1.99	95
5	R	1.6	0.6	0.87	95
6	R	1.6	0.6	0.48	95
7	R	1.6	1	3.21	95
8	R	1.6	1	1.47	95
9	R	1.6	1	0.80	95
10	R	2.8	0.4	1.25	166
11	R	2.8	0.4	0.57	166
12	R	2.8	0.4	0.31	166
13	R	2.8	0.6	1.99	166
14	R	2.8	0.6	0.87	166
15	R	2.8	0.6	0.48	166
16	R	2.8	1	3.21	166
17	R	2.8	1	1.47	166
18	R	2.8	1	0.80	166
19	SR	1.6	0.4	0.75	95
20	SR	1.6	0.4	0.88	95
21	SR	1.6	0.4	1.25	95
22	SR	1.6	0.4	1.86	95
23	SR	1.6	0.4	4.78	95
24	SR	2.8	0.4	0.75	166
25	SR	2.8	0.4	0.88	166
26	SR	2.8	0.4	1.25	166
27	SR	2.8	0.4	1.86	166
28	SR	2.8	0.4	4.78	166

Table 3.2. Summary of the natural plants studied with different plant–to-plant distances, diameters, Reynolds number of the grid (Re_G) and morphology. For each set-up the oscillation frequencies were 1.6 and 2.8 Hz. The height of the plants was 17 cm.

Run no.	Canopy model	f (Hz)	d (cm)	ppd (cm)	Re_G	Morphology
1	*C. mariscus*	1.6	0.45	5.06	95	5 – 10 leaves, vertically distributed
2	*C. mariscus*	2.8	0.45	5.06	166	
3	*P. nodosus*	1.6	0.45	5.06	95	10 – 25 leaves, horizontally distributed
4	*P. nodosus*	2.8	0.45	5.06	166	
5	*M. verticillatum*	1.6	0.45	5.06	95	> 100 leaves, horizontally distributed
6	*M. verticillatum*	2.8	0.45	5.06	166	
7	*R. maritima*	1.6	0.45	5.06	95	10 – 25 leaves, vertically distributed
8	*R. maritima*	2.8	0.45	5.06	166	

3.3. Theory / Calculation

The turbulence generated by an OGT with square bars is based on grid parameters, such as the mesh size (M) and stroke (s), and on the oscillating frequency (f) and the depth from the virtual origin (z_m). According to previous researchers (Hopfinger and Toly, 1976; and DeSilva and Fernando, 1994), the variations in the horizontal (u_0, v_0) and vertical (w_0) root-mean-square velocities as well as the length scale of turbulence (ℓ_0) with distance z_m can be expressed as:

$$\sqrt{\overline{u'^2}} = \sqrt{\overline{v'^2}} = u_0 = v_0 = C_1 \cdot s^{3/2} \cdot M^{1/2} \cdot f \cdot z_m^{-1} \qquad (3.1)$$

$$\sqrt{\overline{w'^2}} = w_0 = C_2 \cdot s^{3/2} \cdot M^{1/2} \cdot f \cdot z_m^{-1} \qquad (3.2)$$

$$\ell_0 = C_3 \cdot z_m \qquad (3.3)$$

where $C_1 = 0.22$, $C_2 = 0.26$ and $C_3 = 0.10$ are widely accepted constants that depend on the grid's geometry (DeSilva and Fernando, 1994).

To calculate the TKE profile for stationary velocity records, the instantaneous velocities at each point (u, v, w) were decomposed into the sum of time-averaged velocities (U, V, W) and the turbulent components (u', v', w'), which means that the TKE can be calculated from the following equation:

$$TKE = \frac{1}{2}\rho_w\left(\overline{u'^2} + \overline{v'^2} + \overline{w'^2}\right) \qquad (3.4)$$

where ρ_w is the water density.

To calculate the grid's Reynolds number, Re_G, the equation of DeSilva and Fernando (1994), $Re_G = u_0 \cdot \ell_0 / \nu$, which by using Eqs. (3.1) and (3.3) can be written as follows:

$$Re_G = \frac{C_1 \cdot C_3 \cdot s^{3/2} \cdot M^{1/2} \cdot f}{\nu} \qquad (3.5)$$

where ν is the kinematic viscosity ($0.93 \cdot 10^{-6}$ m^2/s).

Thus, the Re_G does not depend on the distance from the grid but is a function of the f. In this experiment f = 1.6 and 2.8 Hz, which correspond to Reynolds numbers of 95 and 166 respectively, from which we assumed that the flow within the tank was fully turbulent (Serra et al., 2008).

3.4. Results

The results from the non-dimensional model under the different tested conditions are presented in Figures 3.4, 3.5, and 3.6 and cover the 36 experiments that were carried out (Table 3.1 and Table 3.2).

As suggested by Hopfinger and Toly (1976) and DeSilva and Fernando (1994), the decay of turbulence with distance away from the grid follows Eqs. (3.1) and (3.2) that depends on the geometric parameters of the grid, the oscillation frequency and the distance from the grid, which may be rewritten as follows:

$$\frac{u_0}{fs} = C_1\left(\frac{s}{M}\right)^{1/2} \cdot \left(\frac{z_m}{M}\right)^{-1} \tag{3.6}$$

$$\frac{w_0}{fs} = C_2\left(\frac{s}{M}\right)^{1/2} \cdot \left(\frac{z_m}{M}\right)^{-1} \tag{3.7}$$

Due to the fact that the stroke and mesh have not been varied in our experiment, the relation between them is considered to be the same as that found by Hopfinger and Toly (1976) and DeSilva and Fernando (1994). However, in our study we considered the geometry of the plants. Thus, the parameters governing the turbulence evolution in our system are d and ppd (parameters of the rigid canopy model), and z_m, M, s and f (parameters of the set-up geometry). As such, any dependent parameter $\mathscr{P}$ can be expressed as:

$$\mathscr{P} = \mathscr{P}\ (TKE_0, s, z_m, M, f, d, ppd)) \tag{3.8}$$

where $\mathscr{P}$ denotes a function.

In order to obtain a non-dimensional model for TKE we used the Buckingham pi-theorem, which is based on the assumption that physical laws should be independent of the units used to express the variables (Evans, 1972). This theorem defined the non-dimensional model as the relation among the number of dependent variables (n) with the number of physical dimensions (m). According to the definition, we have five dependent variables (M and s could be variables but in our experiment we did not vary them) with two dimensions (length and time), so n-m = 3 will be the number of non-dimensional parameters required for this model ($TKE_0/f^2 \cdot s^2$, d/ppd, z_m/M). Therefore, the non-dimensional form of $\mathscr{P}$ in (8) becomes:

$$\pi = \pi'\left(\frac{TKE_0}{f^2 \cdot s^2}, \frac{d}{ppd}, \frac{z_m}{M}\right) \tag{3.9}$$

Then, the governing variables used to quantify the behaviour of the turbulence at $z_m/z_c < 1$ and at $z_m/z_c > 1$ can be written according to non-dimensional scales as follows:

$$\frac{TKE_0}{f^2 \cdot s^2} \propto \left(\frac{d}{ppd}\right)^{\alpha} \cdot \left(\frac{z_m}{M}\right)^{\beta} \qquad (3.10)$$

where α and β are exponents.

Considering Eq. (3.10), we plotted $TKE_0/(f^2 \cdot s^2)$ versus d/ppd (not shown). From the representation, two behaviours could be distinguished: $z_m/z_c < 1$ and $z_m/z_c > 1$. The region placed at $z_m/z_c < 1$ presented a trend with a slope of 0.03. The second region, located at $z_m/z_c > 1$ (from 0.12 to 0.05 cm from the bottom of the tank), presented a linear trend with a slope of -0.23. In addition, the plot of $TKE_0/(f^2 \cdot s^2)$ vs z_m/M (not shown) presented also two regimes clearly distinguished at $z_m/z_c < 1$ and at $z_m/z_c > 1$. The experimental data show that at $z_m/z_c < 1$ the turbulent kinetic energy decays with a slope near -2. On the other hand, at $z_m/z_c > 1$ a change in the behaviour of the turbulence is appreciated as a change in the exponent of the power law. In this zone the slope between TKE_0 and z_m was found to be -3.

Two flow regimes within submerged aquatic vegetation can be distinguished depending on the vertical position relative to the canopy. Following the results presented in Figure 3.4, the non-dimensional model can be described, depending on the ratio z_m/z_c, as:

$$\frac{TKE_0}{f^2 \cdot s^2} = 0.43 \cdot \left(\frac{d}{ppd}\right)^{0.03} \cdot \left(\frac{z_m}{M}\right)^{-2} \quad \text{for } z_m/z_c < 1 \qquad (3.11)$$

$$\frac{TKE_0}{f^2 \cdot s^2} = 1.55 \cdot \left(\frac{d}{ppd}\right)^{-0.23} \cdot \left(\frac{z_m}{M}\right)^{-3} \quad \text{for } z_m/z_c > 1 \qquad (3.12)$$

where the regression coefficients are r = 0.89 and r = 0.67 respectively.

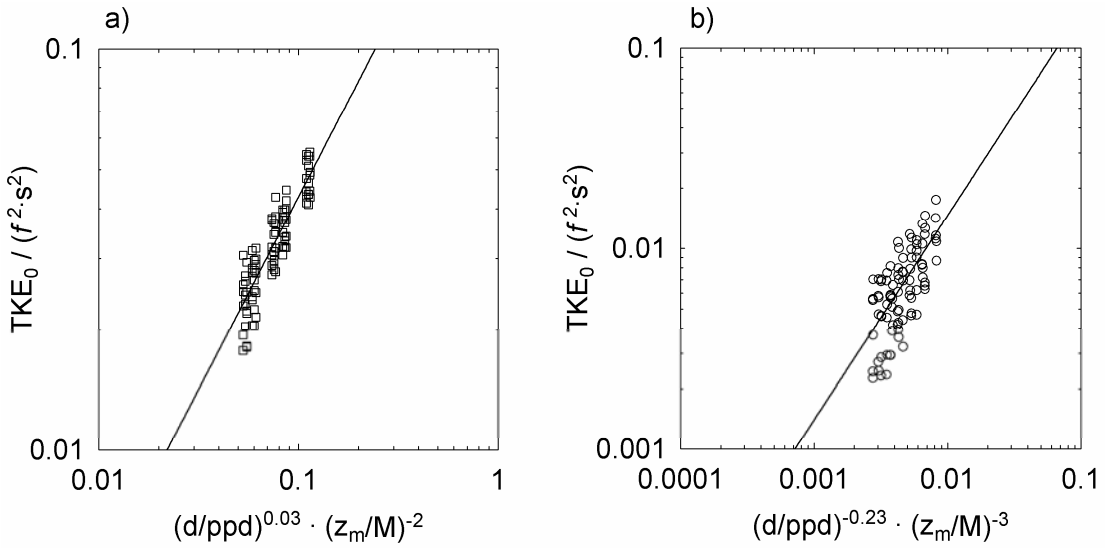

Figure 3.4. Non-dimensional number for rigid canopy model: a) $z_m/z_c < 1$, r = 0.89 (n = 90, 99% of confidence); b) $z_m/z_c > 1$, r = 0.67 (n = 89, 99% of confidence).

Results reveal that the behaviour of the vertical profile of TKE at $z_m/z_c < 1$ depends only on the distance from the virtual origin, due to the fact that the dependence with d/ppd can be considered negligible. However, at $z_m/z_c > 1$, two significant changes could be observed. First, the TKE depends on d/ppd with a dimensionless relation with an exponent of -0.23. And second, the relation between TKE_0 and z_m/M has been intensified, producing an increase in the reduction of the TKE at $z_m/z_c > 1$ with depth as the exponent of z_m/M changed to -3.

The empirical relations found with the semi-rigid canopy are shown in Figure 3.5. At $z_m/z_c < 1$ (Fig. 3.5a), both the semi-rigid and natural plant experiments reveal a slope close to -2 for the decay with z_m/M, like that found for the rigid canopy model. At $z_m/z_c > 1$ (Fig. 3.5b), the semi-rigid canopy model fitted fairly well to the non-dimensional model defined in Eq. (3.12). For natural plants, as shown in Figure 3.6, the relationship between the non-dimensional functions follows those found in the previous models, both for $z_m/z_c < 1$ (Fig. 3.6 a) and $z_m/z_c > 1$ (Fig. 3.6b). For $z_m/z_c > 1$ the constant derived from Eq. (3.10) is found to be lower than that found in Eq. (3.12) for the rigid canopy model, indicating that the complex morphology of plants can cause a decrease of the TKE inside the canopy.

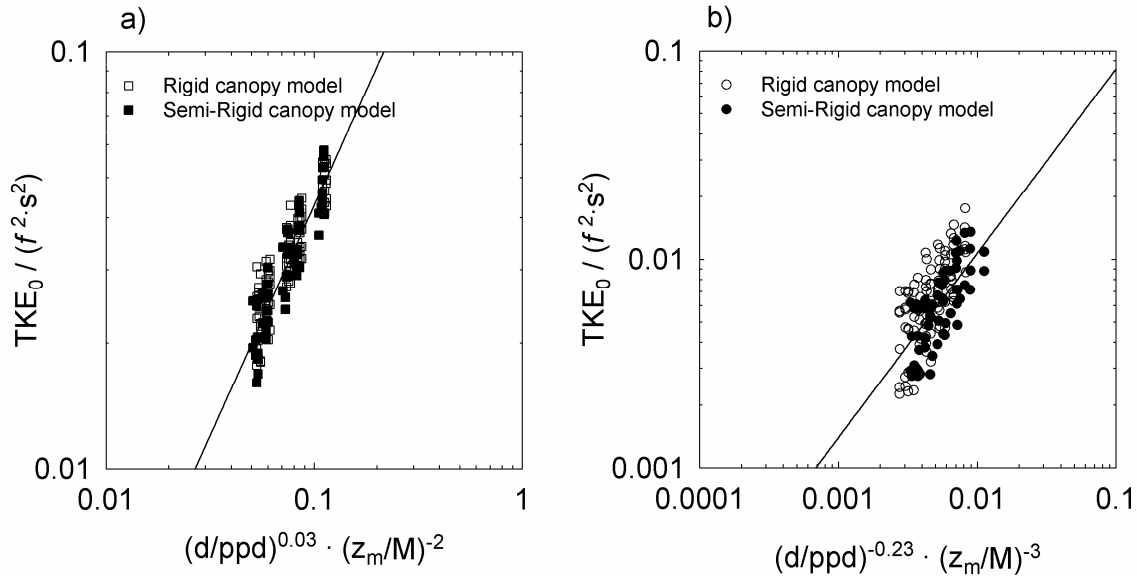

Figure 3.5. Comparison between non-dimensional number for rigid and semi-rigid canopy model: a) $z_m/z_c < 1$, r = 0,9 (n = 60, 99% of confidence); b) $z_m/z_c > 1$, r = 0.74 (n = 60, 99% of confidence).

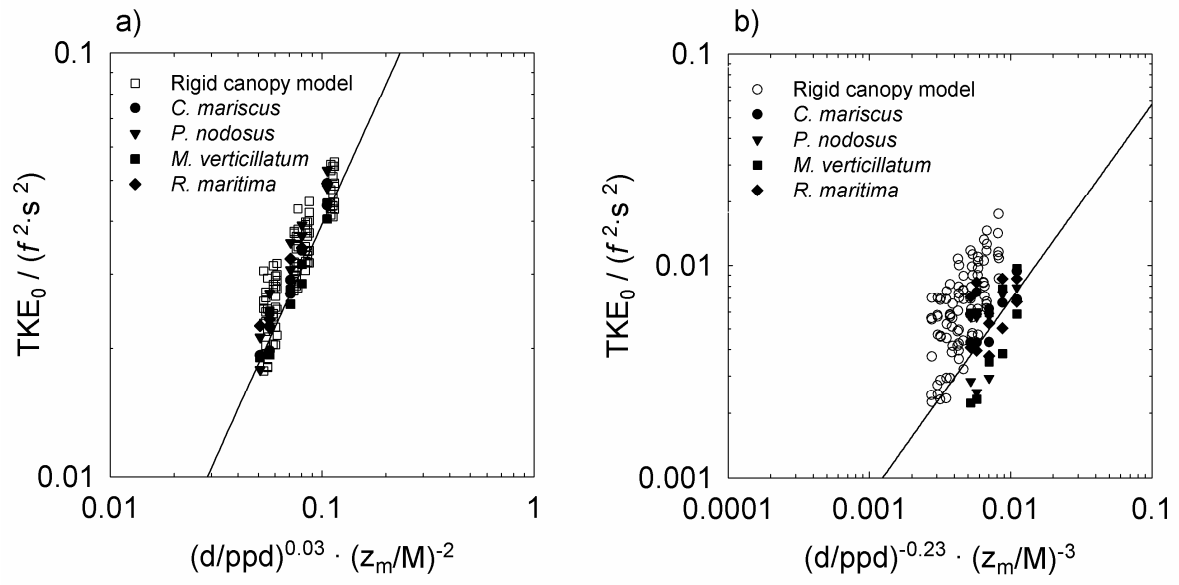

Figure 3.6. Comparison between non-dimensional number for rigid canopy model and natural plants: a) $z_m/z_c < 1$, r = 0.73 (n = 40, 99% of confidence); b) $z_m/z_c > 1$, r = 0.40 (n = 38, 95% of confidence).

3.5. Discussion

As found in Pujol et al. (2010), two zones can be distinguished based on the vertical decay of TKE with depth in a turbulent system with submerged aquatic vegetation. The first zone corresponds to $z_m/z_c < 1$ and the second to $z_m/z_c > 1$. The power law of the decay of the TKE (Eq. 3.11) for $z_m/z_c < 1$ is in accordance with results found by other authors (Hopfinger and Toly, 1976; DeSilva and Fernando, 1994). In their experiments without vegetation, they varied f, z_m, *s* and M to find a non-dimensional model following the dependences in Eqs. (3.6) and (3.7). In our experiments we did not vary the last two parameters (s and M). The decay of TKE for z_m/z_c was found to be $TKE_0 \sim z_m^{-2}$, in accordance with Orlins and Gulliver (2003). For the present study, from the non-dimensional model found for the decay of the turbulence for $z_m/z_c < 1$ we can conclude that the only parameters governing the flow dynamics do not depend on the canopy characteristics. The relationship between $TKE_0/(f^2 \cdot s^2)$ and d/ppd is discarded, taking into account that the exponent (0.03) is very low. Therefore, the upper part of the canopy acted like a false floor.

The results at $z_m/z_c > 1$ reveal a significant change in the behaviour of the TKE with the canopy structure, which is explained by the development of sheltering, i.e. the effects of submerged aquatic vegetation on turbulence. Some authors have pointed out the development of sheltering or dampening for $z_m/z_c > 1$. Unlike the results found for $z_m/z_c < 1$, in this lower zone, the results demonstrated that the behaviour of the TKE, and consequently the sheltering, depends on both the distance from the virtual origin near the grid with a slope of -3, thereby enhancing the sheltering, and the geometric characteristics of the plants, such as stem diameter and plant-to-

plant distance with an exponent of -0.23 (Eq. 3.12). For a given set of plants, as the stem diameter increases, the ppd decreases, producing less void spaces, diminished turbulence and enhanced sheltering by plants. Also, for a constant d, as ppd increases (which means less plant density), the TKE increases as turbulence can penetrate through the plant system or, inversely, when ppd decreases, TKE inside the canopy decreases, thereby enhancing the sheltering process.

Although the size of eddies defined by ℓ_0 was not directly measured in the experiment, according to Eq. (3.3), the calculated ℓ_0 was found to be 1.95 cm at the top of the canopy, which was larger than the ppd at the same depth. Thus, we suggest the hypothesis that eddies impinging the top of the canopy may break into smaller eddies and lose a portion of their energy, thereby producing a change of the TKE regime from z_m^{-2} ($z_m/z_c < 1$) to z_m^{-3} ($z_m/z_c > 1$). Only for stem diameters of 0.6 and 1 cm would the ppd be larger than the eddy length scale (1.99 and 3.21 cm respectively). Consequently, at the top of the canopy the TKE could penetrate at $z_m/z_c > 1$ without too much difficulty. Specifically, for a stem diameter of 0.6 cm the ℓ_0 would be larger than the ppd at z_m = 20.5 cm (1 cm below the top of the canopy). But, for a stem diameter of 1 cm the ℓ_0 is larger than the ppd at z_m = 31.5 cm (5 cm from the bottom of the tank). For this case, well inside the canopy, the length scale is smaller than the ppd. This may allow the eddy to reach the core of the canopy, thus inhibiting sheltering. Raupach (1992) defined sheltering or dampening as a combination of reduced velocity in the wake produced behind the plant and a lower pressure differential around the plant and thus a lower drag. Other authors have described sheltering in the same terms as Leonard and Croft (2006) and Neumeier and Amos (2006), although unlike our study, their experiments were carried out with advection instead of turbulence.

At $z_m/z_c < 1$ results for semi-rigid and natural plants reveal a slope close to the slope found with the rigid canopy model. However, while at $z_m/z_c > 1$, the semi-rigid canopy fit the model well enough, the natural plants do not have a constant close to the model solution as found with the semi-rigid canopy. This difference could be explained by the complex vertical density distribution of the natural plants, i.e. *C. mariscus* has a similar morphology to *R. maritima*: both have stem diameters of less than 2 mm. However, while *R. maritima* leaves are narrower, *C. mariscus* leaves are stiffer and wider. *Myriophyllum verticillatum* has compound and divided leaves, like feathers, with stems around 4 mm in diameter. *P. nodosus* has a long stem with wide horizontal leaves and a diameter between 4 and 5 mm. Both *P. nodosus* and *M. verticillatum* have leaves that grow at each level of the stem and perpendicular to it. All these configurations might reduce the turbulent kinetic energy well inside the canopy.

3.6. Implications for sediment bottom dynamics in wetlands

The presence of SAV in salt marshes modifies the flow dynamics with direct implications for a series of biophysical and geophysical processes (Raupach, et al., 1996). Sheltering, one of the most important geophysical processes, not only promotes sedimentation as a result of longer particle residence times (Ward et al., 1984; Eckman et al., 1989), it also decreases the resuspension of sediment from the bottom and consequently reduces its erosion, relative to unimpeded flows (Shi et al., 1996; Leonard and Croft, 2006; Kosten et al., 2009) and to high energy events (Granata et al., 2001). These geophysical processes, which determine the budget of particle transport in the vegetated area, have biological consequences such as an increase in food availability (Irlandi and Peterson, 1991) and the provision of shelter (Wilson et al., 1987).

The differences between stiff and flexible canopies were described by Peralta et al. (2008). They concluded that a stiff canopy had a greater potential capacity to trap sediment, with the lateral expansion of the rigid canopy's populations resulting as a consequence of increased sedimentation. However, a flexible canopy was more efficient at reducing erosion, so flexible shoots provide efficient protection against erosive forces. In addition, turbulence generated by branches of the canopy could be the only turbulence in water motion at the right scale to enhance nutrient uptakes and affect the exchange of gases and solutes (Anderson and Charters, 1982). Finally, canopy morphology also played an important role in the hydrodynamics of the canopy. Different vegetation morphologies may facilitate different uptake rates for nutrients, such as CO_2 and NH_4^+, which are crucial for plant growth (Morris et al., 2008).

In a larger context, wetland vegetation is an important ecosystem that may attenuates short-period waves (Möller et al., 1999) with a length scale from centimetres to tens of meters and a time in the order of the seconds. Extremes events such as storm surges or tsunamis are long-period waves with hundreds of kilometres of length, a wave celerity from 10 to 100 times faster than standard ocean waves and a wave that quickly floods the coast over several minutes to days. Therefore, it is obviously that in these situations the wetland vegetation could not reduce the effects of storm surges or tsunamis (Feagin et al., 2010).

3.7. Conclusions

For $z_m/z_c < 1$ the decay of the turbulence follows the power law that depends on s, M, f and z_m as demonstrated by other authors, with TKE ~ z_m^{-2}. Most of the experiments carried out with different sizes of d and ppd produced void spaces smaller than the length scale of the eddy at the top of the canopy. Therefore, the canopy acts like a false floor, preventing larger eddies from entering the canopy. In this zone, the relation between the geometric characteristic of the plant and TKE could be considered negligible. Unlike at $z_m/z_c < 1$, at $z_m/z_c > 1$ the decay of the TKE and the consequent sheltering is governed not only by the z_m, which is still the most important parameter (with an exponent of -3), but also by the geometric characteristics of the plants. Finally, the analytical solution for TKE depending on z_m, d and ppd fits well enough for semi-rigid and natural plants. Only slight deviations from the above non-dimensional have been found for TKE values inside the vegetation for natural plants. These differences have been attributed to the complex vertical distribution of this natural vegetation.

Acknowledgements This research was funded by the *Ministerio de Ciencia e Innovación* of the Spanish Government through grant CGL 2010-17289 to the University of Girona. Dolors Pujol was supported by research fellowship BR08/11 of the University of Girona. We would like to acknowledge the contributions of Xicu Gómez and Teresa Martí of the Department of Physics at the University of Girona and those of Amélie Dasre from the *Institut Universitaire et Technologique du Creusot* (France).

References

Anderson, S.M., Charters, A.C., 1982. A fluid dynamics study of seawater flow through *Gelidium nudifrons*. Limnology and Oceanography, 27, 399-412.

Atkinson, J.F., Damiani, L., Harleman, D.R.F., 1987. A comparison of velocity-measurements using a laser anemometer and a hot-film probe, with application to grid-stirring entrainment experiments. Physics of Fluids, 30, 3290-3292.

Bates, B.C., Kundzewicz, Z.W., Wu, S., Palutikof, J.P., 2008. Climate change and water. Technical paper of the Intergovernmental Panel on Climate Change, IPCC Secretariat, Geneva, pp. 210.

Boon, J.D., Green, M.O., Suh, K.D., 1996. Bimodal wave spectra in lower Chesapeake Bay, sea bed energetics and sediment transport during winter storms. Continental Shelf Research, 16, 1965-1988.

Bouma, T.J., van Duren, L.A., Temmerman, S., Claverie, T., Blanco-Garcia, A., Ysebaert, T., Herman, P.M.J., 2007. Spatial flow and sedimentation patterns within patches of epibenthic

structures: Combining field, flume and modelling experiments. Continental Shelf Research, 27, 1020-1045.

Brumley, B.H., Jirka, G.H., 1987. Near-surface turbulence in a grid-stirred tank. Journal of Fluid Mechanics, 183, 235-263.

Christiansen, T., Wiberg, P.L., Milligan, T.G., 2000. Flow and sediment transport on a tidal salt marsh surface. Estuarine Coastal and Shelf Science, 50, 315-331.

Colomer, J., Fernando, H.J.S., 1999. Resuspension of sediments by multiple jets. Journal of Hydraulic Engineering-Asce, 125, 765-770.

Connolly, J.P., Armstrong, N.E., Miksad, R.W., 1983. Adsorption of hydrophobic pollutants in estuaries. Journal of Environmental Engineering-ASCE, 109, 17-35.

Desilva, I.P.D., Fernando, H.J.S., 1994. Oscillating grids as a source of nearly isotropic turbulence. Physics of Fluids, 6, 2455-2464.

Eckman, J.E., 1987. The role of hydrodynamics in recruitment, growth, and survival of *Argopecten-irradians* (L) and *Anomia-simplex* (Dorbigny) within eelgrass meadows. Journal of Experimental Marine Biology and Ecology, 106, 165-191.

Eckman, J.E., Duggins, D.O., Sewell, A.T., 1989. Ecology of understory kelp environments. 1. Effects of kelps on flow and particle-transport near the bottom. Journal of Experimental Marine Biology and Ecology, 129, 173-187.

Evans, J.H., 1972. Dimensional analysis and Buckingham pi theorem. American Journal of Physics, 40, 1815-&.

Feagin, R.A., Lozada-Bernard, S.M., Ravens, T.M., Moller, I., Yeager, K.M., Baird, A.H., 2009. Does vegetation prevent wave erosion of salt marsh edges? Proceedings of the National Academy of Sciences of the United States of America, 106, 10109-10113.

Feagin, R.A., Mukherjee, N., Shanker, K., Baird, A.H., Cinner, J., Kerr, A.M., Koedam, N., Sridhar, A., Arthur, R., Jayatissa, L.P., Lo Seen, D., Menon, M., Rodriguez, S., Shamsuddoha, M., Dahdouh-Guebas, F., 2010. Shelter from the storm? Use and misuse of coastal vegetation bioshields for managing natural disasters. Conservation Letters, 3, 1-11.

Fernando, H.J.S., Desilva, I.P.D., 1993. Note on secondary flows in oscillating-grid, mixing-box experiments. Physics of Fluids A-Fluid Dynamics, 5, 1849-1851.

Fonseca, M.S., Cahalan, J.A., 1992. A Preliminary Evaluation of Wave Attenuation by 4 Species of Seagrass. Estuarine Coastal and Shelf Science, 35, 565-576.

Gambi, M.C., Nowell, A.R.M., Jumars, P.A., 1990. Flume observations on flow dynamics in *Zostera-marina* (Eelgrass) Beds. Marine Ecology-Progress Series, 61, 159-

Granata, T.C., Serra, T., Colomer, J., Casamitjana, X., Duarte, C.M., Gacia, E., 2001. Flow and particle distributions in a nearshore seagrass meadow before and after a storm. Marine Ecology-Progress Series, 218, 95-106.

Green, M.O., Black, K.P., Amos, C.L., 1997. Control of estuarine sediment dynamics by interactions between currents and waves at several scales. Marine Geology, 144, 97-116.

Gruber, R., 2009. Interactions between an estuarine submersed plant bed and its physical and biogeochemical environment: seasonal and spatial variation. Ph.D. thesis, University of Maryland (College Park, Md.), United States of America.

Hopfinger, E.J., Toly, J.A., 1976. Spatially decaying turbulence and its relation to mixing across density interfaces. Journal of Fluid Mechanics, 78, 155-175.

Huppert, H.E., Turner, J.S., Hallworth, M.A., 1995. Sedimentation and entrainment in dense layers of suspended particles stirred by an oscillating grid. Journal of Fluid Mechanics, 289, 263-293.

Irlandi, E.A., Peterson, C.H., 1991. Modification of animal habitat by large plants - mechanisms by which seagrasses influence clam growth. Oecologia, 87, 307-318.

Knutson, P., Brochu, R., Seelig, W., Inskeep, M., 1982. Wave damping in *Spartina alterniflora* marshes. Wetlands, 2, 87-104.

Kosten, S., Lacerot, G., Jeppesen, E., Marques, D.D., van Nes, E.H., Mazzeo, N., Scheffer, M., 2009. Effects of submerged vegetation on water clarity across climates. Ecosystems, 12, 1117-1129.

Leonard, L.A., Croft, A.L., 2006. The effect of standing biomass on flow velocity and turbulence in *Spartina alterniflora* canopies. Estuarine Coastal and Shelf Science, 69, 325-336.

Leonard, L.A., Luther, M.E., 1995. Flow hydrodynamics in tidal marsh canopies. Limnology and Oceanography, 40, 1474-1484.

Lynch, J.F., Irish, J.D., Gross, T.F., Wiberg, P.L., Newhall, A.E., Traykovski, P.A., Warren, J.D., 1997. Acoustic measurements of the spatial and temporal structure of the near-bottom boundary layer in the 1990-1991 STRESS experiment. Continental Shelf Research, 17, 1271-1295.

Madsen, T.V., Warncke, E., 1983. Velocities of currents around and within submerged aquatic vegetation. Archiv Fur Hydrobiologie, 97, 389-394.

Manning, A.J., Dyer, K.R., 1999. A laboratory examination of floc characteristics with regard to turbulent shearing. Marine Geology, 160, 147-170.

Matsunaga, N., Sugihara, Y., Komatsu, T., Masuda, A., 1999. Quantitative properties of oscillating-grid turbulence in a homogeneous fluid. Fluid Dynamics Research, 25, 147-165.

Moller, I., Spencer, T., French, J.R., Leggett, D.J., Dixon, M., 1999. Wave transformation over salt marshes: A field and numerical modelling study from north Norfolk, England. Estuarine Coastal and Shelf Science, 49, 411-426.

Morris, E.P., Peralta, G., Brun, F.G., van Duren, L., Bouma, T.J., Perez-Llorens, J.L., 2008. Interaction between hydrodynamics and seagrass canopy structure: Spatially explicit effects on ammonium uptake rates. Limnology and Oceanography, 53, 1531-1539.

Nepf, H.M., 1999. Drag, turbulence, and diffusion in flow through emergent vegetation. Water Resources Research, 35, 479-489.

Neumeier, U., Amos, C.L., 2006. The influence of vegetation on turbulence and flow velocities in European salt-marshes. Sedimentology, 53, 259-277.

Nokes, R.I., 1988. On the entrainment rate across a density interface. Journal of Fluid Mechanics, 188, 185-204.

Orlins, J.J., Gulliver, J.S., 2003. Turbulence quantification and sediment resuspension in an oscillating grid chamber. Experiments in Fluids, 34, 662-677.

Peralta, G., van Duren, L.A., Morris, E.P., Bouma, T.J., 2008. Consequences of shoot density and stiffness for ecosystem engineering by benthic macrophytes in flow dominated areas: a hydrodynamic flume study. Marine Ecology-Progress Series, 368, 103-115.

Peterson, C.H., Luettich, R.A., Micheli, F., Skilleter, G.A., 2004. Attenuation of water flow inside seagrass canopies of differing structure. Marine Ecology-Progress Series, 268, 81-92.

Pujol, D., Colomer, J., Serra, T., Casamitjana, X., 2010. Effect of submerged aquatic vegetation on turbulence induced by an oscillating grid. Continental Shelf Research, 30, 1019-1029.

Raupach, M.R., Finnigan, J.J., Brunet, Y., 1996. Coherent eddies and turbulence in vegetation canopies: the mixing-layer analogy. Boundary-Layer Meteorology, 78, 351-382.

Raupach, M.R., 1992. Drag and drag partition on rough surfaces. Boundary-Layer Meteorology, 60, 375-395.

Serra, T., Colomer, J., Logan, B.E., 2008. Efficiency of different shear devices on flocculation. Water Research, 42, 1113-1121.

Shi, Z., Pethick, J.S., Burd, F., Murphy, B., 1996. Velocity profiles in a salt marsh canopy. Geo-Marine Letters, 16, 319-323.

Thompson, S.M., Turner, J.S., 1975. Mixing across an interface due to turbulence generated by an oscillating grid. Journal of Fluid Mechanics, 67, 349-369.

Ward, L.G., Kemp, W.M., Boynton, W.R., 1984. The influence of waves and seagrass communities on suspended particulates in an estuarine embayment. Marine Geology, 59, 85-103.

Wilson, K.A., Heck, K.L., Able, K.W., 1987. Juvenile blue-crab, *Callinectes-sapidus*, survival - an evaluation of eelgrass, *Zostera-marina*, as refuge. Fishery Bulletin, 85, 53-58.

Chapter 4

Flow structure in canopy models dominated by progressive waves

Pujol, D.[1], Serra, T.[1], Colomer, J.[1], Casamitjana, X.[1]

[1]Department of Physics, Escola Politècnica Superior-II, Campus Montilivi, 17071 Girona, Catalonia, Spain

Journal of Hydrology (in press)

Abstract Laboratory experiments were carried out to study the flow structure both inside and above different canopy models which were dominated by progressive waves. A set of experimental conditions were considered in a laboratory flume: three vegetation models (submerged rigid, submerged flexible and emergent rigid), three plant densities (128, 640 and 1280 stems m^{-2}) and three wave frequencies (f = 0.8, 1 and 1.4 Hz).The progressive waves followed the second-order Stokes theory in the intermediate depth range. The observations revealed that submerged and emergent rigid vegetation models modified the wave-induced velocities i.e., both mean current and wave velocity. The submerged rigid vegetation model for plant densities higher than 640 plants m^{-2} and wave frequency higher than 1 Hz acted akin to a false floor, confining the mean current to above the plant bed. A penetration depth around 2 cm below the top of submerged rigid vegetation was found. For the other runs, the vertical profile of mean current did not present changes with respect to runs without plants. The emergent rigid vegetation model reversed the direction of the induced mean current, with the highest velocity corresponding to the highest plant density. In contrast, the submerged flexible vegetation model had a weak effect on the mean current, with the vertical velocity profile similar to that found in experiments without vegetation. The wave velocities inside the vegetation for the densest submerged rigid vegetation were found to be reduced by 20%, when compared to the wave velocities without vegetation, while in emergent rigid vegetation this reduction was of 45%.

Keywords Aquatic vegetation model; progressive waves; second-order Stokes' theory; mean current; wave attenuation.

4.1. Introduction

Along and within the coastal zone, the sea, land, and air interact to produce a favourable habitat for many species (Pergent-Martini, 2006). Seagrass meadows are an economically important component of that habitat due to the link between seagrass and fish production. For example, together with wetlands, seagrass beds support more than 80% of the annual fish yield in the Mediterranean (Batisse and Jeudy de Grissac, 1995). Seagrass meadows reduce waves and currents (Gambi et al., 1990), and provide a refuge for fish, invertebrates and plankton. By reducing near-bed velocities, seagrasses reduce local resuspension and promoting the retention of sediment (Fonseca and Fisher, 1986; Fonseca and Cahalan, 1992; Gleason et al., 1979; Granata et al., 2001; Reusch and Chapman, 1995). The reduction of resuspension improves water clarity, which in turn provides greater light penetration and consequently an increase in productivity, thus creating a positive feedback for seagrass growth (Ward et al., 1984). Furthermore, wave-induced forces are believed to set the distribution of seagrass populations (Fonseca and Bell, 1998). Specifically, waves have been noted to determine the upper depth limit distribution of submerged aquatic vegetation such as *Posidonia oceanica* (Infantes et al., 2009) and influence species size, morphology, and distribution patterns (Blanchette, 1997; Lewis, 1968; Menge, 1976).

Within shallow-water environments where seagrasses are abundant, local hydrodynamics can be drastically altered depending on vegetation density and flow conditions. There is a significant body of literature which describes unidirectional flow through submerged canopies. Previous studies have successfully described the flow structure for aquatic vegetation subjected to unidirectional flow using rigid and flexible vegetation models (Folkard, 2005; Ghisalberti and Nepf, 2006; Lefebvre et al., 2010; Luhar et al., 2008; Nepf, 1999; Nepf and Vivoni, 2000; Tanino and Nepf, 2008; Chen et al., 2011). However, some authors suggest that biological processes, such as nutrient uptake, may often be controlled by surface wave motion rather than the steady component of velocity that has received considerably more attention (Koch and Gust, 1999; Lowe et al., 2005b; Thomas and Cornelisen, 2003).

Flows in natural systems are a combination of steady, oscillatory and turbulent flows. Some authors have studied the effects of seagrass or coral reef structures on a wave dominated flow in laboratory experiments (Coops et al., 1996; Gambi et al., 1999; Lowe et al., 2005a; Luhar et al., 2010; Reidenbach et al., 2007). Experiments carried out to study the wave-induced currents inside a seagrass bed (Luhar et al., 2010) revealed that a unidirectional current is generated in the direction of wave propagation within the seagrass bed when it is forced by purely oscillatory wave-driven flow, which is analogous to a viscous layer near the bed. Luhar et al. (2010) designed a model to predict the magnitude of this mean current in flexible plants. The model indicated that the magnitude of the mean current is controlled primarily by wave parameters and did not depend on the canopy parameters. However, how the conditions under this equation applies (equation 21 in Luhar et al., 2010) is dependent on the ratio of blade spacing and wave

excursion. This unidirectional mean current plays a major role in determining both the health of the seagrass beds and their ecological contribution. This current could, for example, speed up the rate of water renewal within a meadow thus enhancing nutrient cycling, the dispersion of seeds and pollen as well as influencing net sediment transport (Luhar et al., 2010). Although the impact of aquatic vegetation on the control of mass transport has been studied for oscillatory flows, it is still unclear how different canopy structures modify the mean current associated with waves within and above the meadow.

The wave velocity attenuation, or dissipation, has been widely studied in field and laboratory experiments (Hansen and Reidenbach, 2012; Lowe et al., 2005a). Lowe et al. (2005a) proposed a theoretical model to estimate the flow inside a submerged canopy, such as a coral reef. Their model was developed by considering the momentum balance around individual canopy elements within a larger canopy. They demonstrated that the flow inside a canopy was always lower than above the canopy, and that the degree of flow attenuation varied as a function of canopy geometry parameters, such as the height and spacing of the elements, as well as coefficients that parameterize the effects of various forces exerted by the canopy element (drag coefficient, C_d, friction coefficient, C_f, and inertial force coefficient, C_m). Hansen and Reidenbach (2012) found that wave velocity within an eelgrass bed was reduced by 20% compared to the flow above the bed. However, this attenuation depended on the stem density and submergence ratios (i.e. canopy height to water depth ratio). Furthermore, bottom shear stress generated with a wave field and over bare soil, was found to be 5 times greater than in the presence of an eelgrass meadow (Hansen and Reidenbach, 2012), which indicates that the presence of vegetation might have important implications for sediment stabilization. Therefore, wave velocity attenuation is an important aspect of canopy flows which has not yet been compared with different seagrass structures.

Our experiments are aimed at studying the relationship between flow structure and vegetation model in terms of a wide variety of parameters; three vegetation models, three vegetation densities and three wave frequencies. We quantified the vertical distribution of mean current (U_c), oscillatory velocity (U_w) above and within different types of vegetation.

4.2. Material and methods

The study was conducted in a wave flume of 6 m x 0.5 m x 0.5 m. A schematic of the setup is shown in figure 4.1a. The mean water height, h, was 0.3 m. A plywood beach with a slope of 1:3 and covered with a 7 cm layer of foam rubber was located at the end of the tank. A vertical paddle, called a flap type wavemaker, was placed at the beginning of the tank and was driven by a variable-speed motor located outside the tank. We define the longitudinal direction as x, and x = 0 at the wavemaker. y is the lateral direction and y = 0 at the centreline of the tank, and z is the vertical direction, with z = 0 at the flume bed.

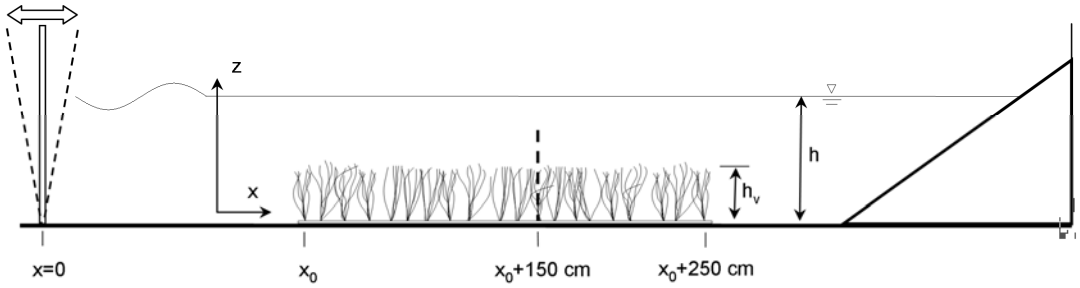

Figure 4.1. Scheme of the laboratory experiments. (a) Experiments were conducted in a 6 m long flume. The streamwise coordinate is denoted by x, with x positive in the downstream direction, and x = 0 at the mean position of the wavemaker. The vertical coordinate is z, with z = 0 at the bed. The mean water depth, d, is 30 cm. The mean plant height in still water is h_{SRV} = 14 cm for submerged rigid and flexible vegetation and h_{ERV} = 29 cm for emergent rigid vegetation. The model meadow was 250-cm long. The vertical dashed line indicates the position of the velocity profile measured using a Sontek MicroADV and a Nortek Vectrino. Note that dimensions in the figure are given in cm and the beach slope at the end of the tank is not scaled; (b) photo of submerged rigid vegetation model; (c) photo of flexible submerged vegetation model and (d) photo or emergent rigid vegetation model.

4.2.1. Vegetation quantification

To construct the meadow, individual plants were inserted into a predrilled baseboard of 2.5 m long. The characteristics of plants vary greatly in terms of height, plant density, and morphology (Fig 4.1b, c and d). In order to obtain features in the laboratory similar to those in the field, 30 different situations were studied featuring three canopy models (submerged rigid, submerged flexible and emergent rigid vegetation, where emergent vegetation was defined as that plant whose height was emergent the half part of the wave cycle) with two canopy heights (h_V = 14 and 29 cm), and three oscillating frequencies (f = 0.8, 1 and 1.4 Hz) (Table 4.1). The rigid canopy model consisted of rigid cylinders made of PVC and 1 cm in diameter. The density of the canopy was quantified by three different SPF. According to Serra et al. (2004) the SPF can be defined as the fractional plant area at the bottom occupied by stems:

$$SPF(\%) = \left(\frac{n \cdot \pi \cdot (d/2)^2}{A} \right) \cdot 100 \qquad (4.1)$$

where n is the number of plants, d is the diameter of the plant and A is the total area. SPFs of 1%, 5% and 10% were used for this study. The vegetation pattern for each SPF was made at random by means of a computer function

A flexible canopy was constructed from polyethylene (high density) blades attached with a plastic band to a 2 cm long and a 1 cm in diameter PVC dowel. The model plants were dynamically and geometrically similar to typical seagrasses, as described by the parameters λ_1 and λ_2 (Ghisalberti and Nepf, 2002). The similarity is based on two independent ratios of the drag force; $F_d = \rho_w A_f C_d U_c^2$, the buoyancy force, $F_B = (\rho_w - \rho_s) g h_v w_b t_b$, and the restoring force due to blade rigidity, $F_r = EI/h_v^2$ (Luhar and Nepf, 2011):

$$\frac{F_B}{F_R} \sim \lambda_1 = \frac{(\rho_w - \rho_s) \cdot h_v^3}{E \cdot t_v^2} \qquad (4.2)$$

$$\frac{F_R}{F_D} \sim \lambda_2 = \frac{E \cdot t_v^3}{h_v^3 \cdot U_c^2} \qquad (4.3)$$

where ρ_w is the density of the water (1000 kg m^{-3}); A_f is the frontal area of the blade; C_d is the blade drag coefficient; U_c is the mean in-canopy velocity; ρ_s is the density of the blades (956.5 kg m^{-3}); g is the gravitational constant (9.8 m s^{-2}); h_v is the height of the vegetation (0.14 m); w_b is the width of the blade; t_b is the thickness of the blade ($0.075 \cdot 10^{-3}$ m); $I = w_b t_b^3/12$ is the second moment of area; and E is the modulus of elasticity ($3 \cdot 10^8$ Pa). As noted by Ghisalberti and Nepf (2002), the dependence of λ_2 on U_c^2 makes λ_2 to vary tremendously in the field, so λ_1 was chosen as the critical design parameter. For the blade model used in this study, λ_1 is 0.07 s^2 m^{-1}. Using the measurements given by Folkard (2005) for *Posidonia oceanica*, (ρ_s is 910 ± 110 kg m^{-3}; h_v is 0.25 m; E is 4.7± 0.6 ·108 Pa; and t_b is $0.2 \cdot 10^{-3}$ m), we obtain λ_1 = 0.075 s^2 m^{-1}, which shows that our prototpye vegetation is dynamically similar to *Posidonia*.

As a result, 30 wave flow experiments were conducted, denoted as WP 1 – WP 3 for experiments without plants; SRV 1 – SRV 9 for submerged rigid vegetation model; SFV 1 - SFV 9 for submerged flexible vegetation model and ERV 1 - ERV 9 for emergent rigid vegetation model (Table 4.1).

Table 4.1. Summary of the wave and vegetation parameters for each experiment.

Run	Canopy model	h_v (cm)	h_v/h	SPF (%)[a]	S/d	n_s (stems/m^2)	S (m)	f (Hz)	k (m^{-1})[b]
WP 1	Without							0.8	3.36
WP 2	vegetation							1	4.53
WP 3								1.4	7.64
SRV 1	Submerged rigid	14	0.47	1	7.8	128	0.078	0.8	3.36
SRV 2	vegetation model							1	4.53
SRV 3								1.4	7.64
SRV 4				5	2.9	640	0.029	0.8	3.36
SRV 5								1	4.53
SRV 6								1.4	7.64
SRV 7				10	1.5	1280	0.015	0.8	3.36
SRV 8								1	4.53
SRV 9								1.4	7.64
SFV 1	Submerged	14	0.47	1	7.8	128	0.078	0.8	3.36
SFV 2	flexible							1	4.53
SFV 3	vegetation model							1.4	7.64
SFV 4				5	2.9	640	0.029	0.8	3.36
SFV 5								1	4.53
SFV 6								1.4	7.64
SFV 7				10	1.5	1280	0.015	0.8	3.36
SFV 8								1	4.53
SFV 9								1.4	7.64
ERV 1	Emergent rigid	29	0.96	1	7.8	128	0.078	0.8	3.36
ERV 2	vegetation model							1	4.53
ERV 3								1.4	7.64
ERV 4				5	2.9	640	0.029	0.8	3.36
ERV 5								1	4.53
ERV 6								1.4	7.64
ERV 7				10	1.5	1280	0.015	0.8	3.36
ERV 8								1	4.53
ERV 9								1.4	7.64

[a] The SPF was calculated by equation 4.1

[b] The k was calculated by dispersion equation

4.2.2. Measuring technique

The Eulerian velocity field was defined as (u, v, w) in the (x, y, z) directions, respectively. The three components of velocity were recorded with a downwards looking Acoustic Doppler Velocimeter (Sontek/YSI16-MHzMicroADV). The acoustic frequency was 16 MHz, the sampling volume was 0.09 cm^3 and the distance to the sampling volume was 5 cm. The ADV instrument was configured to transmit 50 acoustic signals per second with a sampling time interval of 10 minutes (i.e. 30000 recordings per sample). To avoid any spikes or beam correlations from ADV measurements lower than 70%, values of instantaneous velocities higher than two standards deviation were discarded. The ADV, which was operated manually, was mounted on a movable vertical frame that operated from the bottom (z = 1 cm) up to z = 23 cm, and was limited at the upper part by both the wave shape and the 5 cm distance from the ADV to the sampling volume. Another Doppler velocity sensor (Nortek/side-looking Vectrino) was used in order to obtain velocity measurements of the layer situated at the upper part of the water column; that is from z = 24 cm to z = 27 cm. It was configured to transmit 25 acoustic signals per second with a sampling time interval of 10 min (i.e. 15000 recordings per sample).

For each experiment, a vertical profile was taken over a height range of z = 1-27 cm at 1 cm velocity space-intervals from the bottom of the tank. Vertical velocity profiles were measured at one longitudinal location, which corresponded to an antinode created by reflections from the downstream end of the flume. The longitudinal measurements of the velocity were at an anti-node, in order to eliminate the lower-order spatially periodic variation in wave and velocity amplitude associated with the 10% reflection (Luhar et al., 2010). Then, the model bed was shifted longitudinally along the flume in order to measure at 150 cm from the vegetation edge. In order to obtain valid data acquisition within the canopy, just a few stems were removed to avoid blocking the pathway of the ADV beam, as was done by Luhar et al. (2010).In order to obtain valid data acquisition within the canopy, just a few stems were removed to avoid blocking the pathway of the ADV beams, as was done by Neumeier and Ciavola (2004), Pujol et al. (2010, 2012). To minimize the effect of this 'hole', its shape was specifically designed to allow the ADV acoustic receivers and the acoustic transmitter to perform properly. At some specific heights above the bed (8 cm and 20 cm) low correlation was obtained due to what are called "weak spots", which are related to the pulse-coherent or pure-coherent technique used by the ADV to calculate the velocity. This technique uses two pulses of sound separated by a time lag; the sensors measure the phase of the return signal from each pulse. The change in phase divided by the time between pulses is directly proportional to the velocity of the particles in the water. The weak spots occur when the first pulse, which comes from the bottom, matches in time and space with the second pulse at the sampling volume. As the time lag depends on the velocity range this problem is solved by changing the ADV velocity range from 30 cm s^{-1} to 10 cm s^{-1} for measurements at 8 cm and 20 cm height from the bottom (Sontek/YSI, Acoustic Doppler Velocimeter, Technical Documentation).

4.2.3. Methods of analysis

This paper is focused on the study of the effects of canopy on a wave dominated flow. It is well known that for general wave flows, the instantaneous velocity is the sum of steady velocity, wave motion, and turbulent velocity. The waves generated in our flume followed the Stokes' theory. The second order Stokes theory adds an 'extra' harmonic wave term, written as the wave steepness raised to the secon power. One of the most important effects from the addition of second order terms is the incomplete closure of particle paths, resulting in a net momentum transport in the direction of wave propagation. This velocity is called Stokes drift (Stokes, 1847). In this theory, Stokes (1847) assumed perfectly inviscid and irrotational motion near the bottom. Longuet-Higgins (1953) investigated the effect of the viscosity in a finite domain. Four boundary conditions were introduced: both components of velocity on the bottom and both components of stress at the free surface must vanish, so that the flow becomes rotational near the boundary layer, while it remains irrotational in the main body of the water column. As pointed out by Longuet-Higgins (1953), near the bottom there is a boundary layer where horizontal oscillatory velocity decays to zero at the bed because of viscosity. This modification by viscosity causes a phase shift in the oscillatory velocities. The horizontal and vertical velocities are no longer exactly 90º out of phase, creating a steady, nonzero wave stress which is analogous to the turbulent Reynolds stress. Wave stress represents a time-invariant momentum transfer out of the oscillatory flow and generates a mean current in the boundary layer. With the above mentioned assumptions, Longuet-Higgins (1953) found that the vertical profile of this mean current is:

$$\frac{U_C}{\left(\frac{\pi H}{\lambda}\right)^2 \cdot C} = \frac{1}{4\sinh^2 kh}\left(A + 3 + B + D\right) \qquad (4.4)$$

where $A=2\cosh[2kh(\mu-1)]$, $B=kh\sinh(2kh)(3\mu2-4\mu+1)$, $D=3[(\sinh2kh/2kh)+(3/2)](\mu2-1)$, $\mu = z/h$ and $C = \omega/k$, z is the vertical direction, H is the height of the wave and λ is the wavelength. The frequency (f), wave number (k) and water height (h) are related by the dispersion relation, $\omega^2 = (kg)\tanh(kh))$, where ω is the radian frequency and g is the gravity constant (9.8 m s^{-2}). Just beyond the boundary layer the mass-transport velocity is as follows:

$$U_c = \frac{5a^2\omega k}{4\sinh^2(kh)} \qquad (4.5)$$

where a is the amplitude of the wave. For laminar flows, the thickness of the boundary layer is in the order of $O[(\nu/\omega)^{1/2}]$, where ν is the kinematic viscosity ($1\cdot10^{-6}$ m^2 s^{-1}).

Therefore, instantaneous velocity, e.g. U_i, can be decomposed as:

$$U_i = U_c + U_w + U' \tag{4.6}$$

where U_c is the steady velocity associated with the current, U_w is the unsteady wave motion which represents spatial variations in the phase averaged velocity field, and U' is the turbulent velocity. U_c is the space and phase-averaged velocity found as (Lowe et al., 2005a; Luhar et al., 2010; Perrin et al., 2007, Sung and Yoo, 2001):

$$U_c = \frac{1}{2\pi}\int_0^{2\pi} U_i(\varphi)\,d\varphi \tag{4.7}$$

where $U_i(\varphi)$ is the instantaneous velocity according to the phase. Wave velocity, U_w, was obtained by using a phase averaging technique. For that, the Hilbert transform was used to average oscillatory flow velocities with a common phase, as in Wlezien and Way (1979). In order to compare the magnitude of the flow at different heights in the water column, the root mean squared (rms) velocities were calculated according to the following operation:

$$U_{w,rms} = \sqrt{\frac{1}{2\pi}\int_0^{2\pi}\left(U_i(\varphi) - U_c\right)^2 d\varphi} \tag{4.8}$$

Hereafter the subscript (w) refers to oscillatory flows or unsteady wave motion (U_w), subscript (c) refers to unidirectional flows or steady velocity (U_c) and turbulent velocities are represented by prime symbols (U').

To calculate the attenuation of the unsteady wave motion (U_w) a parameter defined by Lowe et al. (2007) is used:

$$\alpha_w = \frac{\overline{U}_w^{rms}}{U_{\infty,w}^{rms}} \tag{4.9}$$

where $\overline{U}_w^{rms}$ represents a vertical average root-mean-square wave velocity over the canopy height and $U_{\infty,w}^{rms}$ represents the wave velocity root-mean-square unaffected by the canopy roughness, called free-stream velocity. Parameter α_w provides a measure of the reduction of the in-canopy flow from its above-canopy potential flow value; values of $\alpha_w \approx 1$, indicating a weak or negligible effect of the vegetation on the wave. In contrast, values of $\alpha_w \approx 0$ means high wave attenuation, indicating that minimal flow passes through the canopy.

Lowe et al. (2005a) generated a theoretical model to estimate flow inside a submerged canopy driven by oscillatory flow:

$$\frac{\partial\left(\bar{U}_w - U_{\infty,w}\right)}{\partial t} = \frac{\left|U_{\infty,w}\right|U_{\infty,w}}{L_s} - \frac{\left|\bar{U}_w\right|\bar{U}_w}{L_d} - \left(\frac{C_M\lambda_p}{1-\lambda_p}\right)\frac{\partial\bar{U}_w}{\partial t} \qquad (4.10)$$

where, $\bar{U}_w$ is the oscillatory velocity inside the canopy; $U_{\infty,w}$ is the free stream velocity; L_s is a canopy shear length scale ($L_s = 2h_c/C_f$); L_d is a canopy drag length scale ($L_d = 2h_c(1-\lambda_p)/(C_d\lambda_f)$) and $(C_m\lambda_p)/(1-\lambda_p)$ is the canopy inertia force; friction and drag coefficients (C_f and C_d, respectively), related to steady flow terms, are assumed to be $C_d = 2.5$ and $C_f = 0.01$ for rigid vegetation (Lowe et al., 2005a) and $C_d = 1$ and $C_f = 0.01$ for flexible vegetation (Luhar et al., 2010). C_m is an inertia force coefficient (2 for potential flow around circular cylinders (Dean and Dalrymple, 1991) The inertia coefficient, C_m, is defined as the pressure gradient required to accelerate the fluid that exerts a so-called "buoyancy" force on an object. This coefficient is calculated as the sum of two terms, $C_m = 1+k_m$, where k_m is called the added mass, and which depends on the shape of the object. To our knowledge, measurements of inertia coefficients for biological shapes such as flexible canopies are scarce; however, for two-dimensional flow through rigid obstacles with elliptical or rectangular cross sectionals, k_m can be estimated as w_b/t_b (Lamb, 1945; Luhar et al., 2010; Mendez and Losada, 2004; Vogel, 1994). In our experiment for flexible vegetation, every eight blades are pasted around a cylindrical dowel and they are free to twist around its main axis. Therefore, the position of each blade in front of the wave field is different due to the spatial orientation around the dowel and the movements of the blade, thus in our study, k_m can be between 0.2 and 5. After fitting our experimental data to the model, the best bit of the model to our experimental data was found in the lower limit, when $k_m = 0.2$ and therefore $C_m = 1.2$. λ_f and λ_p are canopy parameter defined as $\lambda_f = h_c d/(S+d)^2$ and $\lambda_p = (\pi d^2/4)/(S + d)^2$, where S is the distance between stems ($S = n_s^{-1/2}-d$).

The equation (4.10) is a balance between steady flow and inertial terms. Three force terms are used in this model: shear stress, drag and inertia. To determine the relative magnitude of each term, a scaling analysis is performed. Then, three dimensionless parameters are found: A_∞^{rms}/L_s, A_∞^{rms}/L_d and $(C_m\lambda_p)/(1-\lambda_p)$, where A_∞^{rms} is the rms wave orbital excursion length of the free-stream potential flow ($A_\infty^{rms} = U_{w,\infty}^{rms}/\omega$); Since the dimensionless variables are all of order one, the magnitude of these parameters determines the relative importance of each term. Four regimes are proposed: canopy independent flow ($\alpha_w = 1$), inertia force dominated ($\alpha_w = \alpha_i = (1-\lambda_p)/[1+(C_m-1)\lambda_p]$), general flow ($\alpha_w = \alpha_w(A_\infty^{rms}/L_s,\ A_\infty^{rms}/L_d,\ C_m\lambda_p/1-\lambda_p)$) and unidirectional limit ($\alpha_w = \alpha_c = \sqrt{L_d/L_s}$).

4.3. Results

Waves generated in the flume corresponded to waves travelling at intermediate depths, which result when the water depth is between $\lambda/20$ and $\lambda/2$. Wave conditions in the present study correspond to the laminar regime, i.e. to wave Reynolds number, $Re_w = U_{w,\infty},A_\infty/\nu < 10000$ (Fredsoe and Deigaard, 1992).

4.3.1. Steady flow associated with the current (U_c)

Figure 4.2 shows the mean current of the vertical profile for run WP 2 and WP 3. WP 2 shows a positive mean current generated close to the bed, whereas from z = 3 cm to 27 cm it is negative with a positive tendency from z = 20 cm. The positive tendency of mean velocity is maximum at the measurement position closest to the bed (z = 1 cm, $U_c = 0.23\pm0.25$ cm s^{-1}, where ± refers to the accuracy of the instrument) and a maximum negative mean current is measured near the surface (z = 20 cm, $U_c = -1.26 \pm 0.25$ cm s^{-1}). The magnitude of this mean current at the bottom is consistent with the laminar boundary layer solution from equation 4.5, which predicts that the drift will be $U_c = 0.26$ cm s^{-1}. The vertical profile of mean current for run WP 3 is similar to that found for experiment WP 2. However, near the bottom, the mean current in WP3 is also negative (z = 1-2 cm, $U_c = -0.85\pm0.25$ cm s^{-1}). For WP 3 a maximum negative current of $U_c = -1.27\pm0.25$ cm s^{-1} at z = 16 cm is also found. Physical limitations due to the shape of the wave prevented the measurement of the velocity near the surface (from z = 28 to 30 cm). Qualitative observations using a passive tracer (vegetable coloring) indicate that for any frequency, the mean current near the surface is positive and confined to a thin surface layer, while it is negative below this layer, thus balancing the mass transport.

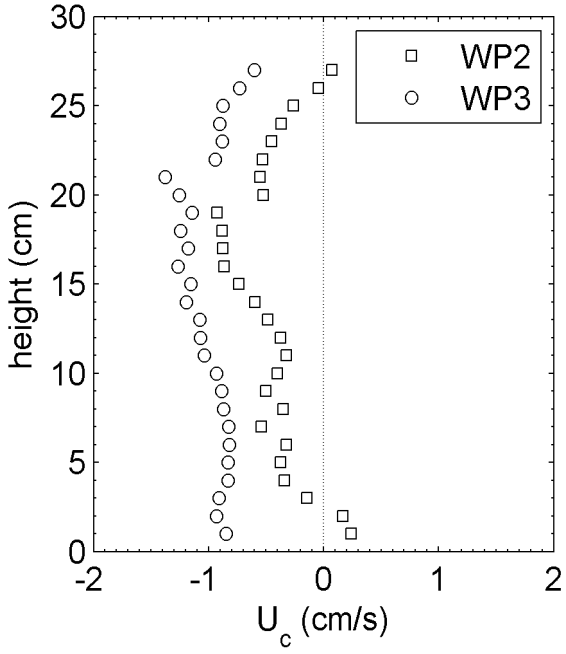

Figure 4.2. Vertical profile of mean current,Uc(z), without vegetation. White squares represent the WP 2 run and white circles represent the WP 3 run.

As an example, the velocity measurements made for run SRV 3, SRV 6 and SRV 9 are shown in figure 4.3a and are compared with those found for run WP 3. SRV 3 shows a vertical profile similar to that found without plants. Experiments carried out with the largest SPF values, corresponding to SRV 6 and SRV 9, show a deviation from WP 3 and SRV 3. Above the meadow, the vertical profile of the mean current increases with height up to z = 23 cm where the maximum negative velocity was found. At z = 23 cm the mean current changed towards positive velocity values. Inside the meadow, a positive mean current was generated from d_p = 2 cm below the top of the canopy and decreasing slightly downwards. d_p is called the penetration depth, (situated at z = 12 cm, U_c = 1.03±0.25 cm s^{-1}). Vertical profiles of SFV 3, SFV 6 and SFV 9, corresponding to flexible vegetation and WP3 are shown in figure 3b. The figure shows small differences for runs with vegetation and without it. Only near the surface, from z = 20 to 27 cm, the highest plant density seems to increase the mean current velocity. Experiments carried out with emergent vegetation (ERV 3, ERV 6 and ERV 9) can be seen in figure 4.3c. From z = 1 cm to z = 17 cm, the velocity remains nearly constant U_c = -2±0.25 cm s^{-1}. For ERV 9 this negative mean current is slightly larger, attaining a maximum negative value of U_c = -2.5±0.25 cm s^{-1} between z = 13 cm and 15 cm. However, from z = 7 cm to z = 20 cm the negative velocity is quite constant. Only, from z = 6 cm to z = 1 cm above the bottom does the velocity seem to slow down. In contrast, the current reverses above z = 23 cm towards positive values, also balance the mass transport in the water column.

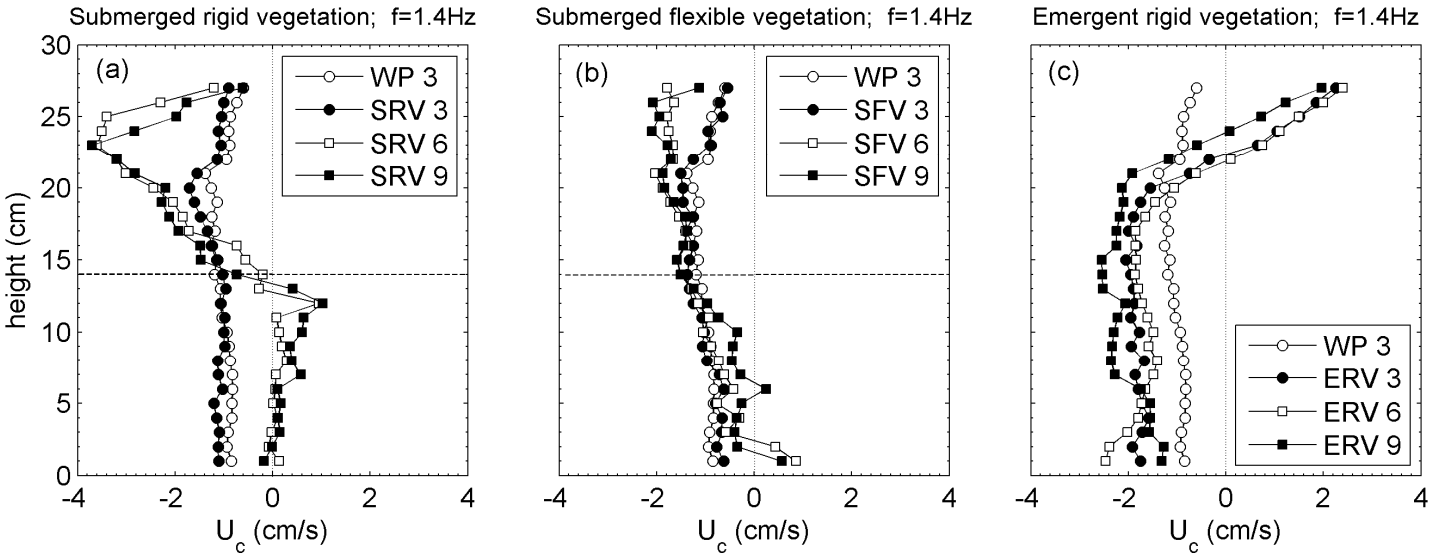

Figure 4.3. Comparison of vertical profile of mean current, $U_c(z)$, for different experiments. (a) WP 3, SRV 3, SRV 6 and SRV 9; (b) WP 3, SFV 3, SFV 6 and SFV 9, and (c) WP 3, ERV 3, ERV 6 and ERV 9. The horizontal dashed lines in Fig. 4.3a-b show the height of the canopy.

The progressive waves generated in the flume followed Stokes' wave theory for intermediate depths. Visual observation confirms the theory, i.e., waves do not follow a sinusoidal wave, but they are vertically asymmetrical around the mean sea level. Figure 4.4 compares experimental results and theoretical predictions based on the model proposed by equation (4.4). The mean current velocity for present experiments are non-dimensionalized, ($<U_c>/[(\pi \cdot H/\lambda)^2 \cdot C]$), and plotted versus the non-dimensional water depth (z/h). Experimental values of WP 2 and WP 3, in figure 4a and b respectively, are compared with the predicted values. While the model is able to explain the velocity profile in WP 2 it does not explain the velocity profile for WP 3. Run WP 3 is characterized by a wave frequency of 1.4Hz and a wave height of 0.065 m. The model (equation (4.4)) is also compared to the results found for experiments with the presence of vegetation, but it is only applied to the layer above the penetration depth. Figures 4c and d show the results found in SRV 8 and SRV 9, respectively. In both figures, figure 4c and 4d, the 0 in the vertical axis corresponds to the penetration depth, i.e. z = 12 cm. Therefore, the value of water height, h, in the model is 18 cm. In addition, the height of the wave, H, decreases due to the vegetation drag (H = 0.038 m for f = 1 and 1.4 Hz). Taking into account these variations both runs, SRV 8 and SRV 9, are in the range of the second-order Stokes' theory. Figures 4e and 4f show results found for SFV 8 and SFV 9, respectively. For run SFV 8 the penetration depth is found to increase by the bottom. In this case the whole water column velocities are closely similar to the values predicted by the model. While experimental values found for SFV 8 agree well with model predictions, experimental values found for SFV 9 can not be explained by the model proposed by Longuet-Higgins (1953).

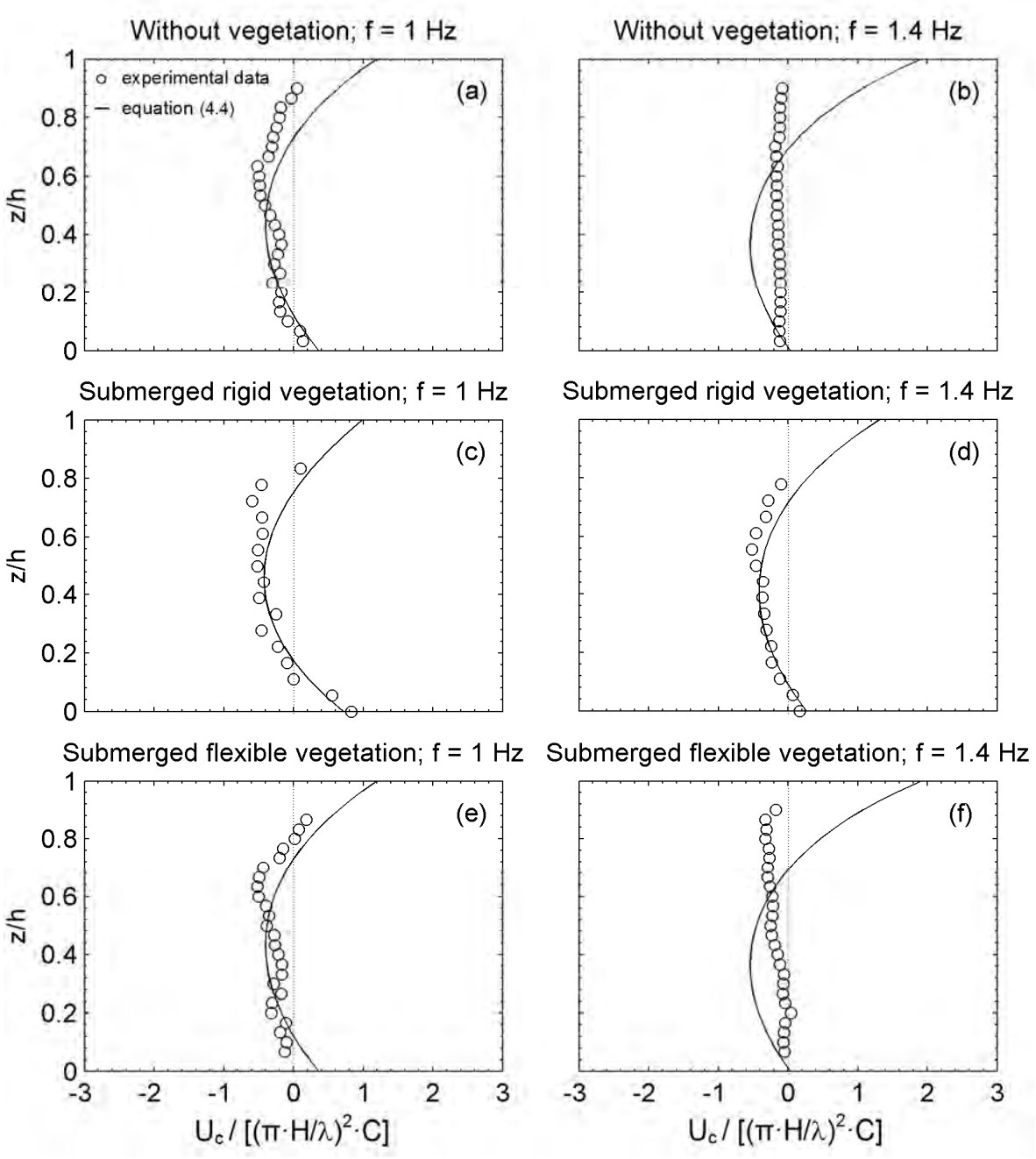

Figure 4.4. Vertical profile of adimensionalized mean current. (a) WP 2; (b) WP 3; (c) SRV 8; (d) SRV 9; (e) SFV 8 and (f) SFV 9.

4.3.2. Wave velocity (U_w^{rms})

Figure 4.5 shows profiles of U_w^{rms} measured for experiments with submerged rigid vegetation (Fig. 4.5a), submerged flexible vegetation (Fig. 5b) and emergent rigid vegetation (Fig. 4.5c), non-dimensionalized by U_w^{rms} without plants. The vertical profile of dimensionless U_w^{rms} for run SRV 3 is similar to that of WP 3. Experiments carried out with the largest plant density, (SRV 6:

SPF = 5% and SRV 9: SPF = 10%) show a slightly higher U_w^{rms} above the meadow than without vegetation at the same depth. In contrast, within the vegetation, U_w^{rms} is below 1, indicating that U_w^{rms} within the vegetation is smaller than U_w^{rms} without vegetation at the same depth. The highest reduction of U_w^{rms} is observed in the 2 cm below the top of the vegetation (with the value for the unvegetated zone decreasing to 20%). From that depth downwards U_w^{rms} remains constant. Vertical profiles of U_w^{rms} for flexible vegetation are shown in figure 4.5b. From the figure no differences can be appreciated when compared to those without vegetation, either above or within the vegetation. Experiments carried out for emergent vegetation are shown in figure 4.5c (ERV 3, ERV 6 and ERV 9). The lowest density run (ERV 3: SPF = 1%) presents a vertical profile of U_w^{rms} similar to that of without vegetation. ERV 6 and ERV 9, corresponding to the highest plant densities (SPF = 5% and 10%, respectively), show a stronger reduction of U_w^{rms}. In particular, for run ERV 9 there is a 45% attenuation of U_w^{rms}, whereas for run ERV 6 there is 25% attenuation.

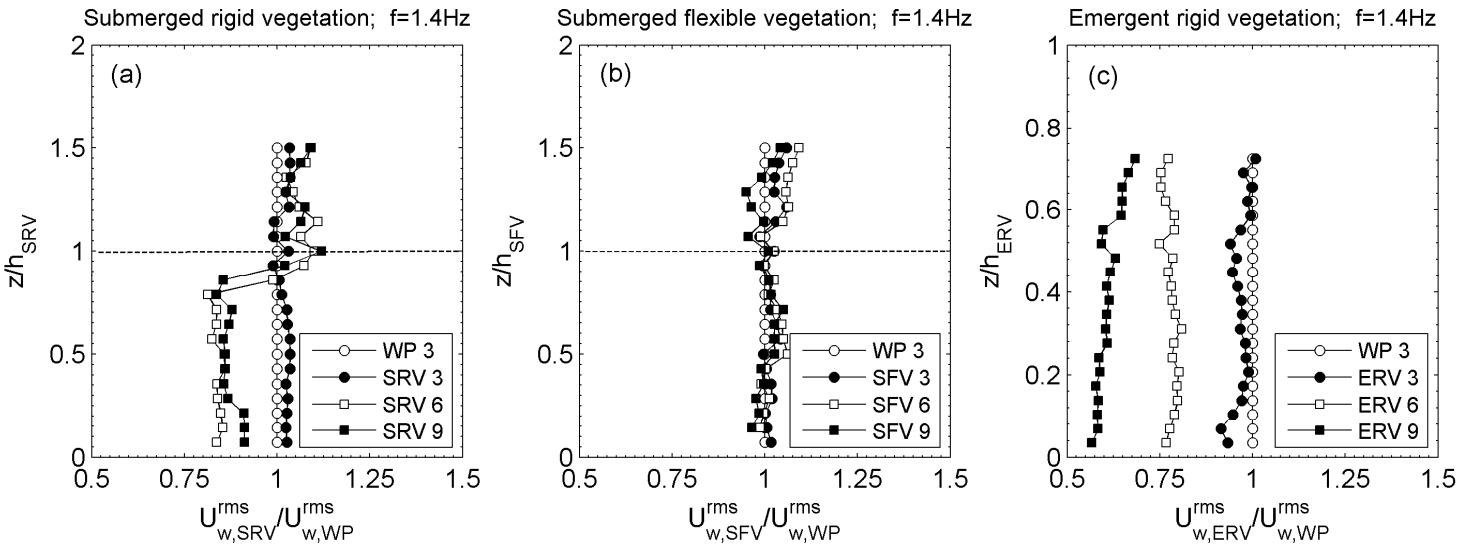

Figure 4.5. Comparison of vertical profile of adimensionalized RMS wave velocity, for different experiments. (a) WP 3, SRV 3, SRV 6 and SRV 9; (b) WP 3, SFV 3, SFV 6 and SFV 9, and (c) WP 3, ERV 3, ERV 6 and ERV 9. The horizontal dashed lines in figure 4.3a-b show the height of the canopy.

To calculate the attenuation of the wave motion, α_w, for submerged vegetation, equation (4.9) is used. For this purpose and knowing that present waves did not follow linear wave theory, $U_{\infty,w}^{rms}$ at $z = h_v$ was estimated according to Lowe et al. (2005a) and fitting the velocities in the canopy free flow to the function:

$$U_{\infty,w}^{rms} = a \cdot \cosh(bz) \qquad (4.11)$$

where a and b are constants. Profiles of $U_{\infty,w}^{rms}(z)$ obtained using this fitting method for experiments SRV 5 and SRV 6 are shown in figures 4.6a and 4.6b. Figures 4.7a and 4.7b show the canopy flow attenuation parameter, α_w, for the submerged rigid and flexible vegetation used in the experiment plotted as a function of the ratio of wave orbital excursion length and distance between stems, A_w^{rms}/S. In general there is a good match between model proposed by Lowe et al. (2005a) and present experiments (figure 4.7a and b). Independent of the density of the vegetation, our experiments are in the range of inertial force dominated, where reducing A_∞^{rms}/S has no effect on α_w. Submerged rigid vegetation presents a slightly higher attenuation than submerged flexible vegetation for the same stem density or S/d. As an example, for $n_s = 1280$ stems m^{-2} or S/d = 1.5, α_w for rigid vegetation is 0.78, whereas for flexible vegetation $\alpha_w = 0.83$.

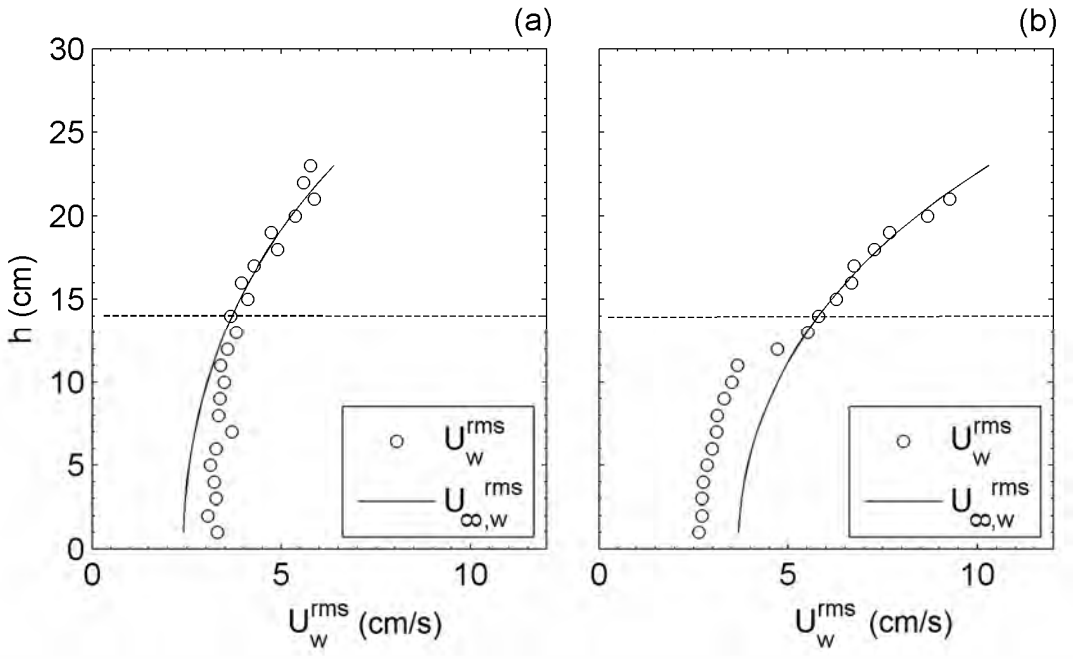

Figure 4.6. Comparison of RMS wave velocity, $U_w^{rms}(z)$ with the predicted potential flow field $U_{\infty,w}^{rms}(z)$ extrapolated into the canopy region using the fitting method in equation (4.11). (a) SRV 5 and (b) SRV 6.

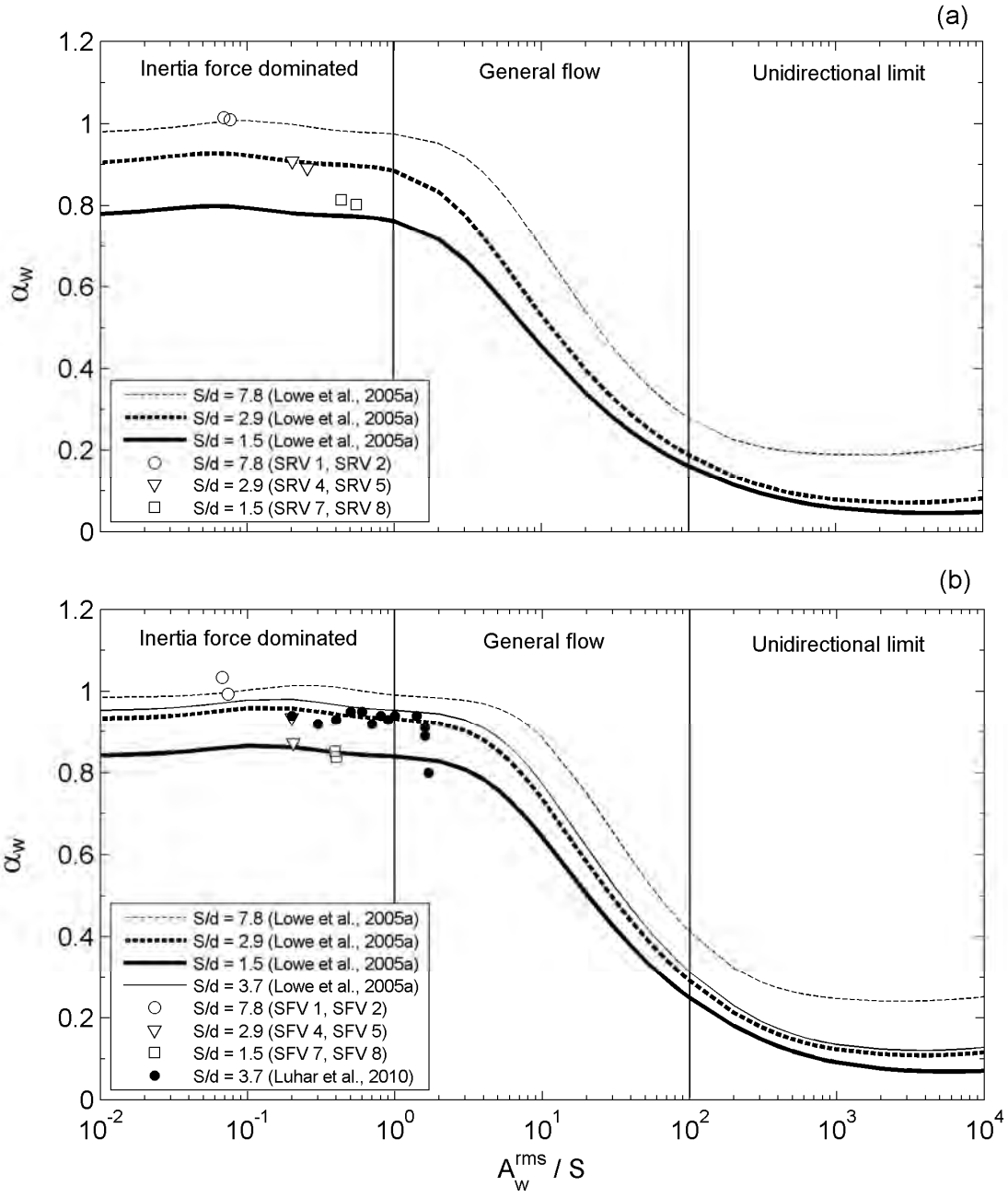

Figure 4.7. Canopy flow attenuation parameter α_w, plotted as a function of the ratio of wave orbital excursion length and the distance between stems, A_∞^{rms}/S. Lines correspond to the three densities or S/d used in the experiments and calculated by solving equation (10). (a) Experiment for submerged rigid vegetation. (b) Experiment for submerged flexible vegetation Vertical lines show the three flow regimes.

4.4. Discussion

Results demonstrate that the presence of vegetation modifies not only the mean current associated with an oscillating flow but also the orbital wave velocity.

4.4.1. Steady velocity associated with the current (U_c)

The presence of submerged rigid vegetation shifts the mean current upwards, generating an induced-current 2 cm downwards from the top of the canopy (SPF ≥ 5%). Unlike that without vegetation, where the thickness of the boundary layer at the bottom is ≈ 0.1 cm, the thickness of the boundary layer with the presence of vegetation is 12 cm, which could be considered the roughness of the bottom boundary layer. The presence of submerged rigid vegetation reduces the free water column available for the establishment of the mean currents (from z = 12 cm to the top of the water surface, i.e. h = 0.18 m).The current velocity agrees with the predicted values of the model proposed by Longuet-Higgins (1953) in equation (4.4) which has also observed by other authors in wave boundary layers (Luhar et al., 2010). Therefore, second-order Stokes theory is able to explain the mean current when the ratio H/h is lower than 0.21, considering h as the free water surface from the mean current to the top of the water surface.

Flexible submerged vegetation model has a weak effect on the mean current, i.e., the velocity profile is similar to that found in experiments without plants. Although the density of the plants (calculated as the ratio of the number of stems over the surface) is the same for both canopy models, the vertical structure of the vegetation is not the same. Flexible vegetation has a higher level of porosity, which in turn allows the penetration of the wave. Luhar et al. (2010) found a maximum mean current of 7.3 cm s^{-1} at z = 4 cm from the bottom. The difference in the result found between the present experiments ($U_c \approx$ -0.24±0.25 cm/s at z = 4 cm) and those of Luhar et al. (2010) is attributed to both the type of the wavemaker and the amplitude of the wave. Luhar et al. (2010) used a piston type wavemaker, whereas in the present study a flap type wavemaker is used. According to Dean and Darlymple (1991) the volume of water displaced over a whole stroke (S) for a piston wavemaker is $(H/S)_{piston} = kh$, whereas the volume of water displaced by a flap wavemaker is $(H/S)_{flap} = kh/2$.

For experiments conducted using the emergent rigid vegetation model (h_{ERV} = 29 cm), the flow structure is confined and completely changed the mean current in the water column. These observations are consistent with Lowe et al. (2008) whose experiments indicated a transition zone between h/h_V = 2.3 and 2.9. They defined a confined zone where shear layer began to dominate the flow structure. In such case, the ratio of the water depth to canopy height increases to a point where the flow structure becomes independent of further increases of depth.

Figure 4.8 shows a conceptual map of the mean current induced by waves for different flow conditions (unidirectional and oscillatory flow corresponding with dashed and solid lines, respectively) and different canopy structures: submerged rigid, submerged flexible and emergent rigid vegetation. Over a bare bed (Fig. 4.8a), the vertical profile of mean current under oscillatory flow shows a positive current, i.e. flowing into the direction of the wave propagation. This positive mean current is situated near the bottom and near the surface, whereas it becomes negative in the middle of the column. In our experiments, the presence of submerged rigid vegetation under oscillatory flow shifts the mean current profile upwards from d_p = 2 cm below the top of the vegetation up to the water surface (Fig. 4.8b). The vertical mean current profile in a canopy of flexible submerged vegetation is represented in Figure 4.8c. For the same oscillatory flow conditions as for submerged rigid vegetation, the flow is unaffected by the flexible vegetation. Finally, emergent rigid vegetation not only does not reduce the mean current under oscillatory flow, but it is stronger and negative inside the vegetation, i.e. in the opposite direction of the wave propagation (Fig. 4.8d). The behaviour of the vertical profile of mean current for oscillatory flow with the presence of submerged rigid vegetation is analogous to that found for unidirectional flows (Nepf and Vivoni, 2000; Reidenbach et al., 2007). These authors showed that the presence of vegetation under unidirectional flow shifts the logarithmic profile from 2 cm below the top of the water surface down to the top of the canopy (Fig. 4.8b).

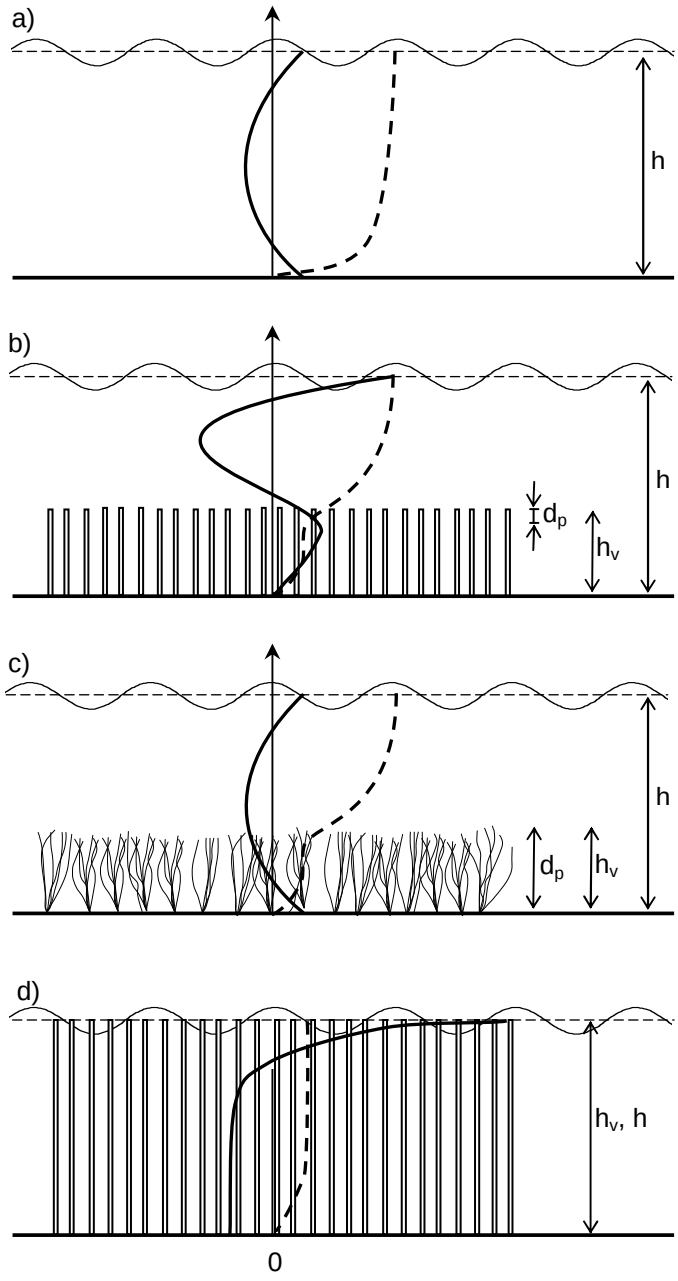

Figure 4.8. Velocity profiles of $U_c(z)$, for three seagrass structures and two height ratios, h_v/h, where h_v is the height of the canopy and h is the height of the water. Solid lines represent the vertical profile $U_c(z)$ under oscillatory conditions and dashed lines represent the vertical profile $U_c(z)$ under unidirectional conditions. (a) without vegetation; (b) submerged rigid vegetation which shift $U_c(z)$ upwards. There is a penetration depth d_p, around 2 cm from the top of the canopy; (c) flexible submerged vegetation and (d) emergent rigid vegetation.

4.4.2. Wave velocity (U_w^{rms})

Vertical profile of wave motion U_w^{rms}, shows a fully developed boundary layer. The reduction of U_w^{rms} inside the submerged rigid vegetation is greater for the largest densities corresponding to SPF = 5% and 10% (20% for SRV 6 and SRV 9, Fig. 4.5a). In addition, for emergent rigid vegetation a larger reduction of wave velocity compared to submerged vegetation for the same plant density is observed (45% for ERV 9, Fig. 4.5c). Therefore both plant density and plant height, modify the wave velocity inside the meadow. This result is in accordance with the values found in the field by Hansen and Reidenbach (2012) who established that the smallest within-canopy flow reduction occurred in the eelgrass with the lowest density and the smallest average blade length. Both parameters, density and blade length, can have an impact on flow processes.

The canopy flow attenuation parameter is calculated using equation (4.9) and plotted as a function of the wave orbital length A_∞^{rms} divided by S and compared to model proposed by Lowe et al. (2005a) (Fig. 4.7). The figure shows that for any submerged vegetation experiments (rigid and flexible, Fig 4.7a and b, respectively), flow conditions were inertia force dominated. The canopy inertia force (C_m) is expected to contribute mostly to the attenuation of the oscillatory canopy flow in that region (Lowe et al., 2005a). As it is said in methods section, the drag and friction coefficients, related to steady flow terms, are assumed to be C_d = 2.5 and C_f = 0.01 for rigid vegetation and C_d = 1 and C_f = 0.01 for flexible vegetation and the inertial force coefficient is assumed to be C_m = 2 for rigid vegetation and C_m = 1.2 for flexible vegetation.

As the model predicts, and the present experiments corroborate, at increasing SPF density for submerged rigid and flexible vegetation, the flow reduction is enhanced compared to the flow above the canopy. In particular, the attenuation coefficient in that region is slightly lower in submerged rigid vegetation than in flexible vegetation, showing that rigid structure better attenuates the wave velocity, in contrast to flexible structures which the movement of the blades allow the path of the wave.

The model proposed by Lowe et al. (2005a) for submerged vegetation can be applied to surface waves when $U_{\infty,w}^{rms}$ varies minimally in depth, which will occur at $kh_v << 1$. In that case, the attenuation of α_w is caused by both the vegetation and bottom drag parameters. Experiments carried out at f = 0.8 and 1 Hz have values of kh_v smaller than 1 (0.4 and 0.63, respectively). However, for f = 1.4 Hz the kh_v found is higher than 1. In this situation, the attenuation of α_w is primarily due to natural attenuation of high frequency wave motions with depth. Therefore, $U_{\infty,w}^{rms}$ varies too much in depth and the procedure above cannot be applied (Fig. 4.6b).

4.4.3. Ecological implications of the ratio h_v/h

The mean current, generated within the model canopy bed when it is forced by purely oscillatory wave-driven flow, is forced by a nonzero wave stress similar to the streaming observed in wave boundary layers. The induced current could play an important role in determining both the health of submerged canopy beds and their ecological contribution. It is well known that the mean current is able to speed up the rate of water renewal within a meadow thus enhancing the nutrient cycling capabilities of canopy, as well as generating net transport of sediments, such as seeds and pollen, in the direction of wave propagation (Luhar et al., 2010). Submerged rigid vegetation with $h_{SRV}/h \approx 0.47$ has a positive mean current in the direction of the wave inside the vegetation, whereas emergent rigid vegetation with $h_{ERV}/h \approx 0.97$ has a stronger negative mean current at the same depth. Therefore, it changes the direction of the mean current which implies a change in the direction of the water renewal, which in turn has effects on the net transport of sediments, nutrients, seeds and pollen. This is crucial in order to understand the dynamics of seed propagation and nutrient renewal when restoring a damaged zone.

4.4.4. Ecological implications of rigidity vs. flexibility

The submerged rigid canopy model used in this experiment could mimic coral reefs. It is well known that many coral communities are located in nutrient limited environments (Falter et al., 2004). Therefore, the capacity of the rate of material transfer between seawater and the coral community will determine the growth rate of this community. Coral reefs do not photosynthesize, but rather have a symbiotic relationship with some algae which do the photosynthesis. In unidirectional flow conditions higher values of turbulent kinetic energy in rigid structures, such as coral reef canopies, rather than in bare beds have been observed (Nepf, 1999). Turbulence found inside the meadow has positive biological consequences, such as improvement in the transfer of CO_2 (in the form of bicarbonate) from the water to the surface layer of leaves. Without turbulence, the only physical mechanism capable of capturing CO_2 would be by means of molecular diffusion from the boundary layer, an extremely inefficient transport mechanism (Denny, 1988). In unidirectional flow, stem-wake turbulence is observed when the stem Reynolds number (Re) exceeds approximately 100 (Zong and Nepf, 2010). The stem Reynolds number is defined by the mean current velocity within the meadow and the stem diameter for rigid plants or blade width for flexible plants. Pujol and Nepf (2012) carried out experiments in a meadow subjected to an isolated breaker, which generated a wave packet. They found high levels of TKE which were attributed to the generation of stem-wake turbulence caused by the elevated near-bed wave velocity during a breaking wave event ($Re_w > 100$, and calculated as the maximum wave velocity within the meadow and the blade width, w_b). In the present experiment, the Reynolds number associated with the mean current is $Re_c \approx 100$ (at $z = 12$ cm) and the Reynolds number associated with the wave velocity $Re_w > 100$. Both

Reynolds numbers indicate a stem-wake presence behind the stem. Therefore, the rigidity could be an important parameter, enhancing the transfer of material between seawater and the benthic community, such as coral reefs.

The submerged flexible vegetation model is dynamically similar to *Posidonia oceanica,* which is found in nutrient rich zones. The mean current induced by waves found within flexible submerged vegetation is too weak to produce stem-wake behind the plants with $Re_c < 100$, compared to the values of $Re_c \approx 100$ found for rigid vegetation. Therefore, under our wave conditions the principal mechanism to generate stem-wake (i.e., turbulence) within the flexible meadow is caused by a wave velocity characterized with a $Re_w > 100$. However, Luhar et al. (2010), who carried out experiments with flexible submerged vegetation, observed an increase in the near-bed turbulence within the meadow as compared with the same wave condition over smooth beds. Those differences are attributed to both the type of the wavemaker and the amplitude of the wave. Furthermore, Bradley and Houser (2009) observed that, as the oscillatory velocity increases the seagrass becomes fully extended and leans in the direction of flow for a longer part of the wave cycle. The blade posture can control light uptake. An increase in the horizontal projected leaf also leads to higher photosynthesis. Therefore, under the wave crest, there is an enhancement of the productivity in seagrass meadows (Zimmerman, 2003).

4.5. Conclusions

This paper considers how the presence of different vegetation structures alters the vertical profiles of current-induced progressive waves. Waves generated in the present experiments followed the second-order and third-order Stokes theory. The vertical profile of the current-induced in second-order waves without vegetation fits well with the model proposed by Longuet-Higgins (1953). Submerged and emergent vegetation clearly modify the current induced by the waves. Submerged rigid vegetation acts like a false floor, shifting the vertical profile of the mean current upward. The Longuet-Higgins' model applied above the vegetation fits well with present experiments with submerged rigid vegetation. A penetration depth around 2 cm below the top of submerged rigid vegetation is observed. Reynolds numbers at this depth are higher than 100, generating a wake-stem behind the plant models. For the other runs, the vertical profile of mean current did not present changes with respect to runs without plants. Emergent rigid vegetation reverses the direction of current-induced waves. That effect has important consequences in understanding the dynamics of the transport of both seeds and nutrients, which, in turn, have important implications for the canopy development and the whole ecosystem itself. Although flexible submerged vegetation reduces wave velocity, it does not generate a mean current. Rigidity could be one of the most important parameters to enhance the transfer rates of material between seawater and benthic community. A 20% reduction in the wave velocity for the densest seagrass for submerged rigid vegetation is also observed, whereas for emergent vegetation the

reduction is even higher, i.e., of 45%. Therefore, the density and height of the plants are the determinants parameters to explain the wave velocity reduction.

Acknowledgements Dolors Pujol was supported by the research fellowship BR08/11 of the University of Girona. We are also grateful to the Spanish Government's support through the *Ministerio de Ciencia e Innovación* with grant CGL 2010-17289 and to the support from the Fundación Biodiversidad through the project 9112019.

References

Batisse M., Jeudy de Grissac A., 1995. Marine region 3: Mediterranean, in: Kelleher G., Bleakley C., Wells S. (Eds.), A global representative system of marine protected areas, Book 1. Great Barrier Reef Marine Park Authority, World Bank, and World Conservation Union,

Blanchette, C.A., 1997. Size and survival of intertidal plants in response to wave action: A case study with *Fucus gardneri*. Ecology 78, 1563-1578.

Bradley, K., Houser, C., 2009. Relative velocity of seagrass blades: Implications for wave attenuation in low-energy environments. J. Geophys. Res-Earth. 114, F01004.

Chen, S-C., Kuo, Y-M., Li, Y-H., 2011. Flow characteristics within different configurations of submerged flexible vegetation. J. Hydrol., 398, 124-134.

Coops, H., VanderVelde, G., 1996. Effects of waves on helophyte stands: Mechanical characteristics of stems of *Phragmites australis* and *Scirpus lacustris*. Aquat. Bot. 53, 175-185.

Dean, R.G., Dalrymple, R.A., 1991. Water wave mechanics for engineers and scientists, 2 printing with corrections ed. World Scientific, Singapore; Teaneck, NJ.

Denny, M.W., 1988. Biology and the mechanics of the wave-swept environment, Princeton University Press, Princeton.

Falter, J., Atkinson, M., Merrifield, M., 2004. Mass-transfer limitation of nutrient uptake by a wave-dominated reef flat community. Limnol. Oceanogr. 49, 1820-1831.

Folkard, A.M., 2005. Hydrodynamics of model *Posidonia oceanica* patches in shallow water. Limnol. Oceanogr. 50, 1592-1600.

Fonseca, M.S., Cahalan, J.A., 1992. A preliminary evaluation of wave attenuation by 4 species of seagrass. Estuar. Coast. Shelf. Sci. 35, 565-576.

Fonseca, M., Bell, S., 1998. Influence of physical setting on seagrass landscapes near Beaufort, North Carolina, USA. Mar. Ecol-Prog. Ser. 171, 109-121.

Fonseca, M., Fisher, J., 1986. A comparison of canopy friction and sediment movement between 4 species of seagrass with reference to their ecology and restoration. Mar. Ecol-Prog. Ser. 29, 15-22.

Fredsøe, J., Deigaard, R., 1992. Mechanics of coastal sediment transport, World Scientific, Singapore; New Jersey.

Gambi, M.C., Nowell, A.R.M., Jumars, P.A., 1990. Flume observations on flow dynamics in *Zostera marina* (eelgrass) beds. Mar. Ecol-Prog. Ser. 61, 159-169.

Ghisalberti, M., Nepf, H., 2006. The structure of the shear layer in flows over rigid and flexible canopies. Environ. Fluid Mech. 6, 277-301.

Ghisalberti, M., Nepf, H., 2002. Mixing layers and coherent structures in vegetated aquatic flows. J. Geophys. Res. Oceans.107, C2.

Gleason, M., Pien, N., Fisher, J., 1979. Effects of stem density upon sediment retention by salt-marsh cord grass, *Spartina-Alterniflora Loisel*. Estuaries 2, 271-273.

Granata, T.C., Serra, T., Colomer, J., Casamitjana, X., Duarte, C.M., Gacia, E., 2001. Flow and particle distributions in a nearshore seagrass meadow before and after a storm. Mar. Ecol-Prog. Ser. 218, 95-106.

Hansen, J.C.R., Reidenbach, M.A., 2012. Wave and tidally driven flows in eelgrass beds and their effect on sediment suspension. Mar. Ecol-Prog. Ser. 448, 271-287.

Infantes, E., Terrados, J., Orfila, A., Canellas, B., Alvarez-Ellacuria, A., 2009. Wave energy and the upper depth limit distribution of *Posidonia oceanica*. Bot.Mar. 52, 419-427.

Koch, E.W., Gust, G., 1999. Water flow in tide- and wave-dominated beds of the seagrass *Thalassia testudinum*. Mar. Ecol-Prog. Ser. 184, 63-72.

Lamb, H., 1945. Hydrodynamics. Dover, New York

Lefebvre, A., Thompson,C.E.L., Amos,C.L., 2010. Influence of *Zostera marina* canopies on unidirectional flow, hydraulic roughness and sediment movement. Cont.Shelf Res. 30, 1783-1794.

LeMéhauté, B., 1976. An introduction to hydrodynamics and water waves, Springer-Verlag, New York.

Lewis, J., 1968. Water movements and their role in rocky shore ecology. Sarsia. 34, 13-36.

Longuet-Higgins, M., 1953. Mass transport in water waves. Philosophical Philos. Trans. R. Soc. London, Ser. A. 245, 535-581.

Lowe, R., Koseff, J., Monismith, S., 2005a. Oscillatory flow through submerged canopies: 1. Velocity structure. J. Geophys. Res. Oceans. 110, C10016.

Lowe, R., Koseff, J., Monismith, S., Falter, J., 2005b. Oscillatory flow through submerged canopies: 2. Canopy mass transfer. J. Geophys. Res. Oceans. 110, C10017.

Lowe, R., Falter, J., Koseff, J., Monismith, S., Atkinson, M., 2007. Spectral wave flow attenuation within submerged canopies: Implications for wave energy dissipation. J. Geophys. Res. Oceans. 112, C5.

Lowe, R., Shavit, U., Falter, J., Koseff, J., Monismith, S., 2008. Modeling flow in coral communities with and without waves: A synthesis of porous media and canopy flow approaches. Limnol. Oceanogr., 53, 2668–2680.

Luhar, M., Rominger, J., Nepf, H., 2008. Interaction between flow, transport and vegetation spatial structure. Environ. Fluid Mech. 8, 423-439.

Luhar, M., Coutu, S., Infantes, E., Fox, S., Nepf, H., 2010. Wave-induced velocities inside a model seagrass bed. J. Geophys. Res. Oceans. 115, C12005.

Luhar, M., Nepf, H., 2011. Flow induced reconfiguration of buoyant and flexible aquatic vegetation. Limnol. Ocean. 56, 2003-2017.

Mendez, F.J., Losada, I.J., 2004. An empirical model to estimate the propagation of random breaking and nonbreaking waves over vegetation fields. Coast.Eng. 51, 2, 103-118.

Menge, B. 1976. Organization of the New England rocky intertidal community: role of predation, competition, and environmental heterogeneity, Ecol. Monogr. 46, 355–393.

Nepf, H., 1999. Drag, turbulence, and diffusion in flow through emergent vegetation. Water Resour. Res. 35, 479-489.

Nepf, H., Vivoni, E.R., 2000. Flow structure in depth-limited, vegetated flow. J. Geophys. Res. Oceans. 105, 28547-28557.

Neumeier, U., Ciavola, P., 2004. Flow resistance and associated sedimentary processes in a *Spartina maritima* salt-marsh. J.Coast.Res. 20, 435-447.

Pergent-Martini, C., Pasqualini, V., Ferrat, L., Pergent, G., 2006. Ecological data in integrated coastal zone management: Case study of *Posidonia oceanica* meadows along the Corsican coastline (Mediterranean sea). Environ.Manage. 38, 889-895.

Perrin, R., Cid, E., Cazin, S., Sevrain, A., Braza, M., Moradei, F., Harran, G., 2007. Phase averaged measurements of the turbulence properties in the near wake of a circular cylinder at high Reynolds number by 2C-PIV and 3C-PIV. Exp. Fluids 42, 93-109.

Pujol, D., Colomer, J., Serra, T., Casamitjana, X., 2010. Effect of submerged aquatic vegetation on turbulence induced by an oscillating grid. Cont. Shelf. Res. 30, 1019–1029.

Pujol, D. Colomer, J., Serra, T., Casamitjana, X., 2012. A model for the effect of submerged aquatic vegetation on turbulence induced by an oscillating grid. Estuar. Coast. Shelf Sci. 114, 23-30.

Pujol, D., Nepf, H., 2012. Breaker-generated turbulence in and above a seagrass meadow. Cont. Shelf. Res. 49, 1-9.

Reidenbach, M.A., Koseff, J.R., Monismith, S.G., 2007. Laboratory experiments of fine-scale mixing and mass transport within a coral canopy. Phys.Fluids 19, 075107.

Reusch, T., Chapman, A., 1995. Storm effects on eelgrass (*Zostera-Marina L*) and blue mussel (*Mytilus-Edulis-L*) beds rid. J. Exp. Mar. Biol. Ecol. 192, 257-271.

Stokes, G., 1847. On the theory of oscillatory waves. Trans. Camb. Phil. Soc. 8, 441–455.

Sung, J., Yoo, J.Y., 2001. Three-dimensional phase averaging of time-resolved PIV measurement data. Meas Sci Technol 12, 655-662.

Tanino, Y., Nepf, H., 2008. Lateral dispersion in random cylinder arrays at high Reynolds number. J. Fluid Mech. 600, 339-371.

Thomas, F., Cornelisen, C., 2003. Ammonium uptake by seagrass communities: effects of oscillatory versus unidirectional flow. Mar. Ecol. Prog. Ser. 247, 51-57.

Vogel, S., 1994. Life in Moving Fluids. Princeton Univ. Press, Princeton,N. J.

Ward, L.G., Kemp, W.M., Boynton, W.R., 1984. The influence of waves and seagrass communities on suspended particulates in an estuarine embayment. Mar. Geol. 59, 85-103.

Wlezien, R.W., Way, J.L., 1979. Techniques for the experimental investigation of the near wake of a circular-cylinder. AIAA J. 17, 563-570.

Zimmerman, R., 2003. A biooptical model of irradiance distribution and photosynthesis in seagrass canopies. Limnol.Oceanogr. 48, 568-585.

Zong, L., Nepf, H., 2010. Flow and deposition in and around a finite patch of vegetation. Geomorphology 116, 363-372.

Chapter 5

Canopy-scale turbulence under oscillatory flow

Pujol, D[1]., Casamitjana, X[1]., Serra, T[1]., Colomer, J[1].

[1]Department of Physics, Escola Politècnica Superior-II, Campus Montilivi, 17071 Girona, Catalonia, Spain

Submitted to: *Continental Shelf Research*

Abstract The aim of this study is to understand the turbulent flow structure inside and above diverse canopy models dominated by progressive waves. A set of experimental conditions was considered in a laboratory flume: three vegetation models (submerged rigid, submerged flexible and emergent rigid), three plant densities (128, 640 and 1280 stems m^{-2}) and three wave frequencies (f = 0.8, 1 and 1.4 Hz). For the submerged rigid model, observations suggested that above the vegetation the turbulent kinetic energy (TKE) remained higher than of that without vegetation, and this was attributed to the redistribution of the TKE at a lower volume, enhanced mainly by the largest plant density. Within the submerged rigid model, larger TKE were found compared with the case without vegetation, therefore the canopy model did not produce any sheltering. The increase of TKE was associated with the penetration of wave velocity which in turn, produced stem-wake turbulence. Sheltering was only found well inside the vegetation for the largest plant density and highest wave frequency. In this case, the generation of stem-wake turbulence and the production of TKE produced a great loss of wave velocity was confined to the very top of the canopy. Sweeps and ejections were the predominant events, enhancing the transfer of mass at the top of the canopy. Within the flexible vegetation, the movement of the blades dissipated the wave energy resulting in lower levels of TKE; a maximum reduction of 46% was found for the highest density and wave frequency when compared to the case without vegetation. For emergent rigid vegetation the TKE was always found to be lower at all depths compared with runs without plants, and this reduction is attributed to the inhibition of the wave energy at all depths. A maximum reduction of 48% was found for the highest density and wave frequency.

Keywords Aquatic vegetation model; progressive waves; wave velocity; stem-wake turbulence; turbulent kinetic energy; reynolds stress.

5.1. Introduction

The role of seagrass meadows in coastal zones has received a lot of attention as it provides a refuge for fish, invertebrates and plankton. The principal mechanism dominating the submerged meadows is the reduction of waves and currents; i.e. the local hydrodynamic can be drastically altered depending on the vegetation density and flow conditions. Wave-induced forces are believed to set the distribution of seagrass populations (Fonseca and Bell, 1998). Specifically, waves have been noted to determine the upper depth limit distribution of submerged aquatic vegetation, such as *Posidonia oceanica* (Infantes et al., 2009), and influence species size, morphology, and distribution patterns (Lewis, 1968; Menge, 1976; Blanchette, 1997).

Previous studies, using rigid and flexible vegetation models, have successfully described the turbulence structure for aquatic vegetation subjected to unidirectional flow (Nepf, 1999; Nepf and Vivoni, 2000; Folkard, 2005; Ghisalberti and Nepf, 2006; Luhar et al., 2008; Tanino and Nepf, 2008; Lefebvre et al., 2010). Some of the current and wave energy dissipated by aquatic vegetation is converted into turbulent kinetic energy within the meadow. Two distinct scales of turbulence have been identified within aquatic canopies. First, turbulence is generated in the wakes of individual blades and stems if the Reynolds number based on the stem-diameter (or blade width) is larger than about 100 (Anderson and Charters, 1982; Tanino and Nepf, 2008). Second, the drag discontinuity at the top of a submerged meadow produces a shear layer that generates canopy-scale turbulence which is transmitted downward into the canopy (Ghisalberti and Nepf, 2002; Neumeier and Amos, 2006). In addition, turbulence generated above the canopy, e.g. by wind-driven stirring, can also penetrate into the canopy. According to Pujol et al. (2010), the penetration of turbulence generated above the canopy is damped by canopy drag.

Turbulence inside the meadow has positive biological consequences such as improving the transfer of CO_2 (in the form of bicarbonate) from the water to the surface layer of leaves. Without turbulence, the only physical mechanism capable of capturing CO_2 would be by means of molecular diffusion from the boundary layer, an extremely inefficient transport mechanism (Denny, 1988). Recent findings suggest that biological processes, such as nutrient uptake, may often be controlled by surface wave motion rather than the steady component of velocity that has received considerably more attention (Koch and Gust, 1999; Thomas and Cornelisen, 2003; Lowe et al., 2005b). As an example, Reidenbach et al. (2007) suggest that wave motion adds a wave-induced enhancement of water motion within a coral canopy, increasing the flux of water (and entrained dissolved and particulate matter) to and from the coral structure.

Some authors have studied the effects of seagrass or coral reef structures on a wave dominated flow in both laboratory and field experiments (Coops et al., 1996; Lowe et al., 2005a; Reidenbach et al., 2007; Luhar et al., 2010; Hansen and Reidenbach, 2012; Infantes et al., 2012; Pujol and Nepf, 2012). Pujol and Nepf (2012) found that the passage of a breaking wave in a seagrass model produced roughly twice as much and even more persistent TKE than of

that without plants. This is attributed to the generation of stem-wake turbulence by the elevated near-bed orbital velocity during the passage of the wave packet. Reidenbach et al. (2007) found that the peaks in normal and shear stresses coincided with regions of separation in the boundary layer as turbulent vortices were shed from the surfaces of the coral during the forward and reverse motions of the wave. This is a key mechanism for imparting mixing and drives the overall exchange with the water column. Although these findings deal with the impact of aquatic vegetation on the turbulence structure for oscillatory flow, it is unclear how differing canopy models (density and typology) modify the turbulence flow within and above the meadow.

Our experiments are aimed at studying the distribution of turbulence structure within vegetation models characterized by a set of plant and wave characteristics such as vegetation height, flexibility, vegetation density and wave frequency. Turbulence structure is described in terms of the vertical distribution of normal stresses, shear stresses, TKE and the production and dissipation of TKE.

5.2. Methods

The study was conducted in a 6 x 0.5 x 0.5 m wave flume. A schematic of the setup is shown in Figure 1a. The mean water height, h, was 0.3 m. A plywood beach, with a slope of 1:3 and covered with a 7-cm layer of foam rubber, was located at the end of the tank. A vertical paddle, called a flap type wavemaker, was introduced at the front of the tank and was driven by a variable-speed motor located outside the tank. We define the longitudinal direction as x, and x = 0 at the wavemaker; y is the lateral direction and y = 0 at the centreline of the tank, and z is the vertical direction, with z = 0 at the flume bed.

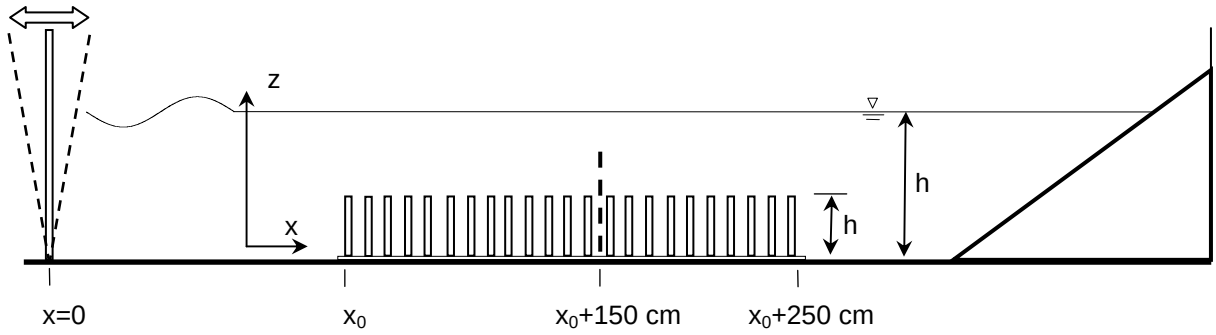

Figure 5.1. Scheme of the laboratory experiments. (a) Experiments were conducted in a 6 m long flume. The streamwise coordinate is denoted by x, with x positive in the downstream direction, and x = 0 at the mean position of the wavemaker. The vertical coordinate is z, with z = 0 at the bed. The mean water depth, d, is 30 cm. The mean plant height in still water is $h_{v,S}$ = 14cm for submerged rigid and flexible vegetation and $h_{v,E}$ = 29 cm for emergent rigid vegetation. The model meadow was 250-cm long. The vertical dashed line indicates the position of the velocity profile measured using a Sontek MicroADV and a Nortek Vectrino. Note that dimensions in the figure are given in cm and the beach slope at the end of the tank are not scaled.

5.2.1. Vegetation quantification

To construct the meadow, individual plants were inserted into a predrilled baseboard of 2.5 m in length. The characteristics of the plants varied greatly in terms of height, plant density, and morphology. In order to obtain features in the laboratory similar to those in the field, 30 different situations were studied featuring three canopy models (submerged rigid, submerged flexible and emergent rigid vegetation), two canopy heights (h_v = 14 and 29 cm), three density of vegetation models (n_s = 128, 640 and 1280 stems m^{-2}) and three oscillating frequencies (f = 0.8, 1 and 1.4 Hz). A flexible vegetation model was constructed from high polyethylene blades attached by a plastic band to a PVC dowel 2 cm long and 1 cm in diameter. The flexible vegetation model was geometrically and dynamically similar to typical seagrasses, as described by the dimensionless parameters λ_1 and λ_2 (Ghisalberti and Nepf, 2002). Therefore, 30 wave flow experiments were conducted and denoted as, WP 1–WP 3 for experiments without plants, SRV 1–SRV 9 for the submerged rigid vegetation model, SFV 1-SFV 9 for the submerged flexible vegetation model and ERV 1-ERV 9 for the emergent rigid vegetation model (Table 5.1).

Table 5.1. Summary of the wave and vegetation parameters for each experiment.

Run	Canopy model	h_v (cm)	n_s(stems/m^2)	f (Hz)
WP 1	Without vegetation			0.8
WP 2				1
WP 3				1.4
SRV 1	Submerged rigid model	14	128	0.8
SRV 2				1
SRV 3				1.4
SRV 4			640	0.8
SRV 5				1
SRV 6				1.4
SRV 7			1280	0.8
SRV 8				1
SRV 9				1.4
SFV 1	Submerged flexible model	14	128	0.8
SFV 2				1
SFV 3				1.4
SFV 4			640	0.8
SFV 5				1
SFV 6				1.4
SFV 7			1280	0.8
SFV 8				1
SFV 9				1.4
ERV 1	Emergent rigid model	29	128	0.8
ERV 2				1
ERV 3				1.4
ERV 4			640	0.8
ERV 5				1
ERV 6				1.4
ERV 7			1280	0.8
ERV 8				1
ERV 9				1.4

5.2.2. Measuring technique

The Eulerian velocity field was defined as (u, v, w) in the (x, y, z) directions, respectively. The three components of velocity were recorded with a downward-looking Acoustic Doppler Velocimeter (Sontek/YSI16-MHzMicroADV). The ADV instrument was configured to transmit 50 acoustic signals per second with a sampling time interval of 10 min (i.e. 30000 records per sample). To avoid spikes, beam correlations from ADV measurements lower than 70% and instantaneous velocities higher than two standard deviations were discarded. The ADV, which was operated manually, was mounted on a movable vertical frame that operated from the bottom (z = 1 cm) up to z = 21 cm. It was limited at the upper part by both, the wave shape and the 5 cm distance from the ADV to the sampling volume.

For each experiment, a vertical profile was taken over a height range of z = 1 – 21 cm at 1 cm space-interval velocity from the bottom of the tank. In order to obtain valid data acquisition within the canopy, just a few stems were removed to avoid blocking the pathway of the ADV beam, as was done by Luhar et al. (2010). To minimise the effect of this 'hole', its shape was specifically designed to allow the ADV acoustic receivers and the acoustic transmitter to perform properly.

5.2.3. Methods of analysis

For general wave flows, the instantaneous velocity, e.g. u_i is decomposed as:

$$u_i = u_c + u_w + u' \tag{5.1}$$

where u_c is the steady velocity associated with the current, u_w is the unsteady wave motion which represents spatial variations in the phase averaged velocity field, and u' is the turbulent velocity. u_c is the space and phase-averaged velocity defined as (Lowe et al., 2005a; Luhar et al.,2010):

$$u_c = \frac{1}{2\pi}\int_0^{2\pi} u_i(\varphi)\,d\varphi \tag{5.2}$$

where $u_i(\varphi)$ is the instantaneous velocity as a function of the wave phase. Wave velocity, u_w, was obtained by using a phase averaging technique. That is, the Hilbert Transform technique was used to average oscillatory flow velocities with a common phase, as in Wlezien and Way (1979), Perrin et al. (2007) and Sung and Yoo (2001). Then, u_w is defined as:

$$u_w = u_i(\varphi) - u_c \tag{5.3}$$

Then, turbulent velocity is calculated by subtracting the mean and the wave velocity from the instantaneous velocity:

$$u' = u_i - u_c - u_w \tag{5.4}$$

Hereafter subscript (w) refers to oscillatory flows or unsteady wave motion (u_w), subscript (c) refers to unidirectional flows or steady velocity (u_c) and turbulent velocities are represented by prime symbols (u').

Then, Turbulent Kinetic Energy (TKE) is calculated as:

$$TKE = \frac{1}{2}\left(\left\langle u'^2 \right\rangle + \left\langle v'^2 \right\rangle + \left\langle w'^2 \right\rangle\right) \tag{5.5}$$

where < > denote the ensemble average of the horizontal and vertical velocities.

The TKE difference between samples with and without plants and expressed as a percentage, is calculated according to:

$$\Delta TKE(z) = \left(\frac{TKE_{vegetation}(z) - TKE_{WP}(z)}{TKE_{WP}(z)}\right)\cdot 100 \tag{5.6}$$

where the $TKE_{vegetation}$ is the TKE measured at z with the presence of vegetation model and the TKE_{WP} is the TKE measured at z without the presence of vegetation model. Negative $\Delta TKE < 0$, indicates a reduction of TKE. In contrast, positive values of $\Delta TKE > 0$ imply TKE generation, indicating that TKE in experiments with plants is higher than in experiments without plants.

The structure of the measured turbulent stress was also analyzed. The turbulent stress is presented as the sum of contributions measured on four quadrants of the (u', w') plane. It provides detailed information on the contribution to the total turbulence production from various events occurring in the flows (Willimarth and Lu, 1972; Wallace et al. 1972). The analysis divides the turbulent stress into four categories according to the signs of u' and w' which, in the following, are called $\langle u'w' \rangle_Q$, where Q means the number of the quadrant corresponding to each category (Q = 1 – 4). Therefore,

$$\left\langle u'w' \right\rangle_Q = \frac{\sum (u'w')_Q}{N_Q} \tag{5.7}$$

The first quadrant is defined as u' > 0 and w' > 0 and which contains outward motion of high-speed fluid ($\langle u'w' \rangle_1$); the second quadrant is u' < 0 and w' > 0 and which contains the motion associated with ejections of low-speed fluid moving away from the top of the canopy ($\langle u'w' \rangle_2$); the third quadrant is u' < 0 and w' < 0 and which contains inward motion of low-speed fluid ($\langle u'w' \rangle_3$) and the forth quadrant is u' > 0 and w' < 0 and which contains an inrush of high-speed

fluid, called sweep event ($<u'w'>_4$). Thus, the second and fourth quadrant events contribute to the negative shear stress (positive production), and the first and third quadrant events contribute to the positive shear stress (negative production) (Kim et al., 1987).

Assuming a homogeneous flow and neglecting viscous stress, the turbulent kinetic energy budget within a canopy may be expressed as (Brunet et al., 1994):

$$\frac{\partial TKE}{\partial t} = 0 = P_s + P_{wk} + \varepsilon + T \qquad (5.8)$$

where the shear production is calculated as $P_s = -<u'w'>\cdot\delta U/\delta z$, and where U can be either u_w or u_c. In the first case, the production is due to shear caused by the wave and in the second case to shear caused by the mean current. The turbulence production associated with canopy wakes is estimated as $P_{wk} = ½\cdot C_D\cdot a\cdot U^3$, where U can be either u_w or u_c and C_D is 1 (Dean and Dalrymple, 1991) where a is the frontal area per volume, called the canopy density, and calculated as $a = n_s.d$. ε is dissipation and T is the transport, estimated as the residual of the remaining terms, as suggested by Brunet et al. (1994).

Dissipation was determined through spectral measurements of the turbulent vertical velocity. The spectra of the vertical velocities (S_{ww}) shows a region characteristic of a -5/3 inertial subrange. According to Reidenbach et al. (2007), the location and magnitude of the inertial subrange is used to estimate dissipation through the equation:

$$S_{ww}(k) = \frac{9}{55}\cdot\left(\frac{4-\cos\theta}{3}\right)\alpha\varepsilon^{2/3}\cdot k^{-5/3} \qquad (5.9)$$

where θ = 90 is the angle from the direction of the mean flow, α = 1.56 is the empirical Kolmogorov constant for velocity, and k and S_{ww} correspond to the wavenumber and power spectral density within the inertial subrange, respectively. By assuming Taylor's frozen turbulence hypothesis, wavenumber space was converted into frequency space using $f = U\cdot k/2\cdot\pi$ (Reidenbach et al., 2006; Reidenbach et al., 2007). Then S_{ww} can be defined as:

$$S_{ww}(f) = C\varepsilon^{2/3}\cdot\left(\frac{u_c}{2\pi}\right)^{2/3}\cdot f^{-5/3} \qquad (5.10)$$

where C = 0.34. Thus by fitting S_{ww} to the frequency spectrum, the dissipation is calculated. The uncertainty in ε was estimated by the standard deviation of the three power spectrum at a given frequency (Gross and Nowell, 1985). In Figure 5.2a dissipation was estimated by fitting the inertial subrange in S_{ww} for the case SRV 9 at z = 13 cm, and in Figure 2b a profile for dissipation is presented for the same case.

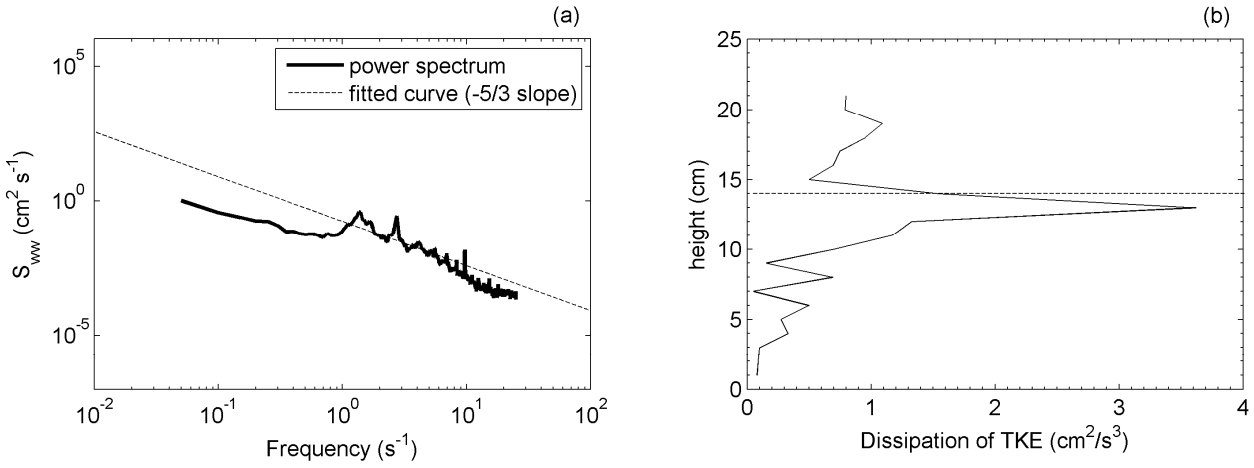

Figure 5.2. (a) Power spectrum for run SRV 9, using the vertical velocity component at z = 13 cm; (b) Dissipation of TKE for SRV 9 at z = 13 cm.

5.3. Results

Waves generated in the flume corresponded to waves travelling at intermediate depths, resulting when the water depth was between λ/20 and λ/2, where λ is the wavelength. Wave conditions in the present study corresponded to the laminar regime, i.e. to wave Reynolds number, $Re_w = u_{w,\infty} \cdot A_\infty / \nu < 10000$ (Fredsoe and Deigaard, 1992), where $u_{w,\infty}$ represents the wave velocity unaffected by the canopy roughness, called free-stream velocity, and A_∞ is the wave orbital excursion length of the free-stream potential flow.

Figures 5.3a, b, c and d show turbulent stresses, $\langle u'^2 \rangle$, $\langle w'^2 \rangle$ and $\langle u'w' \rangle$ profiles for experiments carried out for runs without vegetation (WP 3), submerged rigid vegetation (SRV 9), submerged flexible vegetation (SFV 9) and emergent rigid vegetation (ERV 9), respectively, and corresponding to the case with the densest plant vegetation and the highest wave frequency (n_s = 1280 plants m^{-2} and f = 1.4 Hz). It was observed that without vegetation there was a decrease in depth of both components of the normal stresses, $\langle u'^2 \rangle$ and $\langle w'^2 \rangle$, whereas shear stress, $\langle u'w' \rangle$, showed minimal variations in depth. High $\langle w'^2 \rangle$ compared to $\langle u'^2 \rangle$ from z = 20 to 9 cm was also observed. From 1 to 9 cm $\langle u'^2 \rangle$ become slightly higher than $\langle w'^2 \rangle$. In the experiments carried out with submerged rigid vegetation, SRV 9 (Fig. 5.3b) normal stresses, $\langle u'^2 \rangle$ and $\langle w'^2 \rangle$, were higher than in those without vegetation, and WP 3 (Fig. 5.3a) with $\langle u'^2 \rangle$ slightly higher than $\langle w'^2 \rangle$ (Fig. 5.3b). Within the vegetation, at z = 13 and 12 cm, both normal stresses were larger than in the case without vegetation (Fig. 5.3b). As an example, at z = 13 cm, $\langle u'^2 \rangle$ was calculated to be 1.1 $cm^2 s^{-2}$ for SRV 9 and 0.4 $cm^2 s^{-2}$ for WP 3. Moreover, above the submerged rigid vegetation, shear stress (Fig. 5.3b) was larger than in that without

vegetation (Fig. 5.3a). Within the submerged rigid vegetation at z = 12 cm (Fig. 5.3b) a peak of negative shear stress (0.23 $cm^2\ s^{-2}$) was found.

For the experiments carried out with the submerged flexible vegetation model, profiles of turbulent stresses (Fig. 5.3c) were similar in depth to the experiments carried out without vegetation (Fig. 5.3a). Finally, in the emergent rigid vegetation model, normal stresses (Fig. 5.3d) were smaller than in the model without vegetation (Fig. 5.3a). From z = 1 to 10 cm, $\langle w'^2 \rangle$ was completely attenuated with values near 0 cm s^{-1}. However, $\langle u'^2 \rangle$ was higher than $\langle w'^2 \rangle$, as was found in the experiments without vegetation (Fig. 5.3a).

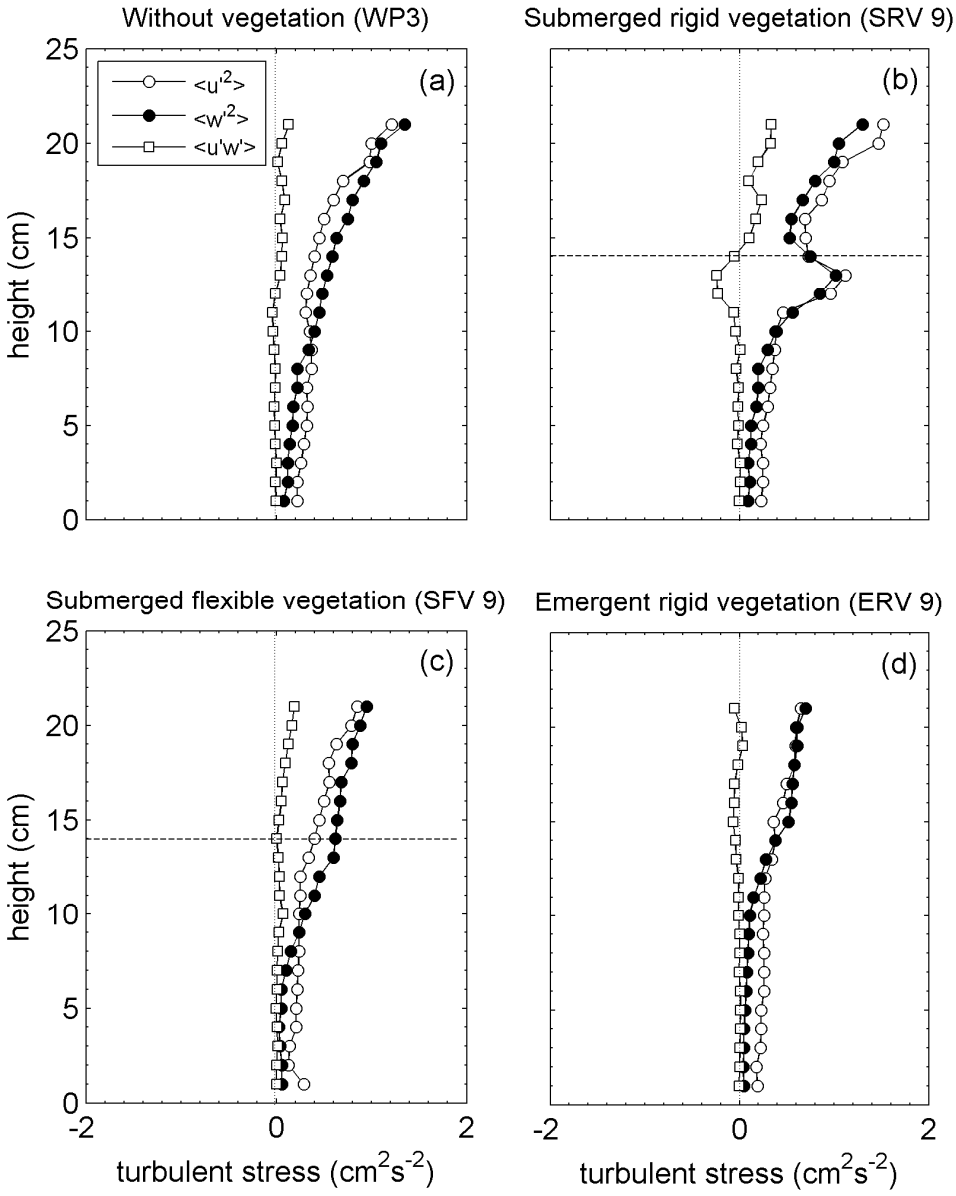

Figure 5.3. Turbulent stresses in a wave-dominated flow. (a) WP3; (b) SRV 9; (c) SFV 9 and (d) ERV 9.

Figure 5.4a shows the vertical profile of turbulent kinetic energy (TKE) corresponding to SRV 8 (f = 1 Hz and n_s = 1280 plants m^{-2}), together with WP 2 (f = 1 Hz, without vegetation). Figure 5.4b show the vertical profile of TKE corresponding to SRV 9 (f = 1.4 Hz and n_s = 1280 plants m^{-2}) together with the case WP3 (f = 1.4 Hz, without vegetation). In Figure 5.4c, SFV 9 (f = 1.4 Hz and n_s = 1280 plants m^{-2}) is depicted together with the case WP 3 (f = 1.4 Hz, without vegetation). And Figure 5.4d illustrates ERV 9 (f = 1.4 Hz and n_s = 1280 plants m^{-2}) together with the case WP3 (f = 1.4 Hz, without vegetation). TKE was calculated following equation (5.5). Without vegetation (WP 2 and WP 3), the TKE decreased in depth. The vertical profile of TKE for submerged rigid vegetation (SRV 8 in Fig. 54a), showed higher TKE above and inside the vegetation compared to those experiments without vegetation, WP2. Figure 5.4b shows that the TKE above the vegetation model was larger than without vegetation. However, well inside the canopy (below z = 10 cm) the TKE profile of SRV 9 was slightly lower than the TKE profile for the vegetation-less case. At the top of the canopy (z = 13 cm) the TKE was higher than in the case without vegetation (1.8 cm^2 s^{-2} at z = 13 cm for SRV 9 and 0.9 cm^2 s^{-2} at z = 13 cm for WP 3).

For the submerged flexible model the profile of the TKE showed that the profile of the TKE above the canopy was similar to WP 3 (Fig. 5.4c). Inside the canopy the TKE was found to be smaller than the TKE found without vegetation. Finally, for the emergent rigid vegetation model, the vertical profile of the TKE was always lower compared to without vegetation (Fig. 5.4d), i.e., from near bottom to z = 10 cm TKE was constant with values of 0.2– 0.3 cm^2 s^{-2}. In addition, vertical profiles of u_w^{rms} were plotted in each figure. In general, the wave velocity profile decayed with depth. However, for SRV 9 (Fig. 5.4b), a drastically reduction of wave velocity at 2 cm below the top of the canopy was observed, corresponding to the zone with a peak in the TKE.

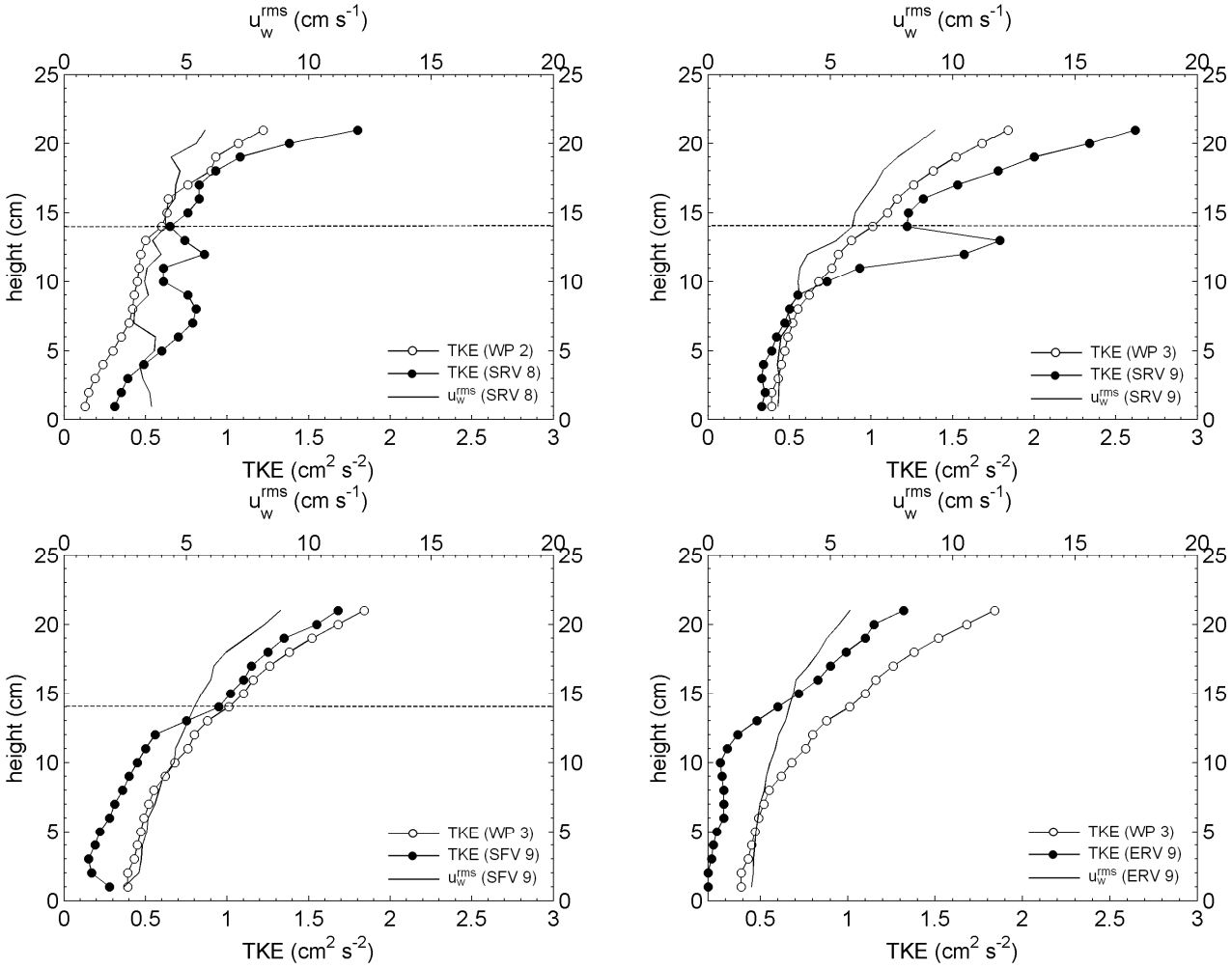

Figure 5.4. Vertical profiles of TKE for comparison between runs with and without plants. a) SRV 8 and WP 2; b) SRV 9 and WP 3; c) SFV9 and WP 3 and d) ERV 9 and WP 3 together with u_w^{rms}.

Table 5.2 shows ΔTKE, Reynolds number associated with the wave velocity (Re_w) and Reynolds number associated with the mean current (Re_c) in three zones of interest: above the canopy model ($h_v < z < 1.5h_v$), at the top of the canopy model ($0.86h_v < z < 0.93h_v$) and well inside the canopy model ($0.07h_v < z < 0.64h_v$), for a comparative analysis between submerged rigid and flexible models for densities of 640 and 1280 plants m^{-2}. In the submerged rigid model, the ΔTKE was positive above the canopy model for both densities, (ranging from 24 – 34%). At the top and well inside the canopy, the ΔTKE for both densities decreased at increasing frequencies. Only SRV 9 (f = 1.4 Hz and n_s = 1280 plants m^{-2}) presented negative ΔTKE well inside the canopy (i.e. -14%), indicating a reduction in the TKE compared to the experiment without plants. In the submerged flexible model, the TKE was found to be generally negative over the whole column and with larger values well inside the canopy.

Table 5.2. ΔTKE (%) for submerged rigid and submerged flexible vegetation above, at the top of the canopy and well inside the canopy.

Run	Canopy model	n_s (stems/m^2)	f (Hz)	$h_v < z < 1.5h_v$	$0.86h_v < z < 0.93h_v$			$0.07h_v < z < 0.64h_v$		
				ΔTKE(%)	ΔTKE(%)	Re_w	Re_c	ΔTKE(%)	Re_w	Re_c
SRV 4	Submerged rigid model	640	0.8	28	201	379	16	87	330	16
SRV 5			1	30	41	370	29	79	331	40
SRV 6			1.4	34	7	509	47	1	344	49
SRV 7		1280	0.8	33	143	311	34	171	328	55
SRV 8			1	24	104	382	70	127	382	90
SRV 9			1.4	26	100	468	72	-14	310	22
SFV 4	Submerged flexible model	640	0.8	9	-10	83	11	-16	89	8
SFV 5			1	2	-6	123	26	-19	96	6
SFV 6			1.4	-2	-9	150	36	-34	104	18
SFV 7		1280	0.8	-15	-10	95	13	-23	77	4
SFV 8			1	-7	-15	112	10	-31	97	75
SFV 9			1.4	-8	-22	150	33	-46	101	11

Table 5.3 shows ΔTKE, Re_w and Re_c for the emergent rigid model. The results are divided into two zones: within the canopy ($0.48h_v < z < 0.72h_v$) and near the bottom ($0.03h_v < z < 0.31h_v$). Within the canopy, ΔTKE decreased at increasing wave frequencies for both densities. Near the bottom the large decrease of ΔTKE was found for the higher density, while for 640 stems m^{-2}, ΔTKE varied between -2 and 3%, indicating that TKE was similar to the case without vegetation.

Table 5.3. ΔTKE (%) for emergent rigid vegetation inside canopy model.

Run	Canopy model	n_s (stems/m^2)	f (Hz)	$0.48h_v < z < 0.72h_v$			$0.03h_v < z < 0.31h_v$		
				ΔTKE(%)	Re_w	Re_c	ΔTKE(%)	Re_w	Re_c
ERV 4	Emergent rigid model	640	0.8	-6	308	25	3	307	64
ERV 5			1	-24	310	37	2	301	118
ERV 6			1.4	-34	286	152	-2	274	183
ERV 7		1280	0.8	2	327	128	-13	261	150
ERV 8			1	-20	269	166	-20	254	167
ERV 9			1.4	-31	310	223	-48	308	177

Re_w was found to be larger for submerged rigid vegetation, between 310 and 509, than for the cases of submerged flexible vegetation which were between 83 and 150 for measurements at the top of the canopy and well inside the canopy (Table 5.2). In contrast, Re_c was found, in all cases, to be lower than Re_w, with a maximum value up to 90 (Table 5.2). For the emergent rigid model, Re_w varied between 254 and 327 with no clear dependence on frequency or density (Table 5.3). Whereas on the contrary, Re_c clearly increased with frequency for both densities (Table 5.3).

Figure 5.5 shows the vertical extent of turbulent stresses, $\langle u'^2 \rangle$ (Fig. 5.5a), $\langle u'w' \rangle$ (Fig. 5.5b), TKE (Fig. 5.5c) and u_w (Fig. 5.5d) with phase (from 0 to 360 º) for experiment SRV 8 (n_s = 1280 plants m^{-2} and f = 1 Hz). A peak of maximum $\langle u'^2 \rangle$ near z = 8 cm was found corresponding to the crest of the wave (180º) and decreased in depth. The shear stress in Fig. 5.5b shows values near 0 at any depths and for all phases. A peak of TKE (Fig. 5.5c) of 1 cm^2 s^{-2} was observed well inside the canopy, situated from z = 5 to z = 10 cm from the crest to 360º.

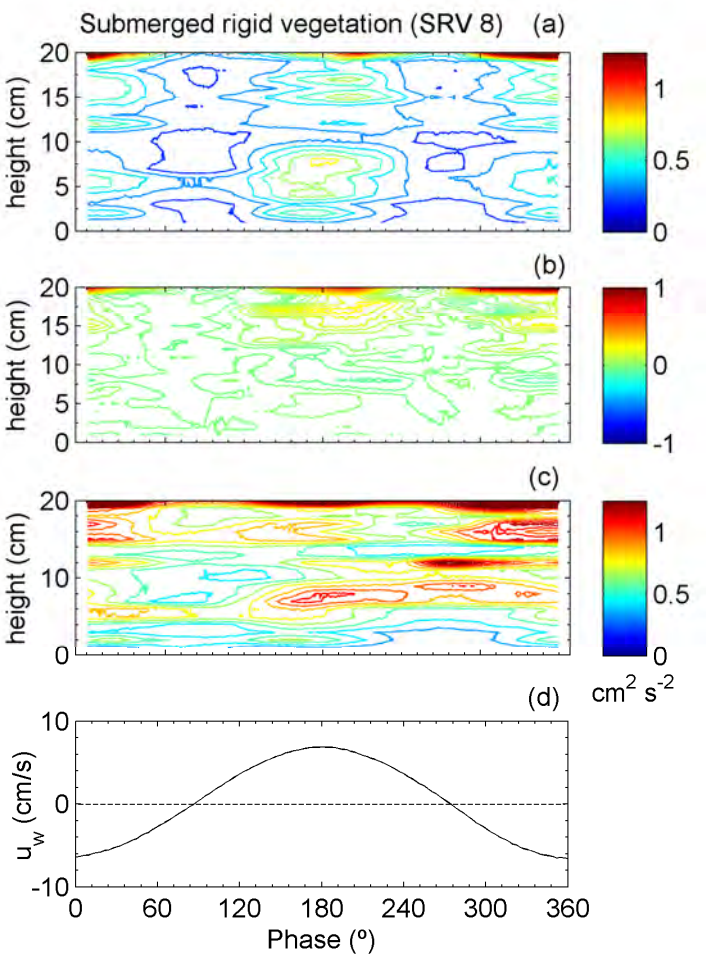

Figure 5.5. Ensemble average turbulent stresses and TKE as a function of phase angle for submerged rigid vegetation (SRV 8): (a) $\langle u'^2 \rangle$; (b) $\langle u'w' \rangle$; (c) TKE and (d) wave velocities.

Figure 5.6, shows the vertical extent of stress distributions for SRV 9: $\langle u'^2 \rangle$ in Fig. 5.6a, $\langle u'w' \rangle$ in Fig. 5.6b, TKE in Fig. 5.6c and u_w in Fig. 5.6d with phase. $\langle u'^2 \rangle$, $\langle u'w' \rangle$ and TKE presented maximum values between z = 12 and 14 cm, i.e. at the top of the canopy, with peaks corresponding to phases 200 and 350 º, and corresponding to the backward facing slope of the wave. Below z = 12 cm, very low values of $\langle u'^2 \rangle$, $\langle u'w' \rangle$ and TKE were found (Figs. 5.6a, 5.6b and 5.6c, respectively). Contour plots for experiments carried out with flexible and emergent vegetation did not present any differences in $\langle u'w' \rangle$ compared without vegetation. The normal stresses and the TKE were close to 0.

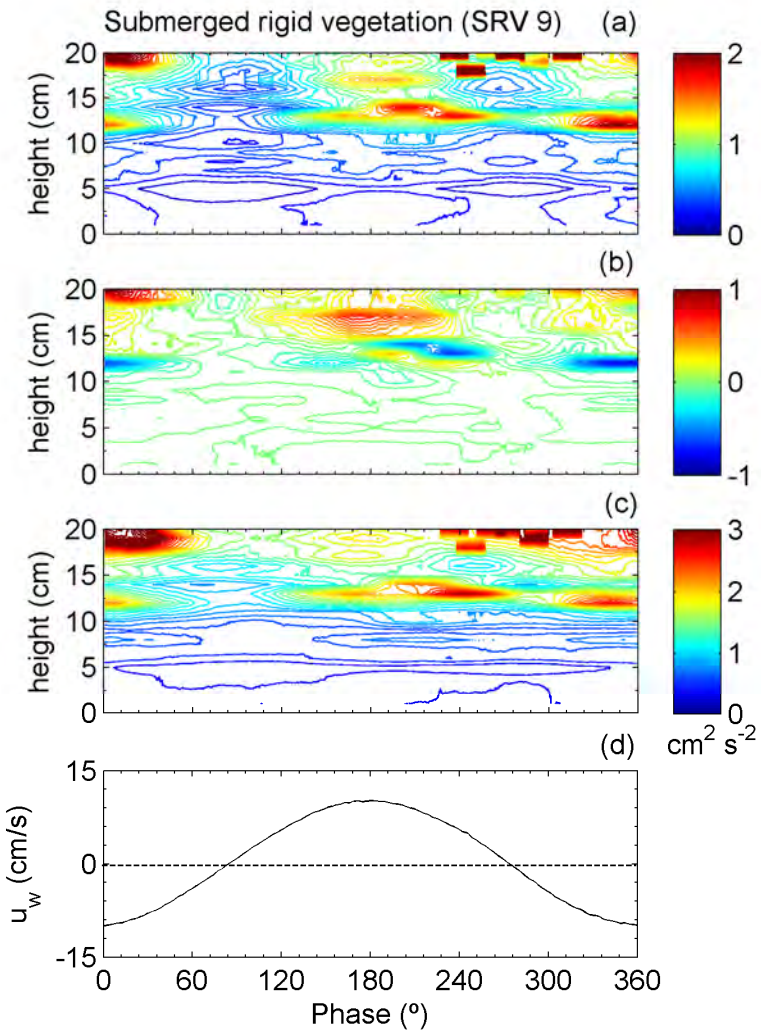

Figure 5.6. Ensemble average turbulent stresses and TKE as a function of phase angle for submerged rigid vegetation (SRV 9): (a) <u'2>; (b) <u'w'>; (c) TKE and (d) wave velocities.

The vertical profiles of the quadrant analysis of shear stress were calculated for runs SRV 8 and SRV 9, and are presented in Figure 5.7. Figure 5.7a shows the quadrant analysis for experiment SRV 8 and Figure 5.7b for run SRV 9. Both figures demonstrate that the contribution of the shear stress decreased with depth. In Figure 5.7a, the vertical profile of $u'w'_4$ coincided with $u'w'_2$, while vertical profile of $\langle u'w' \rangle_1$ was very similar to $u'w'_3$. In contrast, in Figure 5.7b an increase of $\langle u'w' \rangle$ at the top of the canopy, i.e. between z = 12 and 13 cm, was found along with a dominance of both the ejection events ($\langle u'w' \rangle_2$) and the sweep events ($\langle u'w' \rangle_4$) and with an equal contribution of sweeps and ejections. In particular, at z = 12 cm $\langle u'w' \rangle_2$ was -0.64 $cm^2\ s^{-2}$ and $\langle u'w' \rangle_4$ was -0.81 $cm^2\ s^{-2}$, whereas $\langle u'w' \rangle_1$ was 0.4 $cm^2\ s^{-2}$ and $\langle u'w' \rangle_3$ was 0.47 $cm^2\ s^{-2}$.

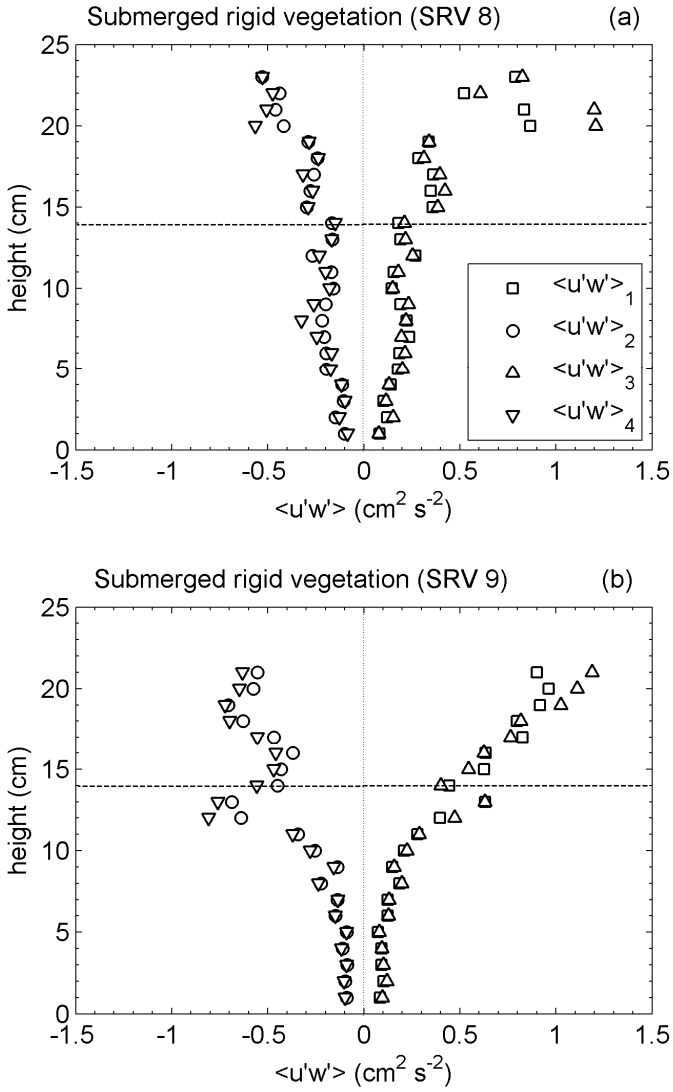

Figure 5.7. Quadrant analysis of the shear stress with $\langle u'w' \rangle_1$, $\langle u'w' \rangle_2$, $\langle u'w' \rangle_3$ and $\langle u'w' \rangle_4$. (a) SRV 8 and (b) SRV 9.

Table 5.4 summarizes the production and dissipation of the TKE for the four main cases described previously (SRV 8, SRV 9, SFV 9 and ERV 9) at z = 12 and 13 cm, and which in the case of submerged vegetation, corresponds to the top of the canopy. For SRV 8 and SRV 9, the TKE production associated with canopy wakes (P_{wk}) due to wave action, was the main contributor to the turbulence production (P_{wk} = 3.5±0.3 and 8±0.3 cm^2 s^{-3}, respectively). The contribution of shear production (P_s) was negligible in SRV 8 and SRV 9; however, for SRV 9 the shear production due to wave action was 1.5±0.2 cm^2 s^{-3}. Dissipation, calculated by equation (5.10), was 2±0.3 cm^2 s^{-3} for SRV 8 and 4±0.3 cm^2 s^{-3}, for SRV 9. For the submerged flexible vegetation, the production terms due to shear were negligible, while P_{wk} was not calculated because Re_c and Re_w < 300 (Table 5.2). For the submerged rigid vegetation, the dissipation was 0.3±0.03 cm^2 s^{-3}. Finally, for the emergent rigid vegetation, the shear production was also very small and there was no wake production because Re_c and Re_w < 300 (Table 5.3). The dissipation in the emergent model was of 0.1±0.03 cm^2 s^{-3}.

Table 5.4. The turbulence kinetic energy production and dissipation for submerged rigid vegetation (SRV 8 and SRV 9), submerged flexible vegetation (SFV 8) and emergent rigid vegetation (ERV 8) between z = 12 and 13 cm.

Run	Canopy model	n_s (stems m^{-2})	f (Hz)	P_s (cm^2 s^{-3})		P_{wk} (cm^2 s^{-3})		ε (cm^2 s^{-3})
				u_c	u_w	u_c	u_w	
SRV 8	Submerged rigid model	1280	1	< 0.1	< 0.1	0.2±0.01	3.5±0.03	2±0.3
SRV 9		1280	1.4	< 0.1	1.5±0.2	0.1±0.01	8±0.04	4±0.3
SFV 9	Submerged flexible model	1280	1.4	< 0.1	< 0.1	--	--	0.3±0.03
ERV 9	Emergent rigid model	1280	1.4	< 0.1	< 0.1	--	--	0.1±0.03

5.4. Discussion

5.4.1. Rigid vs. flexible vegetation

Above the submerged rigid vegetation for all the experiments, the TKE was greater compared to those cases without vegetation (with ΔTKE ranging from 24 to 34%, as shown in Table 5.2). High levels of turbulence were generated within the submerged rigid vegetation (through stem-scale processes) and were transported upwards, above the canopy model. At the very top of submerged rigid model, the TKE was higher than in that without vegetation and ΔTKE varied from 7 to 201%. Well inside the vegetation, ΔTKE ranged from 1 to 171%, indicating the

enhancement of the TKE by the passage of the wave through the stems. ΔTKE was found to decrease in higher wave frequencies, i.e., the highest wave frequency produced lower ΔTKE within the submerged rigid canopy. This result was also suggested by Hansen and Reidenbach (2012), who showed that the rate of energy dissipation was not uniform over a range of wave frequencies, and waves at higher frequencies were attenuated, but waves at lower frequencies were less affected by the seagrass.

The progressive waves generated in this experiment followed the 2nd order Stokes theory in intermediate depths. The presence of the submerged rigid model modified the wave-induced velocities: mean current (u_c) and wave velocity (u_w). Thus, the Reynolds number was calculated considering either the wave velocity, which is defined as the root-mean-square of the horizontal component of the wave-induced velocity, u_w^{rms}, i.e., $Re_w = u_w^{rms} \cdot d/\nu$, or the mean current, defined as $Re_c = u_c \cdot d/\nu$, where ν is the kinematic viscosity (= 1.10^{-6} m^2 s^{-1}). Thus, positive ΔTKE within the canopy coincided with Re_w > 300-310 (Table 5.2). In contrast, mean current velocity generated inside the meadow produced Re_c lower than 100 (Table 5.2), i.e., there was no mean current contribution to stem-wake turbulence. Therefore, only the wave velocity could penetrate inside the meadow and generate TKE due to the stem-wake turbulence.

TKE was also observed to be generated by stem wakes for unidirectional flows (Anderson and Charters, 1982; Tanino and Nepf, 2008), when the stem Reynolds number exceeded approximately 100. This physical process has been shown to inhibit sediment deposition (Zong and Nepf, 2010). Pujol and Nepf (2012), in a meadow subjected to breaker generated turbulence, also found high levels of TKE attributed to the generation of stem-wake turbulence caused by the elevated near-bed wave velocity during a breaking wave event (Re_w > 100).

For the submerged rigid vegetation with the highest density and wave frequency (SRV 9: n_s = 1280 plants m^{-2} and f = 1.4 Hz) a peak of turbulence higher than the experiment without plants, was found between z = 12 and 13 cm (Fig. 5.4b), i.e. ΔTKE was negative. This peak in the TKE coincided with the peaks of $<u'^2>$ and $<w'^2>$ at the same depth. In this experiment, both components $<u'^2>$ and $<w'^2>$, had the same magnitude, therefore contributed equally to the TKE. As shown in Fig. 5.6a, an increase of $<u'^2>$ at 240 º and 350º was found between z = 12 and 13 cm, coinciding with the results of Reidenbach et al. (2007), who found peaks of turbulent velocities at the backward facing slope of the wave at the top of a coral canopy. The increase of $<u'^2>$ at the very top of the vegetation was attributed to the interaction between plants and the passage of the wave packet. The reduction of the TKE within the canopy model, compared to the experiment without vegetation, and which resulted in negative ΔTKE, is called sheltering or dampening of turbulence by the canopy field, and is enhanced by the increase in the plant density of the canopy (Nepf et al., 1997; Neumeier and Amos, 2006; Pujol et al., 2010).

Shear stress for the submerged rigid model (SRV 9), <u'w'> (Fig. 5.6b) showed a maximum negative value, coinciding with a maximum of $<u'^2>$ (Fig. 5.6a) and a maximum TKE (Fig. 5.6c) between 240 and 350º. Reidenbach et al. (2007) also found a maximum of negative <u'w'> during the backward facing slope of the wave. In addition, results of the quadrant analysis (Fig. 5.7b) revealed that at the very top of the canopy, ejection and sweep events were the main events contributing to the shear stress. According to Reidenbach et al. (2007), the peaks in turbulent stresses, $<u'^2>$, $<w'^2>$, <u'w'> coincided with regions of separation of the boundary layer as turbulent vortices were shed from the surfaces of a coral canopy during the backward motion of the wave. The phase of the wave where separation and vortex ejection events occurred was accompanied by considerable TKE. In contrast, for the experiments with submerged rigid vegetation, neither the vertical profile of shear stress nor the quadrant analysis showed any difference compared to the cases without plants.

In contrast to the submerged rigid model, the profile of TKE for the submerged flexible vegetation model above the canopy showed lower TKE compared to the vertical profile of the TKE without plants, with ΔTKE generally negative for all densities and wave frequencies (Table 5.2). Turbulence above the submerged rigid vegetation was caused by the generation of stem-scale turbulence below the top of the canopy. However, submerged flexible canopy moved with the oscillatory flow generating less drag and stem-scale turbulence within the canopy. Although the density of the plants (calculated as the fractional plant area at the bottom occupied by stems) was the same for both canopy models (rigid and flexible), the vertical structure of the vegetation was not the same, i.e. the flexible model had less resistance to flow; therefore, wave flow could penetrate more easily than in the submerged rigid model. In all the experiments with submerged flexible vegetation, Reynolds numbers were $Re_c < 100$ and $Re_w < 150$. Although no wakes were generated behind the stems in our experiments, stem-generated turbulence has indeed been observed in the presence of progressive waves within the flexible vegetation model (Luhar et al. 2010). Luhar et al. (2010), considered progressive waves propagating over beds with and without vegetation (f = 0.7 Hz and the amplitude of the wave was a = 5.2 cm). They observed an increase in the near-bed turbulence within the meadow, compared to the same wave condition without plants (Luhar, personal communication). Specifically, between 1 and 7 cm above the bed (the mean meadow height was about 7 cm), the level of turbulence was almost twice the level found without vegetation. The difference in their findings may be attributed to both the type of wavemaker and amplitude of the wave. Luhar et al. (2010) used a piston type wavemaker, whereas in the present study a flap type wavemaker was used. According to Dean and Darlymple (1991) the volume of water displaced over a whole stroke (S) for a piston wavemaker is $(H/S)_{piston} = kh$, whereas the volume of water displaced by a flap wavemaker is $(H/S)_{flap} = kh/2$.

ΔTKE was found to decrease for both increasing density and wave frequency, i.e., the highest density and highest wave frequency produced lower ΔTKE within the flexible canopy, well inside the canopy (-46%) and at the very top of the canopy (-22%), as shown in Table 5.2. The

relationship between turbulence intensity and canopy density was also found by Hansen and Reidenbach (2012) along a density plant gradient, ranging from 150 to 560 shoots m^{-2}. They reported near-bottom mean velocities to be reduced by 70 to 90% compared to adjacent unvegetated velocities.

The turbulent kinetic energy budget within a canopy was calculated by using equation (5.8). For submerged rigid vegetation the main parameter which contributed to the production of TKE was the production associated with canopy wakes due to $u_{w.}$ When $Re_w > 310$, wakes are formed at the rear of the stems, contributing to the production of turbulence which is the same order as the dissipation (ε = 2±0.3 and 4±0.3 cm^2 s^{-3}, for SRV 8 and SRV 9, respectively). However, there is no balance between production and dissipation and transport of TKE away from the shear would be expected.

Studies of uniform flow in the presence of aquatic vegetation have shown that the flow generally presents a logarithmic velocity profile above the canopy and vegetation may simply be considered as a form of macro-roughness (Nepf and Vivoni, 2000; Neumeier and Ciavola, 2004). The zone below the top of the canopy is characterized by a vertical energy exchange zone, with a zone of predominantly longitudinal energy exchange below it (Nepf and Vivoni, 2000). This zone called the roughness sublayer takes the form of a mixing layer, rather than a boundary layer (Maltese et al., 2007). Ghisalberti and Nepf (2006) found that in the mixing layer, strong sweep was followed by a weak ejection, transferring momentum between the zone below the top of the canopy and above the canopy. Maltese et al. (2007) observed an ejection-dominated region above the seagrass model, whereas a sweep-dominated region was found below the top of the canopy and no dominant quadrant within the canopy. In addition, Pujol et al. (2012) found that submerged rigid vegetation under oscillatory flow acted like a false floor. The presence of submerged rigid vegetation model shifted the vertical profile of the mean current upward and penetrated the canopy 2 cm. In the zone below the top of the canopy, the quadrant analysis revealed an ejection (28%) and sweep-dominated region (35%). Therefore, the vertical profile of mean current below the top of the canopy is analogous to the roughness sublayer at the top of the canopy under uniform flow, characterized by a vertical energy exchange zone

The submerged rigid canopy model used in this experiment could mimic coral reefs. It is well known that many coral communities are located in nutrient limiting environments (Falter et al., 2004). Therefore, the capacity of transfer rates of material between seawater and the coral community will determine the rate of this community. The higher levels of TKE found at the very top of the canopy, together with the increase of $<u'w'>$ ($<u'w'>_2$ and $<u'w'>_4$) at the same depth compared with the experiment without vegetation, could be one of the mechanisms contributing to enhancing the transfer of nutrients in the coral community.

5.4.2. Submerged vs. emergent vegetation

TKE for the emergent rigid vegetation over the whole column was lower than TKE calculated for the experiments without vegetation. ΔTKE was negative or slightly positive and was associated with Re_w being lower than ≈ 310. Wave velocity in emergent rigid vegetation was attenuated 25 and 45% for n_s = 640 and 1280 plants m^{-2}, respectively, compared to runs without plants at f = 1.4 Hz. The largest negative ΔTKE (-48%), was found for n_s = 1280 plants m^{-2} and f = 1.4 Hz at the bottom layer of the canopy. The decrease of ΔTKE with wave frequency for all densities was found within the canopy and associated with an increase of Re_c for the same conditions. High wave frequencies are related to high mean current, which in turn produced high Re_c. The dissipation of TKE in the emergent rigid canopy was lower than in the experiments with submerged rigid vegetation; therefore, dissipation of energy was associated with turbulence generated by waves outside the canopy.

5.5. Conclusion

Three different vegetation models were designed to study the structure of turbulence on a flow dominated by progressive waves. Based on the study of turbulence stresses, turbulent kinetic energy and the production and dissipation of TKE, we found that the submerged rigid, submerged flexible and emergent rigid models clearly modified the flow structure above and well inside the canopy models. Above the submerged rigid model, the TKE was always higher than of that without vegetation, due to the redistribution of TKE at a lower volume. At the top of the canopy and well inside the submerged rigid model, TKE was found to be larger compared to the equivalent experiments without vegetation, and was attributed to the generation of stem-wake turbulence by the elevated near-bed wave velocity during the passage of the wave, characterized by Reynolds wave numbers higher than Re_w > 300 - 310. For the highest plant density and wave frequency, maximum turbulent stresses and TKE were produced during the backward facing slope of the wave and confined to the very top of the canopy. The generation of stem-wake turbulence and the production of TKE at the very top of the canopy were associated with a large reduction in wave velocity. Sweeps and ejections were the predominant events, enhancing the transfer of mass between, above and within the canopy. Only in such conditions was sheltering at well inside the canopy observed. The submerged flexible vegetation TKE progressively decayed inside the vegetation bed as blades dissipated the turbulence, resulting in lower levels of TKE within the vegetation. For the emergent rigid vegetation, the vertical reduction of TKE could be attributed to the vertical reduction of the wave velocity from the top of the water column, a process that was enhanced by increasing the density of the canopy. In summary, our laboratory results indicate that canopy sheltering under oscillatory flow may be observed for submerged flexible vegetation, emergent rigid vegetation and for the highest plant density and wave frequency in the submerged rigid vegetation. In all

the other cases in the submerged rigid model, the production of turbulence was associated with the wave action at the stem scale. In this latter case, TKE increased within the vegetation, therefore sheltering was inhibited.

Acknowledgment Dolors Pujol was supported by the research fellowship BR08/11 of the University of Girona. We are also grateful *Ministerio de Ciencia e Innovación* of the Spanish Government through grant CGL 2010-17289 and Fundación Biodiversidad through the project 9112019.

References

Anderson, S.M., Charters, A.C., 1982. A fluid dynamics study of seawater flow through *Gelidium nudifrons*. Limnol. Oceanogr. 27, 399-412.

Blanchette, C.A., 1997. Size and survival of intertidal plants in response to wave action: A case study with *Fucus gardneri*. Ecology 78, 1563-1578.

Brunet, Y., Finnigan, J., Raupach, M., 1994. A wind-tunnel study of air-flow in waving wheat - single-point velocity statistics. Bound. Layer Meteorol. 70, 95-132.

Coops, H., VanderVelde, G., 1996. Effects of waves on helophyte stands: Mechanical characteristics of stems of *Phragmites australis* and *Scirpus lacustris*. Aquat. Bot. 53, 175-185.

Dean, R.G., Dalrymple, R.A., 1991. Water wave mechanics for engineers and scientists. World Scientific, Singapore; Teaneck, NJ.

Denny, M.W., 1988. Biology and the mechanics of the wave-swept environment. Princeton University Press, Princeton.

Falter, J., Atkinson, M., Merrifield, M., 2004. Mass-transfer limitation of nutrient uptake by a wave-dominated reef flat community. Limnol. Oceanogr. 49, 1820-1831.

Folkard, A.M., 2005. Hydrodynamics of model *Posidonia oceanica* patches in shallow water. Limnol. Oceanogr. 50, 1592-1600.

Fonseca, M.S., Cahalan, J.A., 1992. A preliminary evaluation of wave attenuation by 4 species of seagrass. Estuar. Coast. Shelf. S. 35, 565-576.

Fonseca, M., Bell, S., 1998. Influence of physical setting on seagrass landscapes near Beaufort, North Carolina, USA. Mar. Ecol-Prog. Ser. 171, 109-121.

Fonseca, M., Fisher, J., 1986. A comparison of canopy friction and sediment movement between 4 species of seagrass with reference to their ecology and restoration. Mar. Ecol-Prog. Ser. 29, 15-22.

Fredsøe, J., Deigaard, R., 1992. Mechanics of coastal sediment transport, World Scientific, Singapore; New Jersey.

Gambi, M.C., Nowell, A.R.M., Jumars, P.A., 1990. Flume observations on flow dynamics in *Zostera-Marina* (eelgrass) beds. *Mar. Ecol-Prog. Ser*. 61, 159-169.

Ghisalberti, M., Nepf, H., 2006. The structure of the shear layer in flows over rigid and flexible canopies. Environ. Fluid Mech. 6, 277-301.

Ghisalberti, M., Nepf, H.M., 2002. Mixing layers and coherent structures in vegetated aquatic flows. J. Geophys. Res. Oceans.107, C2

Gleason, M., Elmer, D., Pien, N., Fisher, J., 1979. Effects of stem density upon sediment retention by salt-marsh cord grass, *Spartina-Alterniflora Loisel*. Estuaries 2, 271-273.

Granata, T.C., Serra, T., Colomer, J., Casamitjana, X., Duarte, C.M., Gacia, E., 2001. Flow and particle distributions in a nearshore seagrass meadow before and after a storm. Mar. Ecol-Prog. Ser. 218, 95-106.

Gross, T.F., Nowell, A.R., 1985. Spectral scaling in a tidal boundary layer. J. Phys. Oceanogr. 15, 496 – 508.

Hansen, J.C.R., Reidenbach, M.A., 2012. Wave and tidally driven flows in eelgrass beds and their effect on sediment suspension. Mar. Ecol-Prog. Ser. 448, 271-287.

Infantes, E., Terrados, J., Orfila, A., Canellas, B., Alvarez-Ellacuria, A., 2009. Wave energy and the upper depth limit distribution of *Posidonia oceanica*. Bot. Mar. 52, 419-427.

Infantes, E., Orfila, A., Simarro, G., Terrados, J., Luhar, M., Nepf, H., 2012. Effect of a seagrass (*Posidonia oceanica*) meadow on wave propagation. Mar. Ecol-Prog. Ser. 456, 63-72.

Kim, J., Moin, P., Moser, R., 1987. Turbulence statistics in fully developed channel flow at low Reynolds number. J. Fluid Mech. 177, 133-166

Koch, E.W., Gust, G., 1999. Water flow in tide and wave dominated beds of the seagrass *Thalassia testudinum*. Mar. Ecol-Prog. Ser. 184, 63-72.

Lefebvre, A., Thompson, C.E.L., Amos, C.L., 2010. Influence of *Zostera marina* canopies on unidirectional flow, hydraulic roughness and sediment movement. Cont. Shelf Res. 30, 1783-1794.

Lewis, J., 1968. Water movements and their role in rocky shore ecology. Sarsia, 13-36.

Lowe, R.J., Koseff, J.R., Monismith, S.G., 2005a. Oscillatory flow through submerged canopies: 1. Velocity structure. J. Geophys. Res. Oceans. 110, C10016.

Lowe, R., Koseff, J., Monismith, S., Falter, J., 2005b. Oscillatory flow through submerged canopies: 2. Canopy mass transfer. J. Geophys. Res. Oceans. 110, C10017.

Luhar, M., Coutu, S., Infantes, E., Fox, S., Nepf, H., 2010. Wave-induced velocities inside a model seagrass bed. J. Geophys. Res. Oceans. 115, C12005.

Menge, B., 1976. Organization of the New England rocky intertidal community: role of predation, competition, and environmental heterogeneity, Ecol. Monogr. 46, 355–393

Nepf, H., 1999. Drag, turbulence, and diffusion in flow through emergent vegetation. Water Resour. Res. 35, 479-489.

Nepf, H., Vivoni, E.R., 2000. Flow structure in depth-limited, vegetated flow. J. Geophys. Res. Oceans. 105, 28547-28557.

Neumeier, U., Amos, C.L., 2006. The influence of vegetation on turbulence and flow velocities in European salt-marshes. Sedimentology 53, 259-277.

Pergent-Martini, C., Pasqualini, V., Ferrat, L., Pergent, G., 2006. Ecological data in integrated coastal zone management: Case study of Posidonia oceanica meadows along the Corsican coastline (Mediterranean Sea). Environ. Manage. 38, 889-895.

Perrin, R., Cid, E., Cazin, S., Sevrain, A., Braza, M., Moradei, F., Harran, G., 2007. Phase averaged measurements of the turbulence properties in the near wake of a circular cylinder at high Reynolds number by 2C-PIV and 3C-PIV. Exp. Fluids 42, 93-109.

Pujol, D., Colomer, J., Serra, T., Casamitjana, X., 2010. Effect of submerged aquatic vegetation on turbulence induced by an oscillating grid. Cont. Shelf Res. 30, 1019-1029.

Pujol, D., Nepf, H., 2012. Breaker-generated turbulence in and above a seagrass meadow. Cont. Shelf Res. 49, 1-9.

Reidenbach, M.A., Koseff, J.R., Monismith, S.G., 2007. Laboratory experiments of fine-scale mixing and mass transport within a coral canopy. Phys. Fluids 19, 075107.

Reidenbach, M.A., Monismith, S.G., Koseff, J.R., Yahel, G., Genin, A., 2006. Boundary layer turbulence and flow structure over a fringing coral reef. Limnol. Oceanogr. 51 (5), 1956-1968.

Reusch, T., Chapman, A., 1995. Storm effects on eelgrass (*Zostera-Marina L*) and blue mussel (*Mytilus-Edulis-L*) beds. J. Exp. Mar. Biol. Ecol. 192, 257-271.

Sung, J., Yoo, J.Y., 2001. Three-dimensional phase averaging of time-resolved PIV measurement data. Meas Sci Technol 12, 655-662.

Tanino, Y., Nepf, H., 2008. Lateral dispersion in random cylinder arrays at high Reynolds number. J. Fluid Mech. 600, 339-371.

Thomas, F., Cornelisen, C., 2003. Ammonium uptake by seagrass communities: effects of oscillatory versus unidirectional flow. Mar. Ecol. Prog. Ser. 247, 51-57.

Wallace, J., Eckelmann, H., Brodkey, R., 1972. The wall region in turbulent shear flow. J. Fluid Mech. 54, 39-48.

Ward, L.G., Kemp, W.M., Boynton, W.R., 1984. The influence of waves and seagrass communities on suspended particulates in an estuarine embayment. Mar. Geol. 59, 85-103.

Willimarth, W., Lu, S., 1972. Structure of the Reynolds stress near the wall. J. Fluid Mech. 55, 65-92.

Wlezien, R.W., Way, J.L., 1979. Techniques for the experimental investigation of the near wake of a circular-cylinder. AIAA J. 17, 563-570.

Zong, L., Nepf, H., 2010. Flow and deposition in and around a finite patch of vegetation. Geomorphology 116, 363-372.

Chapter 6

Breaker-generated turbulence in and above a seagrass meadow

Pujol, D.[1], Nepf, H.[2]

[1]Department of Physics, Escola Politècnica Superior-II, Campus Montilivi, 17071 Girona, Catalonia, Spain

[2]Department of Civil and Environmental Engineering, Massachusetts Institute of Technology, Cambridge, Massachusetts, USA

Published in: *Continental Shelf Research*

Abstract In shallow water the turbulence generated by wave breaking can reach the bed, so that the interaction between breaker-generated turbulence and submerged aquatic vegetation (SAV) can be important. The aim of this study is to understand the effect of the submerged aquatic vegetation on the production and dissipation of turbulent kinetic energy associated with the passage of a breaking wave. A model SAV meadow was constructed based on dynamic and geometric similarity to natural plants. The model meadow was subject to an isolated breaker generated within a wave packet, which mimics transient wave breaking in the ocean. The evolution of the turbulent flow field was measured by an Acoustic Doppler Velocimeter. The observations suggest that near the water surface, i.e. above the meadow, the turbulent kinetic energy (TKE) without SAV remains elevated longer than with SAV, and this is attributed to the damping of breaker-generated turbulence by the SAV. In contrast, the TKE measured near the bed is always higher and more persistent with SAV having roughly twice the value observed without SAV. This is attributed to the generation of stem-wake turbulence by the elevated near-bed orbital velocity during the passage of the wave packet. The generation of stem-wake turbulence is associated with a greater loss of wave energy. Specific to the wave and plant conditions considered in this study, in the presence of the SAV a total of 32% wave energy loss was observed; ¾ of this loss (24% loss) can be associated with the breaking event, and ¼ of this loss (8% loss) can be associated with dissipation by meadow drag.

Keywords Seagrass meadow; wave breaking; turbulent kinetic energy; TKE decay; energy losses; stem-wake turbulence.

6.1. Introduction

Within the coastal zone, the ocean, land, and air interact to produce favorable habitat for many species (Pergent-Martini et al., 2006). Seagrass meadows are an economically important component of that habitat, due to the link between seagrass and fish production. For example, together with wetlands, seagrass beds support more than 80% of the annual fish yield in the Mediterranean (Batisse and Jeudy de Grissac, 1995). *Posidonia oceanica,* a common seagrass of the Mediterranean Sea, is included in the Habitats Directive (43/92 EEC, European Economic Community) list as a key species supporting the ecology of this region (http://ec.europa.eu/environment/nature/legislation/habitatsdirective/index_en.htm; last accessed on 23 May 2012). Meadows of *P. oceanica* produce enormous quantities of organic matter (leaves, epiphytes), which constitute the basis of the food web both within and outside the ecosystem (Gobert et al., 2006). Seagrass meadows reduce waves and currents (Gambi et al., 1990), providing refuge for fish, invertebrates and plankton, and stabilizing sediments (Fonseca and Fisher, 1986; Gleason et al., 1979; Granata et al., 2001; Reusch and Chapman, 1995; Ward et al., 1984). Indeed, the disappearance of sandy beaches has been correlated with the regression of meadows (Batisse and Jeudy de Grissac, 1995).

Some of the current and wave energy dissipated by aquatic vegetation is converted to turbulent kinetic energy within the meadow. Two distinct scales of turbulence have been identified within aquatic canopies. First, turbulence is generated in the wakes of individual blades and stems, if the Reynolds number based on the stem-diameter (or blade width) is larger than about 100 (Anderson and Charters, 1982; Tanino and Nepf, 2008). Second, the drag discontinuity at the top of a submerged meadow produces a shear layer that generates canopy-scale turbulence that is transmitted downward into the canopy (Ghisalberti and Nepf, 2002; Neumeier and Amos, 2006). In addition, turbulence generated above the canopy, e.g. by wind-driven stirring, can also penetrate into the canopy. However, Pujol et al. (2010) showed that the penetration of turbulence generated above the canopy is damped by canopy drag.

Turbulence inside a meadow has positive biological consequences, such as enhancing the transfer of CO_2 (in the form of bicarbonate) from the water to the leaf or blade surface (Denny, 1988). The level of turbulence within a meadow may also influence sediment stability. Because the level of turbulence inside a long meadow generally decreases with increasing stem density, the tendency for sedimentation also increases with increasing stem density (Bos et al., 2007; Leonard and Luther, 1995; Neumeier, 2007; Neumeier and Amos, 2006; van Katwijk et al., 2010; Ward et al., 1984).

While many studies have considered seagrasses in the presence of mean currents and waves (references given above), few have considered seagrass interacting with breaking waves. Yet, wave breaking may be an important source of turbulence within a meadow, impacting sediment retention and nutrient uptake. Wave breaking has been shown to

generate turbulent mixing and impose forces on coral reefs (Massel and Gourlay, 2000). Further, wave-induced forces are believed to shape coral reefs and set the distribution of seagrass populations (Fonseca and Bell, 1998; Massel and Gourlay, 2000). Specifically, waves have been noted to determine the upper depth limit for the distribution of submerged aquatic vegetation such as *Posidonia oceanica* (Infantes et al., 2009). Adding to the above studies, this paper characterizes the turbulence generated by a breaking wave event passing over a submerged meadow. Two distinct sources of turbulence within the meadow are identified. First, turbulence generated by the breaking event may penetrate the meadow by vertical turbulent diffusion. Second, the magnification of wave motion near the bed, associated with the wave steepening and approach to breaking, generates stem wake turbulence within the meadow.

The loss of wave energy and turbulence generation associated with two- and three-dimensional wave breaking in open water has been described (Nepf et al., 1998; Rapp and Melville, 1990). Turbulent mixing and air entrainment associated with wave breaking can enhance air-sea gas and heat transfer (Jessup et al., 1997). In addition, turbulence generated by breaking waves causes wide-spread and intense sediment suspension (Ogston and Sternberg, 2002; Teodoro et al., 2004; Ting and Kirby, 1996). We are interested to see whether SAV can modify this response.

Jessup et al. (1997) estimated that the loss of energy from a two-dimensional wave group could range from 10% for a spilling breaker to 25% for a plunging breaker. The resulting turbulence penetrates to depths of three to four wave heights. More than 90% of the energy lost from the waves is dissipated within 4 wave periods, following a temporal power law decay of t^{-1}. In this study we examine how the presence of SAV may impact the wave energy loss associated with and subsequent turbulence decay after a breaking event.

6.2. Methodology

The study was conducted in a 22.6 m x 0.6 m x 0.38 m tank in the Department of Civil and Environmental Engineering at the Massachusetts Institute of Technology. A schematic of the setup is shown in Fig. 6.1. The mean water depth, d, was 0.3 m. The plywood beach located at the end of the tank had a slope of 1:5 and was covered with a 10-cm layer of rubberized coconut fiber. The beach reduced the wave reflection to less than 10% (Luhar et al., 2010). Because we considered a wave packet of finite duration, we were also able to identify the measurements made before wave reflections travel back to the measurement point, and thus eliminate the impact of the reflection on our results.

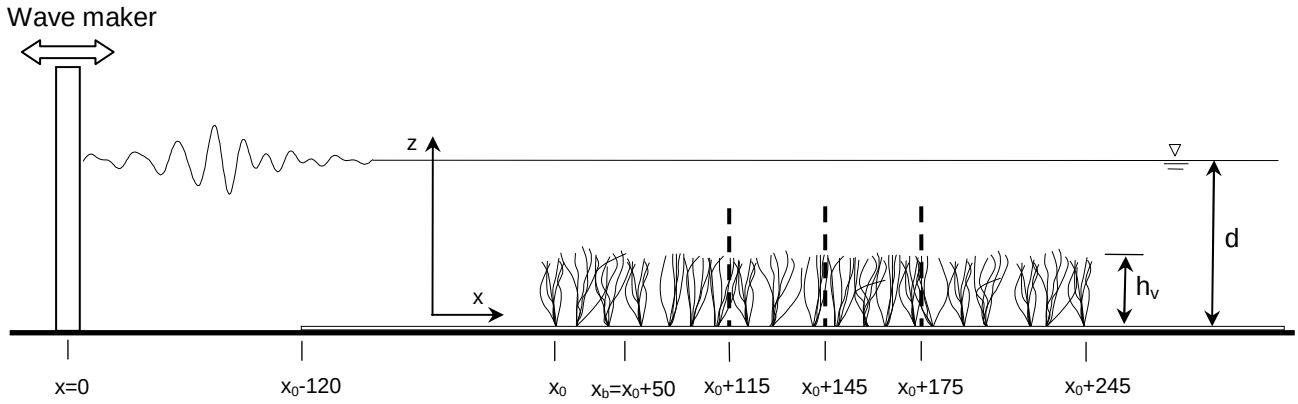

Figure 6.1. Experiments were conducted in at 22.6 m long flume. The streamwise coordinate is denoted by x, with x positive in the downstream direction, and x = 0 at the mean position of the wavemaker. The vertical coordinate is z, with z = 0 at the bed. The mean water depth, d, is 30 cm. The mean plant height in still water is h_v = 13.5 cm. The model meadow was 245-cm long with its leading edge located at x_0 = 285 cm from mean position of the wavemaker. The vertical dashed lines indicate the positions of the velocity profiles measured using a Nortek Vectrino. Surface displacement, which was recorded at the same longitudinal position as the velocity, was measured using a 0.2 mm resolution wavegauge. The single spilling breaker starts at approximately x_b = 335 cm (x_0+50 cm) from the wave maker and continues until x = 550 cm. Note that dimensions in the figure are given in cm.

Each model seagrass plant was constructed from six polyethylene blades attached with a rubber band to a 2-cm long, 0.64-cm diameter wooden dowel. With the rubber band, the average dowel diameter was 0.78 cm. To construct the meadow, individual plants were inserted into two baseboards of 1.25-cm length. The leading edge of the meadow is denoted by x_0 (Fig. 6.1). Two additional baseboards were placed both upstream and downstream of the model vegetation to ensure a uniform bed roughness across the test section (Luhar et al., 2010). The model plants are geometrically and dynamically similar to typical seagrasses, as described by the dimensionless parameters λ_1 and λ_2 (Ghisalberti and Nepf, 2002). The similarity is based on two independent ratios of the drag force, $F_D = \rho_w A_f C_d U_c^2$, the buoyancy force, $F_B = (\rho_w - \rho_s) g h_v w_v t_v$, and the restoring force due to blade rigidity, $F_R \sim EI/h_v^2$ (Luhar and Nepf, 2011), where ρ_w is the density of the water (1000 kg/m^3); A_f is the frontal area of the blade; C_d is the blade drag coefficient, which for simplicity is assumed to be 1; U_c is the mean in-canopy velocity; ρ_s is the density of the blades (920 kg/m^3); g is the gravitational constant (9.8 m/s^2); h_v is the blade length (0.135 m); w_v is the width of the blade; t_v is the thickness of the blade ($0.1 \cdot 10^{-3}$ m); $I = w_v t_v^3/12$ is the second moment of area; and E is the modulus of elasticity ($3 \cdot 10^8$ Pa). Because we exclude parameters that are the same in the model and the field (specifically, gravity and water density), the force ratios become dimensional

$$\frac{F_B}{F_R} \sim \lambda_1 = \frac{(\rho_w - \rho_s) \cdot h_v^3}{E \cdot t_v^2} \qquad (6.1)$$

$$\frac{F_R}{F_D} \sim \lambda_2 = \frac{E \cdot t_v^{\,3}}{h_v^{\,3} \cdot U_c^2} \qquad (6.2)$$

As noted by Ghisalberti and Nepf (2002), the dependence of λ_2 on U_c^2 makes its value vary tremendously in the field, so λ_1 was chosen as the critical design parameter. For the blade model used in this study, λ_1 is 0.066 s^2/m. Using the measurements done by Folkard (2005) for *P. oceanica*, (ρ_s is 910 ± 110 kg/m^3; h_v is 0.25 m; E is 4.7± 0.6 $\cdot 10^8$ Pa; and t_v is 0.2$\cdot 10^{-3}$ m), we obtain λ_1 = 0.075 s^2/m, which shows that our prototype vegetation is dynamically similar to *Posidonia*. The stem density within the meadow, n_s, was chosen to be 1200 stems/m^2, which is representative of a range of field conditions, and each stem consisted of six blades made of polyethylene (Luhar et al., 2010).

Ocean wave breaking is a random, intermittent and unsteady process caused by different mechanisms, such as wind blowing off the tops of waves (Banner and Phillips, 1974), wave-wave interaction, or wave instabilities (Melville, 1982). The most commonly used method for generating a repeatable, unsteady wave-breaking event is the constructive interference method used by Cummins (1962) and Davis and Zarnick (1964) to test ships models. Rapp and Melville (1990) extended this technique to generate an isolated breaker within a wave packet, which mimics transient wave breaking in the ocean. In our study the wave packet was generated by a vertical paddle, which was driven by a Syscomp WGM-101 arbitrary waveform generator. The wave signal was designed to create short period waves at the beginning of the packet and longer period waves at the end of the packet. Based on the linear wave theory, the waves with longer period travel at a higher celerity than those with a shorter period. Therefore, the longer-period waves catch up to the shorter-period waves, and the constructive interference produces a breaking event at a prescribed position and time.

We define the longitudinal direction as x, and x=0 at the wavemaker; y is the lateral direction and y = 0 at the centreline of the tank, and z is the vertical direction, with z = 0 at the flume bed. Time is denoted by t. Following the methods of Rapp and Melville (1990), the free surface displacement generated by the wavemaker, $\eta(x,t)$, was specified to be

$$\eta(x,t) = \sum_{n=1}^{N} a_n \cdot \cos\left[k_n (x - x_f) - 2\pi f_n (t - t_f)\right], \qquad (6.3)$$

where a_n and k_n are the amplitude and wavenumber, respectively, of frequency component n; x_f is the distance from the wavemaker to the theoretical focusing location (x_f = 3.30 m); t_f is the theoretical breaking time (t_f = 9 s); and f_n is the nth frequency component related by the dispersion equation:

$$\omega_n^2 = g k_n \tanh(k_n d), \qquad (6.4)$$

where ω is the angular frequency, defined as $\omega_n = 2\pi f_n$. The signal was generated for 10 s, i.e. t =0 to 10s. The N frequency components were equi-spaced across a bandwidth $\Delta f = f_N - f_1 = 0.789$ Hz. The center frequency was used to characterize the wave, $f_c = 1.08$ Hz, i.e. $f_c = (f_N+f_1)/2$, from which it can be deduced that the central period is $T_c = 0.93$ s, and the central angular frequency, ω_c, is 6.79 rad/s. The dispersion equation (4) gives information about the central wavenumber, k_c, which is 5.15 m^{-1}. A large number of components (N = 32) was chosen to approximate a continuous spectrum, and the values for f_c and Δf were chosen following the recommendations of Rapp and Melville (1990, Fig. 16). Finally, a constant wave-steepness ($a_n k_n$ constant for all frequency components) was used to inhibit premature wave breaking (Rapp and Melville, 1990). Specifically

$$a_n = \frac{G}{K_n}, \qquad (6.5)$$

in which G is the gain factor used to vary the overall intensity of the wave packet.

The Eulerian velocity field was defined as (u, v, w) in the (x, y, z) directions, respectively. The three components of velocity were recorded with a downward-looking Acoustic Doppler Velocimeter (Nortek Vectrino). The sampling volume was located 5 cm below the acoustic transmitter with a sampling volume of 0.4 cm^3. A wave gauge of 0.2 mm accuracy was synchronized with the Vectrino to record the position of the water surface, $\eta(t)$. The analog output from the wave gauge was amplified and logged to a computer using an analog-digital converter (NI-USB6210, National Instruments). Both the Vectrino and the wave gauge were fitted to a trolley moving on precision rails. The sampling rate was 25 Hz. For each wave packet event, the measurements of velocity and surface displacement were manually initiated and sampled for 160 seconds; however, we later analyzed only the first 30 seconds to avoid the reflections of the waves from the end of the tank and velocity values below the noise level. To obtain an ensemble mean measurement, for each measurement position we conducted five runs, with one wave packet per run. We waited 10 minutes between each run to settle the basin and remove the residual motion from the previous run. Ensemble averages of the surface displacement were also estimated. Vertical profiles of velocity were constructed from measurements made at two centimeter intervals between z = 2 cm to z = 18 cm from the bed. A weak spot in the Vectrino response existed between 8 and 10 cm, resulting in reduced data quality at these points. The Vectrino sends out two pulses of sound separated by a time lag, and the sensors measure the phase of the return signal from each pulse. The change in phase divided by the time between pulses is proportional to the velocity of the particles in the water. The weak spots occur when the first pulse, after reflecting off the bottom, matches in time and space with the second pulse at the sampling volume. (Nortek Forum data are available at http://www.nortek.no/en/knowledge-center/forum/velocimeters/30180961; last accessed on 13 January 2012).

The vertical profiles were made at three longitudinal locations within the canopy: x_0+115 cm, x_0+145 cm and x_0+175 cm, where x_0 was located at 285 cm from the mean position of the wavemaker. Additional measurements were made before the breaking point at x_0+25 cm, and after the breaking point at x_0+205 cm and x_0+365 cm at z = 18 cm.

In order to obtain valid data acquisition within the canopy, a hole of between 10 and 15 cm was created within the canopy to avoid blocking the acoustic pathway of the Vectrino. To test the effect of the hole, we measured the velocities near the bed with and without wooden dowels in place at x = x_0+115 cm. A comparison of the two measurements showed an average difference of less than 5% over the time-scale of interest (t = 0 to 20 s).

The turbulence was estimated using an ensemble averaging technique, described in Rapp and Melville (1990). The instantaneous velocity, e.g. u, is decomposed into the sum of the ensemble mean velocity, <u>, and the deviation from the ensemble mean, u':

$$u(x,y,z,t) = <u(x,y,z,t)> + u'(x,y,z,t) \qquad (6.6)$$

The deviation from the ensemble mean reflects three different sources:

$$u' = u'_t + u'_{rw} + u'_{mn}, \qquad (6.7)$$

where: u'_t is the turbulence.

u'_{rw} is the motion associated with random waves generated by the breaking

u'_{mn} is the measurement noise

The variance of the signal is computed as

$$\left\langle [u'(x,y,z,t)]^2 \right\rangle = \frac{1}{M}\sum_{m=1}^{M} [u'(x,y,z,t)]^2 , \qquad (6.8)$$

where M is the number of individual events.

The standard deviation of this quantity is defined as

$$u'_{rms} = \left[\left\langle [u'(x,y,z,t)]^2 \right\rangle \right]^{1/2} \qquad (6.9)$$

The same analysis was used to calculate η_{rms}.

The instrument noise of the Vectrino can be evaluated from the standard deviation of the time series before the passage of the wave packet, at which time there are no turbulent motions and no random waves. In our experiments, the measurement noise was 0.0034 m/s (0.0026C,

where C is the characteristic phase speed calculated as $L_c/T_c = 2\pi f_c/k_c$ = 1.3 m/s) for the horizontal component (Fig. 6.2b) and 0.0015 m/s (0.0011C) for the vertical component, based on records between t = 0 and 5 seconds. These noise levels were much smaller than the velocity rms measured during and after the breaking event (from t = 9 to 20 seconds), indicating that turbulence was measurable above the instrument noise. The random wave component includes the variation in the wave packet between realizations and the generation of short surface waves during breaking, both of which are reflected in the rms-variation of the surface position between realizations, η_{rms}. It is reasonable to assume that the random waves have frequency ω_c, with wavenumber k_c, so that the velocity contribution from the random waves can be estimated from the linear wave theory

$$u'_{rms} = \eta_{rms}\omega_c\left(e^{-k_c(d-z)}\right), \qquad (6.10)$$

and using $C = \eta_{rms}/k_c$, the contribution of random waves to the velocity rms is

$$\left.\frac{u'_{rms}}{C}\right|_{rw} = \eta_{rms}\cdot k_c\cdot\left(e^{-k_c(d-z)}\right) \qquad (6.11)$$

The random wave contribution to u'_{rms}, estimated from (6.11), is shown in Fig. 6.2d. Except at the time of breaking (t = 10 s), the magnitude is comparable to the instrument noise (0.0026C).

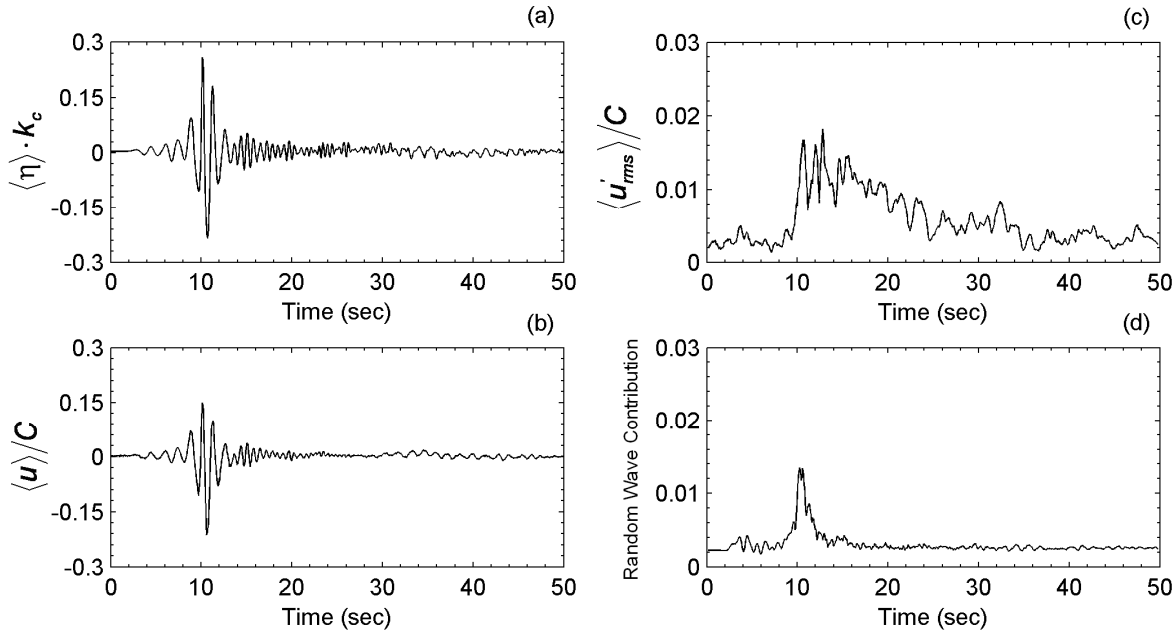

Figure 6.2. Surface displacement and velocity measurements (z = 0.18 m) made at x = x_0+175 cm, downstream of spilling break without vegetation. (a) Ensemble-average surface displacement, $\langle\eta\rangle k_c$; (b) ensemble-average velocity $\langle u\rangle/C$; (c) ensemble-average velocity fluctuation u'_{rms}/C; and (d) estimated contribution of random waves to velocity fluctuation from equation 6.11. The instrument noise is inferred from the rms velocity between 0 and 5 seconds, which represents the period of still water conditions before the arrival of the wave packet.

Finally, there is an uncertainty in u'_{rms}, which we estimate from the confidence interval of a standard deviation following the methods described in Sheskin (2000). To use this technique we assumed that the data were randomly and independently sampled from a Gaussian distribution. For a given value of u'_{rms}/C, the 90% confidence interval is between 0.49 and 1.81.

Having estimated that the noise and random waves make relatively smaller contributions to u'_{rms} (around 20% in Fig. 6.2d), we will use u'_{rms} as a surrogate estimate for the turbulence. Then

$$\left\langle u_t'^2 \right\rangle \approx \left\langle u'^2 \right\rangle = u_{rms}'^2 \qquad (6.12)$$

We repeat the analysis for the v and w components to estimate v'_{rms} and w'_{rms}. Therefore, we obtain the turbulent kinetic energy as

$$TKE = \frac{1}{2}\left(\left\langle u'^2 \right\rangle + \left\langle v'^2 \right\rangle + \left\langle w'^2 \right\rangle\right) \qquad (6.13)$$

To determine the number of individual events (M) needed to characterize the wave and turbulent flow field, we compared the statistics generated by a 5- and a 10-event average (Fig. 6.3). Considering individual time points, the 5-event ensemble average (solid line) deviates from the 10-event ensemble average (dashed line) by as much as 10% (Fig. 6.3c). However, if we smooth the data with a running average (0.4 second averaging, Fig. 6.3d) the two records deviate by less than 6%. Based on the comparison shown in Fig. 6.3 and given the time required to execute each event run, we decided that a 5-event ensemble average would be sufficient for this study.

Energy is lost from the wave packet due to breaking and to the interaction with the meadow. To evaluate the wave energy loss we follow a method described in Rapp and Melville (1990), which is based on the surface displacement variance, $\overline{\eta^2}$ defined as:

$$\overline{\eta^2} = \frac{1}{T}\int_0^T \langle \eta \rangle^2 dt\,, \qquad (6.14)$$

in which T is the integration time chosen to be long enough to capture the passage of the wave-packet through the test section, here 20 seconds, and $<\eta>^2$ is the square of the ensemble-mean surface displacements. Assuming an equi-partition of kinetic and potential energy, the energy flux passing a given cross-section is given by $\rho g<\eta>^2 C_g$, with C_g the group velocity (Dean and Dalrymple, 2002). Then the dissipation of wave energy (D) within the test section is given by the difference in the energy flux observed at the up- and downstream ends of the test section. Assuming that the group velocity is constant, the total loss of wave energy between upstream (subscript 'u') and downstream (subscript 'd') position is then given by

$$D = \frac{\Delta \int_0^T \overline{\eta^2} dt}{\int_0^T \overline{\eta_u^2} dt} \times 100 = \frac{\int_0^T \overline{\eta_u^2} dt - \int_0^T \overline{\eta_d^2} dt}{\int_0^T \overline{\eta_u^2} dt} \times 100 \qquad (6.15)$$

Note that this estimator is unreliable near the breaking point, because the assumption of an equi-partition of kinetic and potential energy is not valid close to breaking, and the group velocity is not constant (Rapp and Melville, 1990). Therefore, the upstream (u) and downstream (d) end points are positioned far from the breaking position.

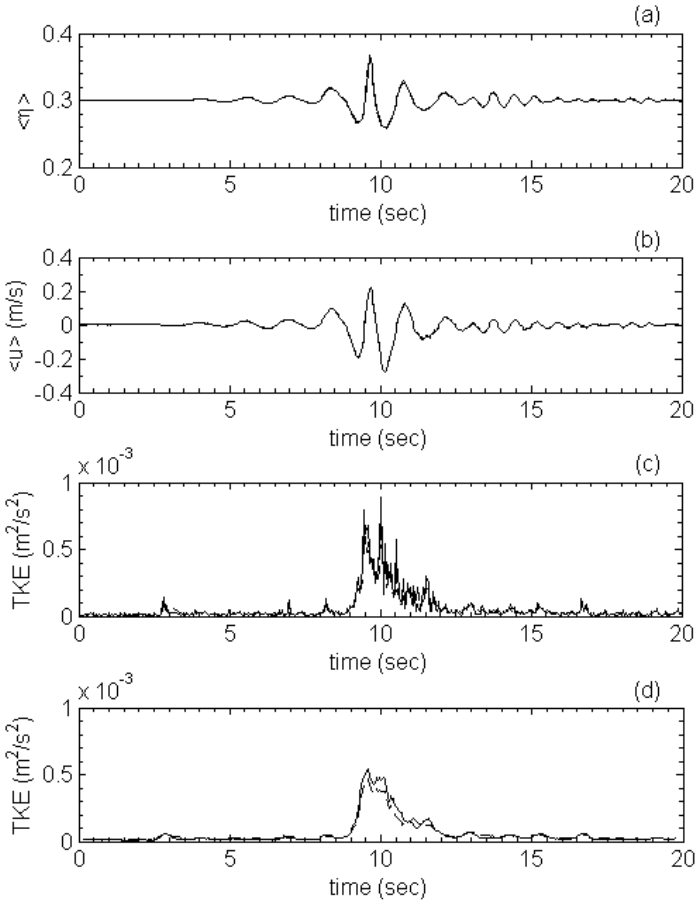

Figure 6.3. Comparison of ensemble average statistics using 5 events (solid line) and 10 events (dashed line) measured at x = x_0+115 cm, y = 0 cm, z = 0.16 m, without SAV: (a) ensemble mean surface displacements, (b) ensemble mean horizontal velocity; (c) ensemble-averaged TKE, and (d) TKE records smoothed by a 0.4 second running average.

6.3. Results and discussion

6.3.1. General observations

The wave packets generated at the paddle were composed of short waves followed by long waves, organized according to equation (6.3) to produce a single breaking wave at the theoretical position x_f = 3.30 m and time t_f = 9 s. The actual breaking point, x_b, was 3.35 m, and the actual breaking time, t_b, was 8.6s. The deviations from theory arose because the dispersion equation used to calculate the wave signal assumed linear, deep-water waves, a condition which was only approximately satisfied in the laboratory channel. Nevertheless, the method produced a breaking event that was initiated at the same time (8.6 s) and position (3.35 m) for each realization, so that the method of ensemble averaging may be applied. After its initiation, breaking and air entrainment continued over a length of 2.15 m, so that the breaking event persisted over a distance of more than one wavelength (L = 1.22 m). Downstream of breaking, the packet dispersed, and the waves again became linear.

The wave steepness, ak_c, predicts the type of breaking event: incipient, spilling and plunging waves correspond to ak_c = 0.25 - 0.26, 0.28 - 0.32 and 0.35 - 0.42, respectively (Rapp and Melville 1990). The wave steepness can be controlled through the gain factor (G) in equation 6.5. For our wave packet ak_c = 0.31, corresponding to spilling waves. Photos taken at the breaking point, but not shown in this article, confirm this. At the point of breaking, the breaking wave has an amplitude of 0.06 m (Fig. 6.3a).

6.3.2. Evolution of turbulence kinetic energy

The passage of the wave packet was recorded in the surface displacement measured at x_0+115 cm, x_0+145 cm and x_0+175 cm in Fig. 6.4a, d and g, respectively. The dashed and solid lines correspond to conditions with and without submerged aquatic vegetation (SAV). The surface displacements were nearly identical with and without SAV. The breaking crest corresponds to the maximum amplitude wave at the center of the packet, which arrived at x_0+115 cm, x_0+145 cm and x_0+175 cm at 9.64, 9.88 and 10.12 s, respectively. The amplitude of the breaking crest was slightly (2%) higher with SAV than without SAV. As an example, at x_0+145 cm the peak amplitude was $0.3460 \pm 0.2 \cdot 10^{-3}$ m and $0.3540 \pm 0.2 \cdot 10^{-3}$ m without SAV and with SAV, respectively.

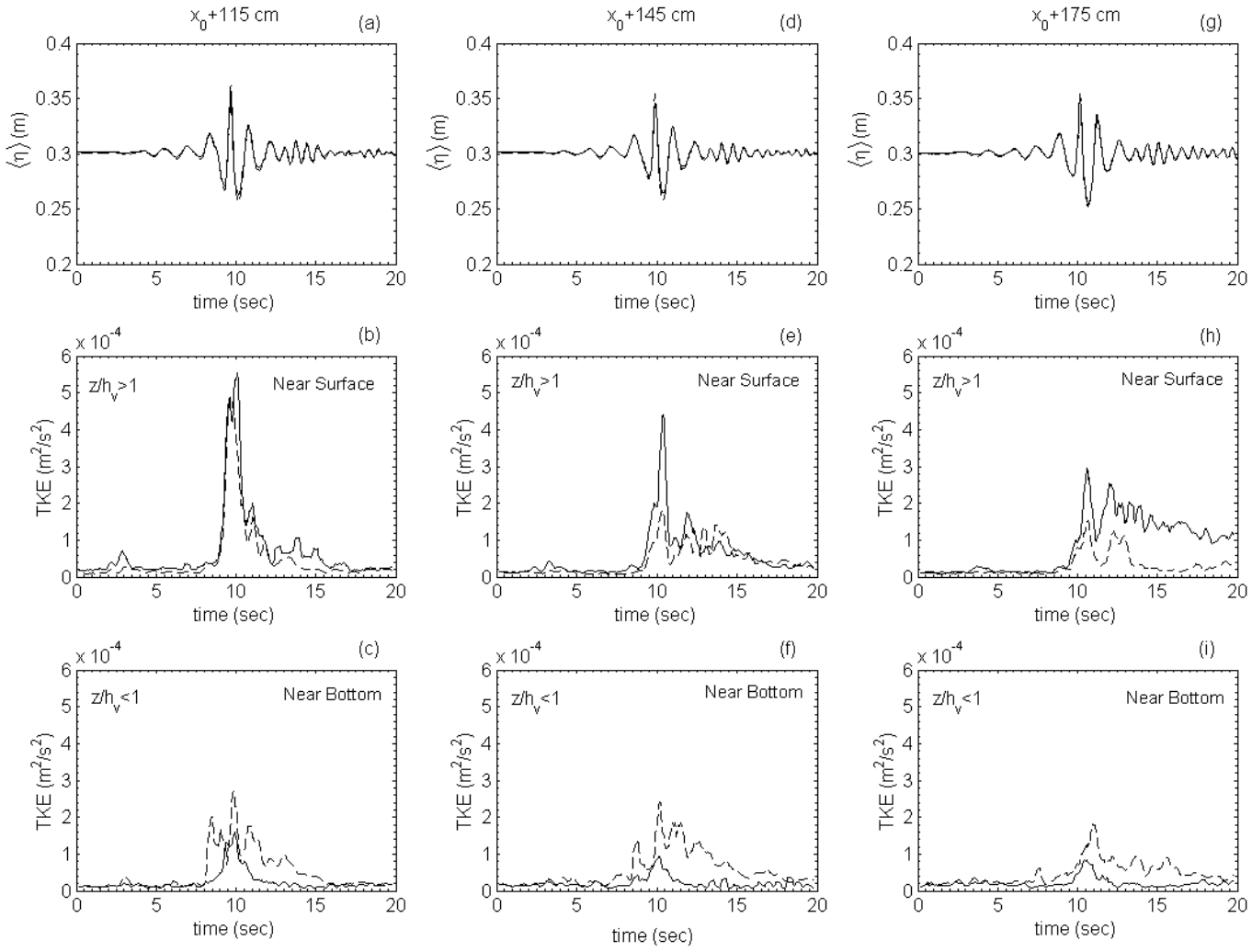

Figure 6.4. Ensemble-mean surface displacement and turbulent kinetic energy statistics for a spilling breaker event. The paddle motion began at t = 0. TKE measurements were vertically averaged across two bands: the near surface (from 0.18 m to 0.14 m), which is above SAV when SAV is present; and near bottom (from 0.06 to 0.02 m, which is within the SAV when SAV is present. The solid and dashed lines correspond to cases without SAV and with SAV, respectively. The records of turbulent kinetic energy were smoothed by a 0.4 seconds running average. (a) Surface displacement at $x = x_0+115$ cm; (b) near-surface turbulent kinetic energy at $x = x_0+115$ cm; (c) near-bottom turbulent kinetic energy at $x = x_0+115$ cm; (d) surface displacement at $x = x_0+145$ cm; (e) near-surface turbulent kinetic energy at $x = x_0+145$ cm; (f) near-bottom turbulent kinetic energy at $x = x_0+145$ cm; (g) surface displacement at $x = x_0+175$ cm; (h) near-surface turbulent kinetic energy at $x = x_0+175$ cm, and (i) near-bottom turbulent kinetic at $x = x_0+175$ cm.

The turbulent kinetic energy was estimated from velocity records made at each vertical position from z = 2 to 18 cm from the bed. In order to simplify the presentation of results, these data were separated into two bands; the near surface band includes z = 18 - 14 cm, which was above the meadow when the meadow was present, and the near bottom band includes z = 6 – 2 cm, which was within the meadow, when the meadow was present. As noted above, a weak spot in the Vectrino response exists between 8 and 10 cm, resulting in reduced data quality, so that we excluded these data. The time records of TKE near the surface (Fig. 6.4b, e, h) and near the bottom (Fig. 6.4c, f, i), are shown for the conditions with (dashed line) and without

(solid line) SAV. In each case, the level of TKE increased rapidly at the time corresponding to the arrival of the breaking crest, i.e. the maximum amplitude wave within the packet. Following this, the TKE declined at different rates, depending on the presence of SAV and the vertical position (near surface vs. near bed). Downstream from the breaking point ($x = x_0$+175 cm), the peak value of TKE near the surface was less than that observed closer to the breaking point ($x = x_0$ + 115 cm), but the duration of elevated turbulence was longer, which is consistent with turbulence introduced at the breaking point subsequently advecting downstream by the wave drift, as also observed by Rapp (1986, page 191).

First, we consider the TKE near the surface, which was above the meadow, when the meadow was present (Fig. 6.4b, e, h). Closest to the breaking point (Fig. 6.4b), the TKE levels were comparable with and without SAV, but moving downstream from the breaking point the TKE level was higher without SAV (Fig. 4h). Recall that the wave packet structure was nearly identical between the two cases (within 2%), so that we may infer that the strength of breaking was the same with and without vegetation. This is consistent with the nearly identical TKE measured closest to the breaking point (Fig. 6.4a). In contrast, the TKE measured later in time and further downstream from the breaking was significantly reduced in the presence of SAV. For example, farthest from the breaking point ($x = x_0$+175 cm, Fig. 6.4h) and in the absence of SAV, the turbulence remains elevated over the entire sampling period (>20 s). At the same position, the TKE measured with SAV was reduced to the noise level (0.0026C) within 5 seconds. The reduction of TKE above the SAV meadow was most likely attributed to the damping of breaker-generated turbulence by the SAV. This is consistent with Pujol et al. (2010), who also observed the damping of the TKE by SAV meadow.

Next, we consider the TKE observed near the bottom (bottom row of Fig. 6.4). Unlike the near surface measurements, the TKE near the bottom was always higher and more persistent with SAV than without SAV (Fig.6.4c, 6.4f, 6.4i). The peak TKE values observed with SAV were 2.7, 2.4 and 1.8 cm^2/s^2 at x_0+115, x_0+145 and x_0+175 cm, respectively, which was roughly twice the values observed without SAV, 1.6, 0.9 and 0.8 cm^2/s^2 at x_0+115, x_0+145 and x_0+175 cm, respectively. Further, at both x_0+145 and x_0+175 cm the peak TKE with SAV was higher within the meadow (Fig. 6.4f and 6.4i) than above the meadow (Fig. 6.4e and 6.4h). Finally, note that elevated TKE was observed within the meadow before breaking occurred at both x_0+115 cm and x_0+145 cm, i.e. before the breaking time point t = 8.48 s and t = 8.84 s at x_0+115 and x_0+145 cm, respectively. The observations given above suggest that the TKE within the meadow was not due to a downward vertical flux from the wave breaking at the surface, but was instead generated directly within the meadow. This result is consistent with previous studies of spilling waves (ak_c = 0.31), for which most of the turbulence generated is confined near the water surface. For example, Rapp and Melville (1990) showed that dye introduced at the surface before a spilling breaking was mixed down to a depth of the order of the wave height. A similar depth of penetration was observed in our dye visualization. A passive tracer (red food coloring) gently sprayed onto the surface before the breaking event made visible the

vertical turbulent transport associated with the breaking event. Photos taken at the breaking point (not shown in the article) suggested that the turbulence generated by breaking at the water surface did not penetrate inside the meadow. We note again that our observations are for spilling breakers. For plunging breakers the turbulence generated by breaking penetrates more deeply (Rapp and Melville 1990), so that for plunging breakers both types of turbulence (breaker-generated and stem-generated) might co-existence within the canopy.

The generation of TKE by stem wakes has been observed in unidirectional flow (Nepf 1999; Tanino and Nepf 2008), and it has been shown to inhibit sediment deposition (Zong and Nepf, 2010). Stem-generated turbulence has also been observed in the presence of progressive waves. Specifically, Luhar et al. (2010) considered non-breaking waves propagating over beds with and without SAV in the same facility used in this study (f = 0.7 Hz and a = 5.2 cm). They observed an increase in near-bed turbulence within the meadow, compared to the same wave condition over smooth bed (personal communication). Specifically, between 1 and 7 cm above the bed (the mean meadow height was about 7 cm), the level of turbulence was almost twice the level found upstream of the meadow. This magnitude difference is similar to our observations, i.e. within our meadow the TKE was almost twice that observed near the bare bed (Fig. 6.4c, 6.4f, 6.4i). Further, the magnitude of the u'^2 observed inside our meadow (u'^2 = 3.1 cm^2/s^2) was comparable to that observed by Luhar et al. (2010) for progressive, non-breaking waves (u'^2 = 1.8 cm^2/s^2). This comparison further supports our conclusion that the magnitude of TKE measured within the SAV was augmented by, and possibly completely determined by, stem-wake production.

In unidirectional flow, stem-wake turbulence is observed when the stem Reynolds number (Re_b) exceeds approximately 100 (Zong and Nepf, 2010). The stem Reynolds number is defined using the velocity within the meadow and the stem diameter (or blade width, b). For wave conditions, we consider the maximum horizontal component of the wave-induced velocity, u_b, i.e. $Re_b = u_b b/\nu$. Within the wave packet at $x = x_0$+115 cm, the measured peak value of u_b is 0.115 m/s, corresponding Re_b = 354. Further, Re_b exceeded the threshold of 100 during 2.5 s of the record, including periods before the arrival of the breaking wave. Specifically, the wave peak at 8.5 s, which comes before the breaking peak, produces conditions for stem wake generation (Re_b > 100), explaining why elevated TKE appears within the meadow before the onset of breaking. These results are comparable to those of Luhar et al. (2010) who found an increase of TKE with SAV with a Reynolds number Re_b = 220 to 1400.

As discussed above, the time necessary for the TKE to decay to the noise level depends on the presence of the meadow and the distance from the breaking point. The time scale for TKE decay is estimated as the difference between the time at which the TKE peaks ($t_{max\ TKE}$) and the time at which the TKE decays to the noise level (t_{bnl}). That is, $t_d = t_{max\ TKE} - t_{bnl}$. These time scales are shown in Table 6.1. Near the surface TKE persists for a longer time (larger t_d) when SAV is absent. In particular, at x_0+175 cm the surface TKE persists over 30 seconds longer

without SAV, than with SAV. In contrast, near the bottom, TKE persists for a longer time with SAV. These results are consistent with the following ideas introduced above. First, the presence of the SAV damps the turbulence generated by the breaking event. Second, stem-wake production contributes significantly to the TKE within the meadow.

Table 6.1. Summary of time-scales at $x = x_0+115$ and $x = x_0+175$ cm, including: the time of initial breaking from η_{rms}, the time at which the maximum TKE was measured, the time at which TKE returns to the noise level, and the time from the initial breaking until the TKE goes back to the noise level.

			$t_{max\ TKE}$	t_{bnl}	t_d
x_0+115 cm	*Near surface*	*Without SAV*	10.1 s	17 s	7 s
		With SAV	9.6 s	15 s	6 s
	Near bottom	*Without SAV*	10.0 s	13 s	3 s
		With SAV	9.8 s	16 s	6 s
x_0+175 cm	*Near surface*	*Without SAV*	10.6 s	>50 s	>39 s
		With SAV	10.6 s	16 s	5 s
	Near bottom	*Without SAV*	10.5 s	12 s	2 s
		With SAV	11 s	22 s	11 s

$t_{max\ TKE}$:is the time for maximum peak of TKE
t_{bnl}: is the time TKE back to the noise level
t_d: is the time from the breaking point to TKE back to the noise level

Previous researchers have observed that the temporal decay of breaker-generated turbulence follows a power law. In particular, Rapp and Melville (1990) observed that beyond four wave periods after breaking, the decay of the total kinetic energy with time was proportional to t^{-1}. The method of Rapp and Melville (1990) has also been used to calculate the power law in the present study. We consider whether SAV alters this relationship by comparing the observed TKE decay to the previously observed -1 slope (Fig. 6.5). Note, the TKE is nondimensionalized by the square of the wave speed (TKE/C^2), and the time is measured relative to the theoretical breaking time, t_f, normalized by the central angular frequency ($\omega_c(t-t_f)$). A log-log plot between the two nondimensional parameters gives the slope. Fig. 6.5 depicts the time interval from 10 seconds to 23 seconds, which extends over 14 wave periods. The noise level ($u'_{rms}/C \approx 0.0026C$ in Fig. 6.2), corresponds to $TKE/C_2 = O(10^{-5})$, which corresponds to $\log_{10}(TKE/C^2) = -5$. We disregard data that falls below the noise level. For reference, the -1 power law is shown as a dashed line in Fig. 6.5. Near the surface (Fig. 5a and 5c), both with and without SAV, TKE decays as t^{-1} with a 95% of confidence, consistent with previous studies of two-dimensional breaking (Rapp and Melville, 1990). There is one exception, the near surface TKE with SAV at $x = x_0+115$ cm, for which the TKE decays as t_{-2} with a 95% of confidence (Fig. 6.5c). Near the bottom (Fig. 6.5b and 6.5d), without SAV the TKE decays as t^{-2}.

Most likely, the bed provides additional damping that accelerates the decay of TKE decay. In contrast, within the meadow the TKE decays as t^{-1}, i.e. TKE decays more slowly near the bed when SAV is present. This is a bit counter-intuitive, since we expect the SAV to damp turbulence. However, as discussed above turbulence is also generated within the meadow through the interaction of the waves with the stems, and this additional source of TKE changes the observed decay rate.

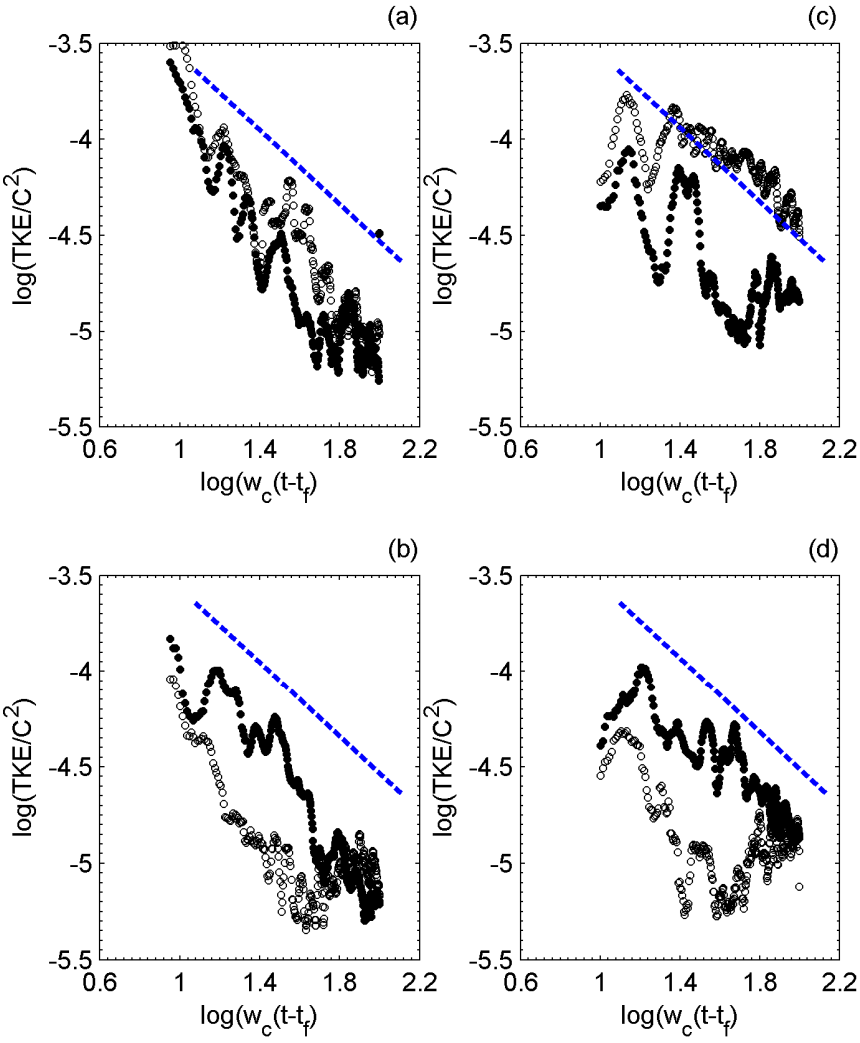

Figure 6.5. Decay of the turbulent kinetic energy as a function of the time. The white and black circles correspond to conditions without and with SAV, respectively. The dashed line represents the slope -1. (a) Near the surface at $x = x_0+115$ cm, for white circles r = 0.89, for black circles r = 0.95; (b) near the bottom at $x = x_0+115$ cm, for white circles r = 0.98, for black circles r = 0.89; (c) near the surface at $x = x_0+175$ cm, for white circles r = 0.95, for black circles r = 0.71, and (d) near the bottom at $x = x_0+175$ cm, for white circles r=0.93, for black circles r = 0.89. Levels of TKE lower than noise level were excluded from fitting.

6.3.3. Energy losses

Six points were chosen to observe the longitudinal evolution of the wave energy, before, during and after the spilling breaker (Fig. 6.6). These points are used to estimate the wave energy dissipation. Keep in mind that the estimator for wave energy dissipation (eq. 6.15) is not valid near the point of breaking (from x_0+115 to x_0+175 cm), where the assumption of kinetic and potential energy equi-partition breaks down and the group velocity is not constant (Rapp and Melville, 1990). For this reason, only the difference between the first and last points in the series (x = 3.1 and 4.9 m) is used as an estimate of the total energy loss from the wave packet. The estimates are given in Table 6.2. The loss of wave energy can be attributed to viscous dissipation in the wall- and bottom-boundary layers, to wave breaking, and to work against the meadow drag, a portion of which shows up in the production of stem-wake turbulence. For the experimental conditions considered here without SAV, the two-dimensional wave packet loses 24% of its energy (Table 6.2). This is larger than the 10% and 9% wave energy loss measured for two-dimensional waves by Rapp and Melville (1990) and by Wu and Nepf (2002), respectively. We attribute the difference to the shallower water depths used in our experiment. Our experiments were in transitional water depths, whereas the previous studies were in deep water. It is not surprising that, with the same packet conditions ($a_n k_c$, f_c, Δf), the shallower water depths used in our study created more vigorous breaking.

For the wave and meadow conditions considered in this study, a 32% wave energy loss was observed with SAV, which was greater than that observed without SAV (Table 6.2). We can estimate the contribution to wave energy loss from meadow drag alone by considering Luhar et al. (2010), who considered progressive, non-breaking waves with wave characteristics similar to the present experiment. For wave frequency 0.7 Hz and an initial amplitude of 5.2 cm, Luhar et al. (2010) observed a wave decay rate of 13% per wavelength, so that over a meadow length of 1.8 m (present study) we would expect a wave decay of 10%. We use this as an estimate of the wave decay associated with meadow drag alone. This value is consistent with the difference between the wave energy loss observed with (32%) and without (24%) SAV, i.e. an 8% difference. From this we conclude that in the presence of the SAV, ¾ of wave energy loss (24% loss) can be associated with the breaking event, and ¼ (8% loss) with dissipation by meadow drag. Note that these values are specific to the meadow stem density and height used in the current study. Different distributions have been observed over corals. Lowe et al. (2005) segregated the fraction of wave dissipation associated with wave breaking and with interaction with a coral reef. For most wave conditions, more than 80% of the wave energy was dissipated by reef bed friction. Only for the largest wave heights did wave breaking provide the dominant contribution (70%) to the total dissipation. Taken together with Lowe et al (2005), our study suggests that to properly model wave evolution over beds with macro-roughness (coral reefs or SAV meadows), one must consider both the bed friction as well as the breaking events.

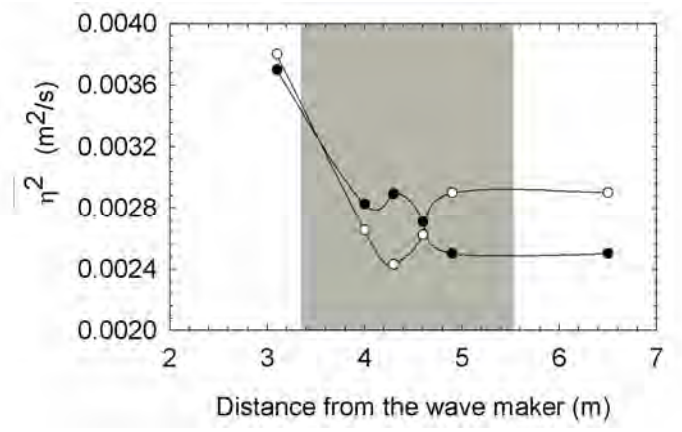

Figure 6.6. Longitudinal variation in surface displacement variance measured at the flume centreline (y = 0). Time-average was taken over t = 0 - 20 seconds. The white and black circles correspond to conditions without SAV and with SAV, respectively. Shadow zone corresponds to the length of breaking waves (= 2.15m)

Table 6.2. Wave energy loss due to breaking and interaction with submerged meadow.

Rapp and Melville (1990)	**Wu and Nepf (2002)**	**Present Experiments (2011)**		**Luhar et al. (2010)** *
Breaking waves		Breaking waves		Non breaking waves
Without SAV		Without SAV	With SAV	With SAV
10%	10%	24%	32%	10%

*Luhar et al. (2010) considered non breaking, progressive waves with a wave period of 1.4 s, a wavelength of 2.4 m, a water depth of 39 cm, a canopy height of 13 cm, and a stem density of 1200 stems/m^2. Luhar energy dissipation rates used to estimate energy loss expected over a meadow of length 1.8 m, as used in the present study.

6.4. Conclusions

This paper considers how the presence of submerged aquatic vegetation (SAV) alters the production and dissipation of turbulent kinetic energy associated with the passage of a breaking wave. Notably, in the presence of SAV the near-bed turbulence is both stronger and more persistent than observed without SAV. This is attributed to the generation of stem-wake turbulence by the elevated near-bed orbital velocity that occurs during the breaking event. The stem-wake production represents a transfer of energy from the wave field into the near-bed turbulence. Indeed, ¼ of the total loss of wave energy is attributed to meadow dissipation, and some fraction of this is fed into the turbulence at the stem scale. In contrast, the turbulence observed near the surface is weaker and more rapidly damped in the presence of SAV (as compared to the same conditions without SAV), consistent with previous studies that document the damping of turbulence generated above a meadow by the meadow drag. Importantly, this study suggests that to properly model wave evolution over beds with SAV, one must consider both the bed friction as well as the breaking events.

Acknowledgements Dolors Pujol was supported by research fellowship BR08/11 of the University of Girona and the *Ministerio de Ciencia e Innovación* of the Spanish Government through grant CGL 2010-17289 to the University of Girona. Funding also provided by US National Science Foundation, OCE 0751358. We also thank Mitul Luhar for helpful discussions and Dr. Jordi Colomer and Dr. Teresa Serra of the Department of Physics at the University of Girona.

References

Anderson, S.M., Charters, A.C., 1982. A fluid dynamics study of seawater flow through *Gelidium nudifrons*. Limnology & Oceanography 27, 399–412.

Banner, M., Phillips, O., 1974. Incipient breaking of small-scale waves. Journal of Fluid Mechanics 65, 647–656.

Batisse, M., Jeudy de Grissac, A., 1995. Marine region 3: Mediterranean. in: Kelleher, G., Bleakley, C., Wells, S. (Eds.), A Global Representative System of Marine Protected Areas. Vol. I. Great Barrier Reef Marine Park Authority. World Bank, and World Conservation Union, pp. 77–104.

Bos, A.R., Bouma, T.J., de Kort, G.L.J., van Katwijk, M.M., 2007. Ecosystem engineering by annual intertidal seagrass beds: sediment accretion and modification. Estuarine Coastal and Shelf Science 74, 344–348.

Cummins, W., 1962. The impulse–response function and ship motion. Schiffstechnik Forschungshefte Schiffbau Schiffsmaschineubau 9, 101–109.

Davis, M., Zarnick, E., 1964. Testing ship models in transient waves. In: Proceedings of the Fifth Symposium on Naval Hydrodynamics, Office of Naval Research, Washington, DC, pp. 509–540.

Dean, R.G., Dalrymple, R.A., 2002. Coastal Processes with Engineering Applications, first ed.. Cambridge University Press, Cambridge.

Denny, M.W., 1988. Biology and the Mechanics of the Wave-swept Environment. Princeton University Press, Princeton.

Folkard, A.M., 2005. Hydrodynamics of model *Posidonia oceanica* patches in shallow water. Limnology & Oceanography 50, 1592–1600.

Fonseca, M., Bell, S., 1998. Influence of physical setting on seagrass landscapes near Beaufort, North Carolina, USA. Marine Ecology Progress Series 171, 109–121.

Fonseca, M., Fisher, J., 1986. A comparison of canopy friction and sediment movement between 4 species of seagrass with reference to their ecology and restoration. Marine Ecology Progress Series 29, 15–22.

Gambi, M.C., Nowell, A.R.M., Jumars, P.A., 1990. Flume observations on flow dynamics in *Zostera marina* (eelgrass) Beds. Marine Ecology Progress Series 61, 159–169.

Ghisalberti, M., Nepf, H.M., 2002. Mixing layers and coherent structures in vegetated aquatic flows. Journal of Geophysical Research C: Oceans 107, C2.

Gleason, M., Elmer, D., Pien, N., Fisher, J., 1979. Effects of stem density upon sediment retention by salt-marsh cord grass, *Spartina alterniflora loisel*. Estuaries 2, 271–273.

Gobert, S., Cambridge, M.L., Velimirov, B., Pergent, G., Lepoint, G., Bouquegneau, J.M., Dauby, P., Pergent-Martini, C., Walker, D.I., 2006. Biology of Posidonia. in: Larkum, A.W.D., Orth, R.J., Duarte, C.M. (Eds.), Seagrasses: Biology, Ecology and Conservation. Springer Verlag, Berlin, pp. 387–408.

Granata, T.C., Serra, T., Colomer, J., Casamitjana, X., Duarte, C.M., Gacia, E., 2001. Flow and particle distributions in a nearshore seagrass meadow before and after a storm. Marine Ecology Progress Series 218, 95–106.

Infantes, E., Terrados, J., Orfila, A., Canellas, B., Alvarez-Ellacuria, A., 2009. Wave energy and the upper depth limit distribution of *Posidonia oceanica*. Botanica Marina 52, 419–427.

Jessup, A., Zappa, C., Yeh, H., 1997. Defining and quantifying microscale wave breaking with infrared imagery. Journal of Geophysical Research C: Oceans 102, 23145–23153.

Leonard, L.A., Luther, M.E., 1995. Flow hydrodynamics in tidal marsh canopies. Limnology & Oceanography 40, 1474–1484.

Lowe, R.J., Falter, J.L., Bandet, M.D., Pawlak, G., Atkinson, M.J., Monismith, S.G., Koseff, J.R., 2005. Spectral wave dissipation over a barrier reef. Journal of Geophysical Resaerch C: Oceans 110, C04001.

Luhar, M., Coutu, S., Infantes, E., Fox, S., Nepf, H.M., 2010. Wave-induced velocities inside a model seagrass bed. Journal of Geophysical Research C: Oceans 115, C12005.

Luhar, M., Nepf, H.M., 2011. Flow induced reconfiguration of buoyant and flexible aquatic vegetation. Limnology & Oceanography 56, 2003–2017.

Massel, S.R., Gourlay, M.R., 2000. On the modelling of wave breaking and set-up on coral reefs. Coast Engineering 39, 1–27.

Melville, W., 1982. The instability and breaking of deep-water waves. Journal of Fluid Mechanics 115, 165–185.

Nepf, H.M., 1999. Drag, turbulence, and diffusion in flow through emergent vegetation. Water Resources Research 35, 479–489.

Nepf, H.M., Wu, C.H., Chan, E.S., 1998. A comparison of two- and threedimensional wave breaking. Journal of Physical Oceanography 28, 1496–1510.

Neumeier, U., 2007. Velocity and turbulence variations at the edge of saltmarshes. Continental Shelf Research 27, 1046–1059.

Neumeier, U., Amos, C.L., 2006. The influence of vegetation on turbulence and flow velocities in European salt-marshes. Sedimentology 53, 259–277.

Ogston, A.S., Sternberg, R.W., 2002. Effect of wave breaking on sediment eddy diffusivity, suspended-sediment and longshore sediment flux profiles in the surf zone. Continental Shelf Research 22, 633–655.

Pergent-Martini, C., Pasqualini, V., Ferrat, L., Pergent, G., 2006. Ecological data in integrated coastal zone management: case study of *Posidonia oceanica* meadows along the Corsican coastline (Mediterranean sea). Environmental Management 38, 889–895.

Pujol, D., Colomer, J., Serra, T., Casamitjana, X., 2010. Effect of submerged aquatic vegetation on turbulence induced by an oscillating grid. Continental Shelf Research 30, 1019–1029.

Rapp, R.J., 1986. Laboratory Measurements of Deep-water Breaking Waves. Massachusetts Institute of Technology, Cambridge.

Rapp, R.J., Melville, W.K., 1990. Laboratory Measurements of Deep-water Breaking Waves, vol. 331, p. 735.

Reusch, T., Chapman, A., 1995. Storm effects on eelgrass (*Zostera-Marina L*) and Blue Mussel (*Mytilus-Edulis-L*) beds. Journal of Experimental Marine Biology and Ecology 192, 257–271.

Sheskin, D., 2000. Handbook of Parametric and Nonparametric Statistical Procedures, second ed.. Chapman & Hall, Boca Raton.

Tanino, Y., Nepf, H.M., 2008. Lateral dispersion in random cylinder arrays at high Reynolds number. Journal of Fluid Mechanics 600, 339–371.

Teodoro, A.C., Marcal, A.R.S., Gomes, F.V., 2004. Evaluation of total suspended matter concentration in wave breaking zone using. Multispectral Satellite Images 5569, 168–175.

Ting, F.C.K., Kirby, J.T., 1996. Dynamics of surf-zone turbulence in a spilling breaker. Coastal Engineering 27, 131–160.

van Katwijk, M.M., Bos, A.R., Hermus, D.C.R., Suykerbuyk, W., 2010. Sediment modification by seagrass beds: muddification and sandification induced by plant cover and environmental conditions. Estuarine Coastal and Shelf Science 89, 175–181.

Ward, L.G., Kemp, W.M., Boynton, W.R., 1984. The influence of waves and seagrass communities on suspended particulates in an estuarine embayment. Marine Geology 59, 85–103.

Wu, C.H., Nepf, H.M., 2002. Breaking criteria and energy losses for three-dimensional wave breaking. Journal of Geophysical Research C: Oceans 107, 3177.

Zong, L., Nepf, H.M., 2010. Flow and deposition in and around a finite patch of vegetation. Geomorphology 116, 363–372.

Chapter 7: Results and Discussion

This Ph.D. thesis has been prepared as a collection of papers, from Chapters 2 to 6. Each chapter comprises of its own results and discussion. In order not to transcribe the results and discussions again, this chapter aims to produce a more global discussion, comparing our results with the results obtained by other studies, as well as to emphasize the ecological implications of the results obtained in each chapter.

The next section (7.1 Flow dominated by unidirectional flow) shows a summary of the effect of aquatic plants on a flow dominated by unidirectional flow. Although this section does not present results from the experiments carried out in this thesis, it aims to put the results obtained in this thesis into context. Sections 7.2, 7.3 and 7.4 highlight the main results and discussions, while section 7.5 presents the ecological implications for each process.

7.1. Flow dominated by unidirectional flow

Hydrodynamic characteristics of seagrass habitats have a wide range of positive and negative biological effects on the vegetation meadow. Some authors have pointed out the idea that plant movement is important in order to understand the hydrodynamics of the flow, while other authors have suggested that shoot density and plant height need to be taken into consideration to study flow within seagrass beds (Ackerman and Okubo, 1993; Bouma et al., 2007; Ghisalberti and Nepf, 2006; Leonard and Crof, 2006; Nepf et al., 1997; Nepf and Vivoni, 2000; Peralta et al., 2008; Shi et al., 1995). In a laminar flow, it is well known that a highly turbulent flow inside a seagrass meadow resulting from the presence of seagrass blades can be observed. However, this turbulent velocity can vary depending on shoot density. In a low density of stiff shoot canopy (<200 shoots m^{-2}) stems cannot interact with the flow and no significant differences are shown when compared to the case without vegetation (Worcester, 1995). In plant densities higher than 200 shoots m^{-2} stem-wake turbulence is generated, which increases linearly with density (Nepf et al., 1997). At high plant density (>2000 shoots m^{-2}) wake turbulence generated at the rear of stem decreases due to enhanced attenuation in current velocity by the vegetation (Nepf et al., 1997). Nepf (1999) defined sheltering or dampening as a reduction in the in-emergent canopy macroscale diffusion, due to a combination of reduced velocity and reduced eddy-scale relative to unvegetated zones. Because the level of turbulence inside a long meadow generally decreases with increasing stem density, the tendency for sedimentation also increases with increasing stem density (Bos et al., 2007; Leonard and Luther, 1995; Neumeier, 2007; Neumeier and Amos, 2006; van Katwijk et al., 2010; Ward et al., 1984).

7.2. Flow dominated by nearly isotropic turbulence

Results in Chapter 2 showed that within the submerged rigid vegetation model, two zones were able to be distinguished. The first zone was the transition zone, situated a few centimetres below the top of the canopy and characterised by levels of higher TKE than of that without plants. However, as in the unidirectional flow, the depth of transition zone depended on the plant geometric characteristics, stem density and stem diameter, as well as the length of eddies (ℓ_0). In order to quantify the geometric characteristic of the plants, a new parameter was used: plant-to-plant distance (ppd). This parameter allowed both the plant density and the stem diameter in one parameter to be taken into account. The transition zone appeared once $\ell_0 <$ ppd. This may allow the eddy to reach the core of the canopy, thus inhibiting sheltering. The deepest transition zone corresponded to small stem density and large stem diameter.

Well inside the canopy, located below the transition zone, the TKE progressively decayed as the stems dissipated the turbulence, creating a zone where the TKE was lower than that in the zone without plants, i.e., producing sheltering or dampening. This phenomenon was enhanced by a decrease in the stem diameter and an increase in the plant density of the vegetation model, due to the reduction of the plant-to-plant distance. A non-dimensional model was developed in Chapter 3 using the Buckingham pi-theorem, based on Hopfinger and Toly (1976) and DeSilva and Fernando (1994), who found an equation where the decay of the turbulent components was a function of: stroke (s), mesh (M), f (frequency of the grid) and distance from the grid to the measurement point (z_m). Following that equation, we added a new variable: d/ppd. Then, it was found that the decrease of TKE followed: $TKE_0/(f^2 \cdot s^2) \propto (d/ppd)^{-0.25} \cdot (z_m/M)^{-3}$. Therefore, the TKE was not only affected by the distance from the grid to the measured point, but also by the geometric characteristics of the plants (both diameter and plant-to-plant distance).

When implementing a semi-rigid submerged vegetation model the transitional hydrodynamic regime disappeared, resulting in a steep gradient of TKE above and below the plants. This process was attributed to the architecture of the semi-rigid stems, where the thick stem at the base of the plant gradually divided at the top and its branches merged with the branches of its neighbours, resulting in an increase in the SPF at the top of the canopy.

7.3. Flow dominated by progressive waves

Chapters 4 and 5 were focused on studying the relationship between flow structure and different vegetation models over a flow dominated by progressive waves. The progressive waves followed the second-order Stokes theory in the intermediate depth range. The observations revealed that submerged and emergent rigid vegetation models modified the wave-induced velocities, i.e., the mean current, wave velocity and turbulent stress.

7.3.1. Mean current associated with progressive waves

The submerged rigid vegetation model, at plant densities higher than 640 plants m^{-2}, acted like a false floor and confined the mean current to above the plant bed. A penetration depth of around 2 cm below the top of submerged rigid vegetation, which was analogous to a viscous layer near the bed, was found. The behaviour of the vertical profile of mean current for oscillatory flow with the presence of submerged rigid vegetation was analogous to that found for unidirectional flows (Nepf and Vivoni, 2000; Reidenbach et al., 2007). These authors showed that the presence of vegetation under unidirectional flow shifted the logarithmic profile from the top of the water surface down to 2 cm below the top of the canopy. The emergent rigid vegetation model changed the direction of the induced mean current, with the highest velocity corresponding to the highest plant density. In contrast, the submerged flexible vegetation model had a weak effect on the mean current, with the velocity profile similar to that found in experiments without vegetation.

7.3.2. Wave velocity associated with progressive waves

The highest reduction of U_w^{rms} for the densest submerged rigid model (1280 plants m^{-2}) was observed in the 2 cm below the top of the vegetation (with the value for the unvegetated zone decreasing to 20%). From that depth downwards U_w^{rms} remained constant. According to the model proposed by Lowe et al. (2005a), the canopy inertia force (C_m) was expected to contribute mostly to the attenuation of the oscillatory canopy flow in our wave conditions. This coefficient was calculated as the sum of two terms, $C_m = 1+k_m$, where k_m was called the added mass, and which depended on the shape of the object. Submerged flexible vegetation showed a reduction of less than 10%. Unlike the submerged rigid model, the flexible model had a higher level of porosity, which in turn consigned the path of the flow. Furthermore, canopy inertia force was lower than for submerged rigid vegetation, putting up no resistance to the wave velocity which could then penetrate inside the meadow. Emergent rigid vegetation showed a reduction of 45% compared to experiments without vegetation. This result was in accordance with the

values found in the field by Hansen and Reidenbach (2012) who established that the smallest within-canopy flow reduction occurred in the eelgrass with the lowest density and the smallest average blade length.

7.3.4. Turbulent stress associated with progressive waves

The aim of Chapter 5 is to describe the interaction between the TKE and the seagrasses under progressive waves. In general, well inside the submerged rigid model larger TKE was found compared to the experiment without vegetation. This was attributed mainly to the generation of stem-wake turbulence by the elevated near-bed wave velocity during the passage of the wave, with a $Re_w > 300$-310. The maximum peak of TKE was produced during the backward facing slope of the wave, in accordance with Reidenbach et al. (2007). This increase of turbulence is attributed to the generation of stem-wake turbulence caused by the elevated near-bed wave velocity ($Re_w > 100$, calulated by the maximum wave velocity). Therefore, the wave velocity is converted to TKE by means of stem-wakes. This process was also observed in unidirectional flow, when the stem Reynolds number (Re) exceeds approximately 100 (Zong and Nepf, 2010). However, for the highest plant density and wave frequency ($n_s = 1280$ plants m^{-2} and $f = 1.4$ Hz) the increase of TKE was confined to 2 cm below the top of the canopy. Therefore, the generation of stem-wake turbulence was associated with a greater loss of wave velocity below the top of the submerged rigid seagrass model. Specifically for that case, sweeps and ejections were the predominant events in that zone. Below that zone and well inside the canopy a decrease of TKE, compared to the experiment without plants, is observed i.e., sheltering or dampening.

Under the same wave conditions as in the submerged rigid models, the study of the turbulence with the submerged flexible model in a flow dominated by progressive waves showed similar profiles of TKE as to those with no plants. TKE progressively decayed inside the seagrass bed as blade movement dissipated the turbulence, resulting in lower levels of TKE than of those without vegetation (a reduction between 16 and 46%). Reynolds number was $Re_w \approx 100$, i.e. there was an absence of stem-wake turbulence. For the emergent rigid model the TKE was always lower compared to that without vegetation and it was attributed to the reduction of the wave velocity from the top of the water column.

7.4. Flow dominated by breaking waves

Flow dominated by breaking waves was studied in Chapter 6. The observations suggested that the TKE measured near the bed was always higher and more persistent with submerged aquatic vegetation, having roughly twice the value observed than of that without submerged aquatic vegetation. This enhancement of TKE was attributed to the generation of stem-wake turbulence by the elevated near-bed orbital velocity during the passage of the wave packet. This process is also observed for progressive waves when Re_w > 300-310. The generation of stem-wake turbulence is associated with a greater loss of wave energy. Specific to the wave and plant conditions considered in this study, in the presence of the SAV a total of 32% of wave energy loss was observed; ¾ of this loss (24%) could be associated with the breaking event, and ¼ of this loss (8%) could be associated with dissipation by meadow drag.

7.5. Ecological implications

From the collection of experiments carried out in this thesis, it has been demonstrated that seagrass produces sheltering under pure turbulence and progressive waves. Sheltering, one of the most important geophysical processes, not only promotes sedimentation as a result of longer particle residence times (Ward et al., 1984; Eckman et al., 1989), it also decreases the resuspension of sediment from the bottom and consequently reduces its erosion, relative to unimpeded flows (Shi et al., 1996; Leonard and Croft, 2006; Kosten et al., 2009) and to high energy events (Granata et al., 2001). These geophysical processes have biological consequences such as an increase in food availability and provide a refuge for fish, invertebrates and plankton (Wilson et al., 1987; Gambi et al., 1990; Irlandi and Peterson, 1991; Ackerman and Okubo, 1993; Nepf and Vivoni, 2000). The reduction of resuspension improves water clarity, which in turn provides greater light penetration and consequently an increase in productivity, thus creating a positive feedback for seagrass growth (Ward et al., 1984).

On the other hand, under progressive waves in the submerged rigid model and at some specific wave conditions, sheltering was not observed. TKE is higher with plants than without them. However, turbulence generated by the canopy could be the only turbulence in water motion at the right scale to enhance nutrient uptakes and effect the exchange of gases and (Anderson and Charters, 1982). The submerged rigid canopy model could mimic coral reefs. It is well known that many coral communities are located in nutrient limited environments (Falter et al., 2004). Therefore, the capacity to enhance the rate of material transfer between seawater and the coral community will determine the growth rate of that community. Coral reefs do not photosynthesize, but rather have a symbiotic relationship with some algae which do the photosynthesis for them. Turbulence found inside the meadow has positive biological consequences, such as the improvement in the transfer of CO_2 (in the form of bicarbonate) from

the water to the surface layer of leaves. Without turbulence, the only physical mechanism capable of capturing CO_2 would be by means of molecular diffusion from the boundary layer, an extremely inefficient transport mechanism (Denny, 1988). The TKE observed confirms that a stem-wake presence is found in submerged rigid vegetation, whereas in submerged flexible vegetation no stem-wake turbulence is generated. Therefore, rigidity could be a significant parameter, enhancing the transfer of material between seawater and the benthic community, such as coral reefs. In addition, the increase of TKE, together with the increase of -<u'w'> (<u'w'>$_2$ and<u'w'>$_4$) at the same depth when compared with experiment without vegetation, could be one of the mechanisms which contributed to improving the transfer of nutrients in the coral community.

The unidirectional mean current generated within the meadow under wave forcing plays a major role in determining both the health of the seagrass beds and their ecological contribution. It is well known that the mean current is able to speed up the rate of water renewal within a meadow thus enhancing the nutrient cycling capabilities of seagrass, as well as generating net transport of sediments, such as seeds and pollen, in the direction of wave propagation (Luhar et al., 2010). Submerged rigid vegetation has a positive mean current in the direction of the wave inside the vegetation, whereas emergent rigid vegetation has a stronger negative mean current at the same depth. Therefore, it changes the direction of the mean current, i.e., implying a change in the direction of the water renewal, which in turn has effects on the net transport of sediments, nutrients, seeds and pollen. This is crucial in order to understand the dynamics of seed propagation and nutrient renewal when restoring a damaged zone.

References

Ackerman, J.D., Okubo, A., 1993. Reduced Mixing in a Marine Macrophyte Canopy. Funct. Ecol. 7, 305-309.

Anderson, S.M., Charters, A.C., 1982. A fluid dynamics study of seawater flow through *Gelidium nudifrons*. Limnol. Oceanogr. 27, 399-412.

Bos, A.R., Bouma, T.J., de Kort, G.L.J., van Katwijk, M.M., 2007. Ecosystem engineering by annual intertidal seagrass beds: Sediment accretion and modification RID A-9841-2011. Estuar. Coast. Shelf Sci. 74, 344-348.

Bouma, T.J., van Duren, L.A., Temmerman, S., Claverie, T., Blanco-Garcia, A., Ysebaert, T., Herman, P.M.J., 2007. Spatial flow and sedimentation patterns within patches of epibenthic structures: Combining field, flume and modelling experiments. Cont. Shelf Res. 27, 1020-1045 .

Denny, M.W., 1988. Biology and the Mechanics of the Wave-Swept Environment Princeton University Press, Princeton.

Desilva, I.P.D., Fernando, H.J.S., 1994. Oscillating grids as a source of nearly isotropic turbulence. Phys. Fluids. 6, 2455-2464.

Eckman, J.E., Duggins, D.O., Sewell, A.T., 1989. Ecology of understory kelp environments. 1. Effects of kelps on flow and particle-transport near the bottom. Journal of Experimental Marine Biology and Ecology, 129, 173-187.

Falter, J., Atkinson, M., Merrifield, M., 2004. Mass-transfer limitation of nutrient uptake by a wave-dominated reef flat community. Limnol. Oceanogr. 49, 1820-1831.

Gambi, M.C., Nowell, A.R.M., Jumars, P.A., 1990. Flume observations on flow dynamics in *Zostera marina* (eelgrass) beds. Mar. Ecol. Prog. Ser. 61, 159-169.

Ghisalberti, M., Nepf, H., 2006. The structure of the shear layer in flows over rigid and flexible canopies. Environ. Fluid. Mech. 6, 277-301.

Granata, T.C., Serra, T., Colomer, J., Casamitjana, X., Duarte, C.M., Gacia, E., 2001. Flow and particle distributions in a nearshore seagrass meadow before and after a storm. Mar. Ecol. Prog. Ser. 218, 95-106.

Hansen, J.C.R., Reidenbach, M.A., 2012. Wave and tidally driven flows in eelgrass beds and their effect on sediment suspension. Mar. Ecol-Prog. Ser. 448, 271-287.

Hopfinger, E.J., Toly, J.A., 1976. Spatially Decaying Turbulence and its Relation to Mixing Across Density Interfaces. J. Fluid Mech. 78, 155-&.

Irlandi, E.A., Peterson, C.H., 1991. Modification of animal habitat by large plants - mechanisms by which seagrasses influence clam growth. Oecologia, 87, 307-318.

Koch, E.W., 1996. Hydrodynamics of a shallow *Thalassia testudinum* bed in Florida, USA. pp 105-110. In: J. Kuo, R.C. Phillips, D.I. Walker and H. Kirkman [eds.], Seagrass Biology - Proceedings of an International Workshop, Western Australia Museum, Perth, Australia.

Kosten, S., Lacerot, G., Jeppesen, E., Marques, D.D., van Nes, E.H., Mazzeo, N., Scheffer, M., 2009. Effects of submerged vegetation on water clarity across climates. Ecosystems, 12, 1117-1129.

Leonard, L.A., Croft, A.L., 2006. The effect of standing biomass on flow velocity and turbulence in *Spartina alterniflora* canopies. Estuar. Coastal. Shelf Sci. 69, 325-336.

Leonard, L.A., Luther, M.E., 1995. Flow hydrodynamics in tidal marsh canopies. Limnol. Oceanogr. 40, 1474-1484.

Luhar, M., Coutu, S., Infantes, E., Fox, S., Nepf, H., 2010. Wave-induced velocities inside a model seagrass bed. J. Geophys. Res. Oceans 115, C12005.

Nepf, H., 1999. Drag, turbulence, and diffusion in flow through emergent vegetation. Water Resour. Res. 35, 479-489.

Nepf, H., Sullivan, J.A., Zavistoski, R.A., 1997. A model for diffusion within emergent vegetation. Limnol. Oceanogr. 42, 1735-1745.

Nepf, H., Vivoni, E.R., 2000. Flow structure in depth-limited, vegetated flow. J. Geophys. Res. Oceans 105, 28547-28557.

Neumeier, U., 2007. Velocity and turbulence variations at the edge of saltmarshes. Cont. Shelf Res. 27, 1046-1059.

Neumeier, U., Amos, C.L., 2006. The influence of vegetation on turbulence and flow velocities in European salt-marshes. Sedimentology 53, 259-277.

Peralta, G., van Duren, L.A., Morris, E.P., Bouma, T.J., 2008. Consequences of shoot density and stiffness for ecosystem engineering by benthic macrophytes in flow dominated areas: a hydrodynamic flume study. Mar. Ecol. Prog. Ser. 368, 103-115.

Reidenbach, M.A., Koseff, J.R., Monismith, S.G., 2007. Laboratory experiments of fine-scale mixing and mass transport within a coral canopy. Phys. Fluids 19, 075107.

Shi, Z., Pethick, J.S., Pye, K., 1995. Flow structure in and above the various heights of a saltmarsh canopy: a laboratory flume study. J. Coast. Res. 11, 1204-1209.

Shi, Z., Pethick, J.S., Burd, F., Murphy, B., 1996. Velocity profiles in a salt marsh canopy. Geo-Marine Letters, 16, 319-323.

van Katwijk, M.M., Bos, A.R., Hermus, D.C.R., Suykerbuyk, W., 2010. Sediment modification by seagrass beds: Muddification and sandification induced by plant cover and environmental conditions. Estuar. Coast. Shelf Sci. 89, 175-181.

Ward, L.G., Kemp, W.M., Boynton, W.R., 1984. The influence of waves and seagrass communities on suspended particulates in an estuarine embayment. Mar. Geol. 59, 85-103.

Wilson, K.A., Heck, K.L., Able, K.W., 1987. Juvenile blue-crab, *Callinectes-sapidus*, survival - an evaluation of eelgrass, *Zostera-marina*, as refuge. Fishery Bulletin, 85, 53-58.

Worcester, S.E., 1995. Effects of eelgrass beds on advection and turbulent mixing in low current and low shoot density environments. Mar. Ecol-Prog. Ser. 126, 223-232.

Zong, L., Nepf, H., 2010. Flow and deposition in and around a finite patch of vegetation. Geomorphology 116, 363-372.

Chapter 8: General conclusions

Submerged aquatic vegetation (rigid and flexible models as well as real plants) and emergent aquatic vegetation may modify the physical climate (turbulence and waves) by producing sheltering or dampening of the associated energy. The most important conclusions of this thesis are:

a) under pure and nearly isotropic turbulence, sheltering or dampening is enhanced by a decrease in stem diameter and an increase in canopy density i.e., a reduction in the plant-to-plant distance.

b) sheltering under pure and nearly isotropic turbulence is quantified by an adimensional model, which suggests that well inside the canopy the decrease of TKE follows: $TKE_0/\left(f^2 \cdot s^2\right) \propto (d/ppd)^{-0.25} \cdot (z_m/M)^{-3}$, where TKE_0 is TKE/ρ, f is the oscillating frequency, s is the stroke of the grid, d is the stem diameter, ppd is the plant-to-plant distance, z_m is the distance from the grid to the measurement point and M is the mesh.

c) under the progressive wave, sheltering is present for the submerged rigid model at the highest plant density and wave frequency. The sheltering is associated with the reduction of wave velocity at the top of the canopy. The submerged flexible model also shows sheltering. This sheltering is caused by blade movement which dissipated the turbulence, resulting in lower levels of TKE than of that without vegetation. Emergent rigid vegetation shows a high reduction of wave velocity compared to experiments without vegetation. That reduction inhibits the production of TKE, i.e. enhancing the sheltering.

Although under progressive waves sheltering has been observed, for some specific wave conditions and plant densities the TKE increases inside the meadow. An increase of TKE, i.e., the absence of sheltering, has also been observed under a fluid dominated by breaking waves. The wave velocity is converted to TKE by means of stem-wakes, and by the elevated near-bed wave velocity during the passage of the wave when a Reynolds number larger than 300-310. The generation of stem-wake turbulence was associated with a greater loss of wave velocity.

To sum up, submerged and emergent vegetation in shallow-water environments modify the local flow, depending on plant rigidity, stem diameter and canopy density. The vertical flow structure was determined for each environment by whether it was dominated by pure and nearly isotropic turbulence, progressive waves or breaking waves.